

**Dissertation zur Erlangung des Doktorgrades
der Fakultät für Chemie und Pharmazie
der Ludwig-Maximilians-Universität München**



**In vivo and In vitro Analysis of the Retinal Voltage
Dependent L-type Ca^{2+} Channel $\text{Ca}_v1.4$ Function**

**Lior Shaltiel
aus Ramat Gan (Israel)**

2013

Erklärung

Diese Dissertation wurde im Sinne von § 7 der Promotionsordnung vom 28. November 2011 von Herrn Prof. Dr. Christian Wahl-Schott betreut.

Eidesstattliche Versicherung

Diese Dissertation wurde eigenständig und ohne unerlaubte Hilfe erarbeitet.

München, den 14.05.2013

(Lior Shaltiel)

Dissertation eingereicht am	14.05.2013
1. Gutachter	Herr Prof. Dr. Christian Wahl-Schott
2. Gutachter	Herr Prof. Dr. Martin Biel
Mündliche Prüfung am	13.06.2013

*“The highest activity a human being can attain
is learning for understanding,
because to understand is to be free.”*

Baruch Spinoza

To My Family

TABLE OF CONTENTS

Table of Contents

1. INTRODUCTION	7
1.1 Voltage-gated calcium channel.....	10
1.2 L-type calcium channel.....	15
1.2.1 Regulation by voltage and Ca ²⁺ ions	16
1.3 The L-type Calcium Channel Ca _v 1.4	20
1.4 Calcium binding proteins (CaBPs).....	21
1.4.1 CaBP4.....	24
2. OBJECTIVE OF THE STUDY	25
3. MATERIALS AND METHODS	26
3.1 Chemicals, Solutions and Equipment	26
3.2 Molecular biology methods	26
3.2.1 Plasmids.....	26
3.2.2 Generated constructs	28
3.2.2.1 Constructs for electrophysiology.....	28
3.2.2.1.1 Ca _v 1.4 subunits constructs.....	28
3.2.2.1.2 CaBP4 constructs	28
3.2.3 Culture and transformation of bacteria	29
3.2.3.1 Bacteria strains.....	29
3.2.3.2 Culture media and antibiotics	29
3.2.3.3 Bacteria culture.....	30
3.2.3.4 Creation of competent bacterial cells stocks.....	30
3.2.3.5 DNA Transformation into E. coli cells	31
3.2.4 Isolation of plasmid DNA	31
3.2.4.1 Mini-preparation (Miniprep).....	32
3.2.4.2 Maxi-preparation (Maxiprep).....	33
3.2.4.3 Determination of the DNA concentration	33
3.2.5 Polymerase chain reaction (PCR)	33
3.2.5.1 Primers	34
3.2.5.2 Standard genotyping PCR.....	34
3.2.5.3 High Fidelity PCR for cloning.....	35
3.2.5.4 Overlap-PCR	36
3.2.5.5 Quikchange-PCR.....	36
3.2.6 Isolation, purification and quantification of DNA	38
3.2.6.1 Agarose gel	39
3.2.6.2 Polyacrylamide gel electrophoresis (PAGE)	39
3.2.6.3 Isolation of DNA from a gel.....	40
3.2.6.4 Precipitation of DNA	40
3.2.6.5 Isolation of genomic DNA from mouse tissues	40
3.2.6.6 Phenol-chloroform extraction.....	41
3.2.6.7 Sequencing of DNA	41

TABLE OF CONTENTS

3.2.7 Enzymatic modification of DNA	42
3.2.7.1 Restriction digestion	42
3.2.7.2 Dephosphorylation.....	42
3.2.7.3 Ligation	42
3.2.8 Southern-Blot	43
3.2.8.1 Buffers and solutions for Southern blot.....	44
3.2.8.2 Extraction of genomic DNA from mouse tissue	44
3.2.8.3 Restriction digestion of genomic DNA	44
3.2.8.4 Separation of genomic DNA on agarose gel.....	45
3.2.8.5 Depurination of genomic DNA	45
3.2.8.6 Blotting.....	45
3.2.8.7 Amplification of the ³² P-labeled probe	45
3.2.8.8 Hybridization	46
3.2.8.9 Washing and analyzing the membrane.....	46
3.3 Biochemical methods.....	47
3.3.1 Protein extraction from HEK293 cells.....	47
3.3.2 Quantification of protein concentration	47
3.3.3 Electrophoretic separation of proteins by SDS-PAGE.....	48
3.3.4 Western Blot.....	49
3.4 Culture and transfection of eukaryotic cells	51
3.4.1 HEK293 cells culture	51
3.4.2 Establish of HEK293 stable cell lines	51
3.4.3 Transfections.....	52
3.4.3.1 Transient transfection with Fugene.....	52
3.4.3.2 Transient transfection with calcium phosphate	53
3.4.4 Harvesting of HEK293 cells.....	53
3.4.5 Freezing of HEK293 cells	53
3.5 Investigation of Ca _v 1.4 knockout mice	54
3.5.1 The Ca _v 1.4 knockout mice	54
3.5.2 Immunohistochemical methods	54
3.5.3 Electroretinography (ERG)	56
3.5.4 Behavior test - Water maze	56
3.6 Electrophysiology	57
3.6.1 Experimental implementation	57
3.6.2 Patch-clamp protocols.....	58
3.6.3 Data analysis.....	59
3.6.4 Calculation of the liquid junction potential (LJP)	61
3.7 Statistical analysis	61

TABLE OF CONTENTS

4.RESULTS	62
4.1 The regulation properties of retinal Ca _v 1.4 channel by CaBP4.....	62
4.1.1 Ca _v 1.4 channels are regulated by CaBP4	62
4.1.1.1 The calcium dependent inactivation (CDI) in truncated Ca _v 1.4 variants ..	62
4.1.1.2 CaBP4 increases Ca _v 1.4 channel availability by modulating voltage dependent gating of the channel	64
4.1.2 Functional alterations in two CaBP4 human mutations	69
4.1.3 Window conductance and availability of the Ca _v 1.4 channel under physiological extracellular Ca ²⁺ concentrations.....	72
4.1.4 CaBP4 binds to the IQ motif in the C-terminus of Ca _v 1.4	75
4.2 Characterization of the Ca _v 1.4 channels function in-vivo.....	78
5. DISCUSSION	89
5.1 Functional effects of the CaBP4 regulation on the Ca _v 1.4α1.....	89
5.2 The patho-mechanism of CaBP4 mutants	95
5.3 Functional characterization of Ca _v 1.4 deficient mice	96
6. SUMMARY	99
7. LITERATURE	100
8. APPENDIX	114
8.1 Sequence of the murine Ca _v 1.4α1 cDNA	114
8.2 Multiple sequence alignment of the CaBPs	119
8.3 Sequence alignment of the CaBP4 protein variants	121
8.4 Primers and Restriction enzymes	122
8.5 Materials and Equipment	123
8.5.1 Devices	123
8.5.2 Chemicals	124
8.6 Summary of the electrophysiological measurements	125
8.6.1 Voltages for half-maximum activation ($V_{0.5,act}$) and slope values (k_{act}) from the patch clamp measurements	125
8.6.2 Voltages for half-maximum inactivation ($V_{0.5,inact}$) and slope values (k_{inact}) from the patch clamp measurements	125
8.7 List of Abbreviations	126
9. CURRICULUM VITAE	129
10. PUBLICATIONS	130
11. ACKNOWLEDGEMENTS	131

1. Introduction

Intracellular calcium signals are essential for a variety of physiological processes (Berridge, 2004; Catterall, 2010; Turner et al., 2011). They affect virtually all cellular processes, from the excitation-contraction coupling in skeletal and cardiac muscles through signal transduction, hormone and neurotransmitter release, regulation of enzyme activity, gene expression to cell proliferation in different cell types. These signals are generated when calcium enters the cell via voltage gated Ca^{2+} channels in the plasma membrane. Alternatively, intracellular Ca^{2+} can transiently rise upon release from intracellular organelles such as ER, nuclear envelope, mitochondria and lysosomes. Voltage gated Ca^{2+} channels in the plasma membrane belong to the superfamily of voltage gated pore loop ion channels. This superfamily also includes voltage-gated sodium and potassium channels. Voltage gated Ca^{2+} channels open in response to changes in the membrane potential. The opening and the closing of these calcium channels is regulated by hormones, protein kinases, protein phosphatases, and drugs (Hofmann et al., 1999; Minor and Findeisen, 2010). Changes in the function and expression of calcium channels lead to cellular disorders and thereby a number of diseases (Bidaud et al., 2006; Striessnig et al., 2010).

Voltage-gated calcium channels are known to play a key role in synaptic transmission. In the retina, a distinct member of the voltage gated Ca^{2+} channel family is expressed, termed $\text{Ca}_v1.4$. $\text{Ca}_v1.4$ channels are located in specialized synapses of retinal photoreceptors and bipolar cells, so called ribbon synapses. $\text{Ca}_v1.4$ channels are responsible to the tonic glutamate release in the retinal photoreceptors synapses as a result of graded and sustained changes in membrane potential during a light stimulus (Fig. 1.1). In the dark, when the membrane potential is rather depolarized (-40mV), glutamate is released at these synapses. Light induces a hyperpolarization and, hence, switches off neurotransmission (Barnes and Kelly, 2002; Bech-Hansen et al., 1998; Corey et al., 1984; Doering et al., 2005; Mansergh et al., 2005; Morgans, 2001; Strom et al., 1998; Taylor and Morgans, 1998; Thoreson, 2007).

$\text{Ca}_v1.4$ critical for synaptic transmission and mutations in the encoding gene (*CACNA1F*, chromosome Xp11.23) that lead to aberrations in the expression of the $\text{Ca}_v1.4$ protein or to its complete loss have been linked to severe human diseases (Striessnig et al., 2004). Recently, mutations in the gene *CACNA1F* have been

INTRODUCTION

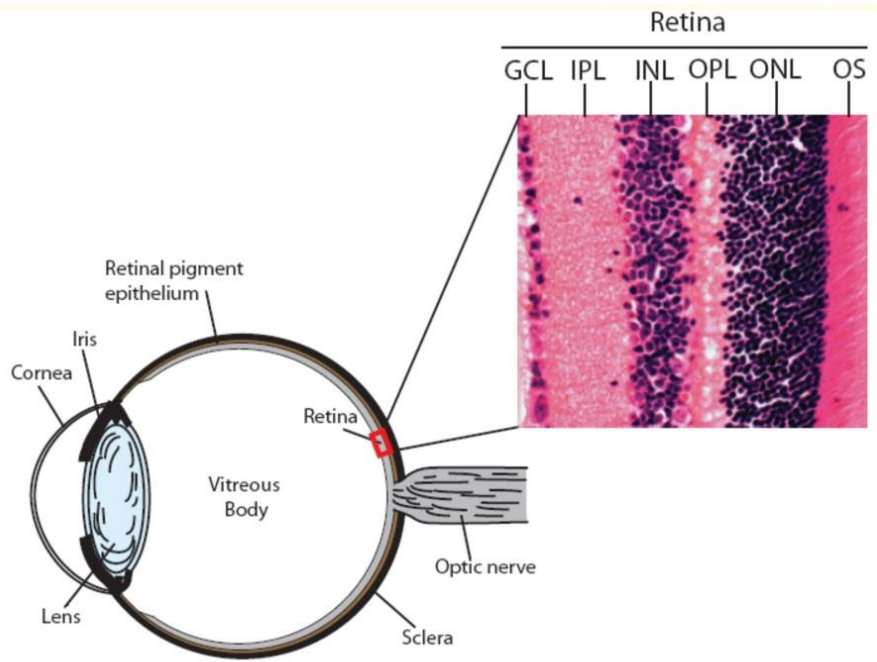
identified in patients who have incomplete X-linked congenital stationary night blindness (CSNB2) (Bech-Hansen et al., 1998; Boycott et al., 2001; Striessnig et al., 2004; Strom et al., 1998; Wutz et al., 2002). Another forms of channelopathies related to malfunctioning of the $Ca_v1.4$ are CORDX3 (x-linked cone-rod dystrophy) which it is an X-linked rod-cone dystrophy type 3 (Jalkanen et al., 2006), and the Åland Iceland eye disease (AIED, Forsius-Eriksson syndrome) (Jalkanen et al., 2007; Vincent et al., 2011).

The symptoms of these diseases range from relatively mild forms of night blindness and decreased visual acuity to severe forms in which myopia, hyperopia, nystagmus, complete vision loss and dystrophy of the photoreceptors may additionally appear. In order to understand the molecular mechanism by which mutations in the $Ca_v1.4$ channel lead to disease two mice lines, which lack the full *CACNA1F* gene for the channel $Ca_v1.4$, have been generated (Mansergh et al., 2005; Specht et al., 2009). Both of the $Ca_v1.4$ KO mice show a CSNB-like phenotype.

The electrophysiological hallmark of these knockout animals is a 'Schubert and Bornschein' type electroretinogram, in which the amplitude of the scotopic b-wave is smaller than the normal a-wave size (Kabanarou et al., 2004). This finding suggests that the pathologic correlate of the disease is localized most likely at the photoreceptor-to-bipolar synapse which may lead to neurotransmission impairment (Mansergh et al., 2005; Specht et al., 2009). In addition, deletion of another component of the $Ca_v1.4$ channel complex, the auxiliary β_2a subunit, in the mouse leads also to CSNB2 like phenotype (Ball et al., 2002).

Since the $Ca_v1.4$ channelopathies are transmitted by X-chromosomal inheritance, the clinical symptoms have occasionally been also observed in heterozygous female carriers (Hemara-Wahanui et al., 2005; Hope et al., 2005; Jalkanen et al., 2007; Rigaudiere et al., 2003). Moreover, the clinical picture is not always restricted to the visual system, there is evidence of an association between mutations in the $Ca_v1.4$ gene locus and neurological disorders such as mental retardation, autism or epilepsy (Hemara-Wahanui et al., 2005; Hope et al., 2005).

A



B

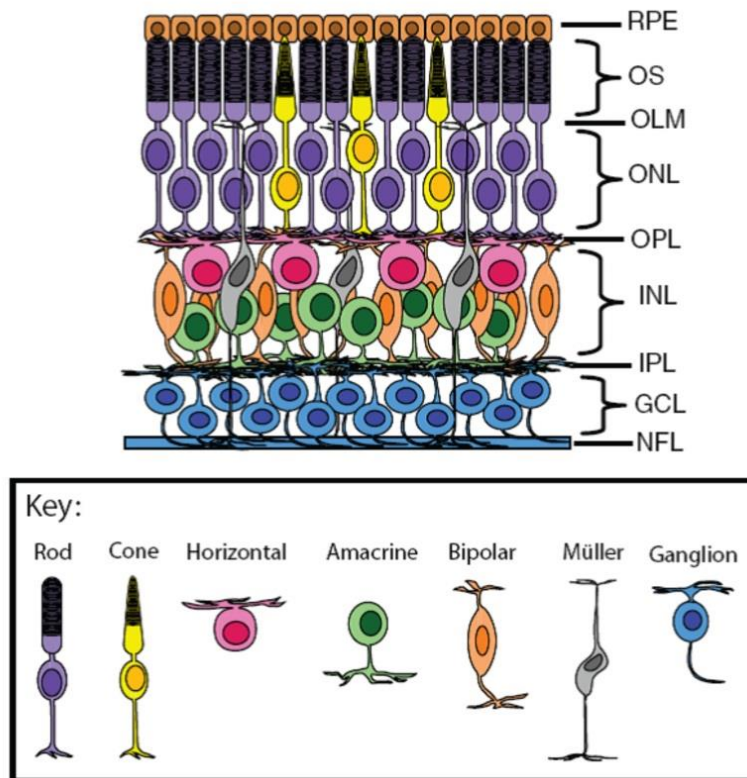


Figure 1.1 – Principal structure of the retinal network. **(A)** The retina is precisely organized into a discrete laminar structure at the back of the eye. **(B)** The retina layers are composed of different neurons and glial cell types, which are derived from a common progenitor cell population. The index of the retina layers: retinal pigment epithelium (RPE), outer segments (OS), outer limiting membrane (OLM), outer nuclear layer (ONL), outer plexiform layer (OPL), inner nuclear layer (INL), inner plexiform layer (IPL), ganglion cell layer (GCL) and nerve fiber layer (NFL). (Poche and Reese, 2009)

1.1 Voltage-gated calcium channel

The voltage gated calcium channels (VGCC, Ca_v) are protein complexes containing 4 to 5 subunits. The pore-forming subunit α_1 with about 190-270kDa is the largest component of the complex. The α_1 subunit is functionally the most important component of the channel and determines its biophysical and pharmacological properties (Catterall, 2000).

In mammals, there are ten different α_1 subunits (Fig. 1.2). The voltage-dependent calcium channels can be divided into high voltage-activated (high voltage activated, HVA) and low voltage-activated (low voltage activated, LVA) calcium channels, according depolarization required for activation (Hofmann et al., 1999; Striessnig, 1999; Yaari et al., 1987).

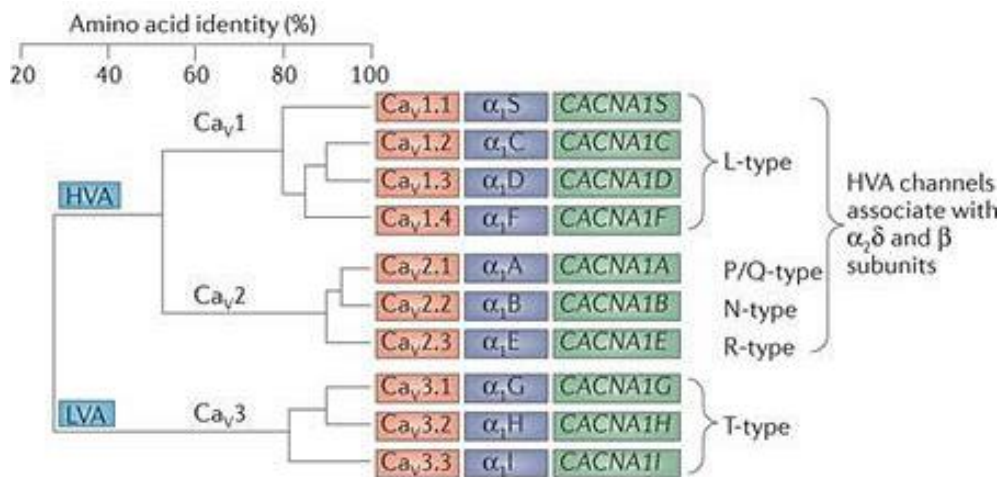


Figure 1.2 – Phylogenetic tree of the voltage-gated calcium channels according to its α_1 -Subunit. L-type channels: $Ca_v1.1$ - $Ca_v1.4$, P / Q-type channel: $Ca_v2.1$, N-type channels: $Ca_v2.2$, R-type channel: $Ca_v2.3$, T-type channels: $Ca_v3.1$ - $Ca_v3.3$. (Dolphin, 2012)

The LVA channels which are also called T-type channels ($Ca_v3.1$ - $Ca_v3.3$) are activated at quite hyperpolarized voltages. On the other hand, the HVA channels need a high depolarization of the membrane potential to open. They open at a membrane potential of $>-30mV$, for example $-30mV$ (for $Ca_v1.2$) and inactive slowly compared to the LVA.

Depending on their pharmacological properties the HVA calcium channels can be distinguished further into subtypes. The first type, the so-called L-type calcium channels (LTCCs) ($Ca_v1.1$ - $Ca_v1.4$), produces a long lasting ("L") current which is

INTRODUCTION

sensitive to organic LTCC blockers including dihydropyridine (DHP), phenylalkylamines and benzodiazepines (Catterall, 2000; van der Heyden et al., 2005).

The P/Q-type (Purkinje), N-type (Neither L- nor T-) and R-type (Remaining) channels ($Ca_v2.1$ - $Ca_v2.3$, respectively) belong to HVA calcium channels but they are only weakly affected by the L-type channel blockers. These channels typically can be blocked by specific polypeptide toxins from snail and spider venoms.

The LVA calcium channels, which lead to the tiny/transient current ("T"), require only weak depolarization for activation and rapidly inactivate. They have a lower conductivity than the HVA. Furthermore, the LVA calcium channels are resistant to subtype-specific channel blockers (Nowycky et al., 1985).

INTRODUCTION

Table 1A shows an overview of the classification of the various voltage-dependent calcium channels.

Nomenclature				primary tissues	antagonists	Citation
HVA	Ca _v 1.1	α _{1S}	L-Type	skeletal muscle	DHP PAA BTZ Mibefradil	(Tanabe et al., 1987)
	Ca _v 1.2	α _{1C}	L-Type	heart, smooth muscle, brain, pancreas		(Biel et al., 1990; Mikami et al., 1989; Moosmang et al., 2006)
	Ca _v 1.3	α _{1D}	L-Type	brain, pancreas kidney, heart, Ovary		(Seino et al., 1992)
	Ca _v 1.4	α _{1F}	L-Type	retina	L- and D-cis-diltiazem DHP	(Strom et al., 1998)
	Ca _v 2.1	α _{1A}	P/Q-Type	brain, cochlea, pituitary gland	ω-Agatoxin	(Mori et al., 1991; Starr et al., 1991)
	Ca _v 2.2	α _{1B}	N-Type	brain, peripheral nervous system	ω-Conotoxin	(Dubel et al., 1992; Williams et al., 1992)
	Ca _v 2.3	α _{1E}	R-Type	brain, cochlea, retina, pituitary gland	SNX-482	(Niidome et al., 1992)
LVA	Ca _v 3.1	α _{1G}	T-Type	brain, heart, peripheral nervous system	Mibefradil	(Perez-Reyes, 1998)
	Ca _v 3.2	α _{1H}	T-Type	heart, brain		(Cribbs et al., 1998)
	Ca _v 3.3	α _{1I}	T-Type	brain		(Lee et al., 1999)

Table 1A – Classification of the voltage-dependent calcium channels: The two main groups of HVA and LVA can be subdivided on the basis of electrophysiological and pharmacological properties into several subtypes. DHP (dihydropyridine), PAA (phenylalkylamine), BTZ (benzothiazepines). Detailed references on the VGCC's nomenclature (Birnbaumer et al., 1994; Ertel et al., 2000; Tsien et al., 1988)

The α₁ subunit contains the channel pore, the voltage sensor and the gating machinery. The α₁ subunit also contains the binding domain of dihydropyridine, benzodiazepines and phenylalkylamines, three classes of calcium channel antagonist (Striessnig, 1999). The α₁ subunit has four homologous domains, which are composed of six α-helix transmembrane segments. The fourth segment of each respective domain serves as a voltage sensor of the channel, the pore loop between the segments 5 and 6 acts as a selectivity filter, as was reported for K⁺ channel at 2.0Å resolution (Zhou et al., 2001) and later by crystal structure of the mammalian

INTRODUCTION

voltage-dependent K^+ channel family (Chen et al., 2010; Long et al., 2005) (Fig. 1.3). The structure determination for K^+ channel could be similar to Ca_v/Na_v channels, since these channels are also a complex of six α -helix transmembrane segments domains.

The carboxy-terminus (C-terminus) contains a variety of regulatory structural elements: (i) the IQ motif (consisting of the amino acids isoleucine and glutamine), for binding calmodulin which can change the open probability of the channel (Zuhlke et al., 2000); (ii) The EF-hand motif translates Ca^{2+} -CaM binding into channel inactivation and essential for calcium dependent inactivation (Peterson et al., 2000); (iii) AKAP150 binding site element enables the interaction between the protein kinase C and the calcium channel (Oliveria et al., 2007); and several phosphorylation sites (Hell et al., 1995). The distal part of the C-terminus was proposed to play an important role in the regulation of transcription of many genes (Dolmetsch et al., 2001).

The remaining subunits are considered to be accessory subunits so-called modulatory proteins which fine-tune the basic properties of the channel complex, as they influence the expression of the channel, also the kinetics and amplitude of the calcium influx (Bers, 2002; Gao et al., 1999). The β subunit plays specially an important role in the channel transport and trafficking to the cell membrane (Shistik et al., 1995). The β subunit (50-72kDa) interacts with the $\alpha 1$ pore subunit in a certain domain (AID), located in the intracellular loop between segments 1 and 2 (Pragnell et al., 1994).

The other accessory subunits are: The δ subunit, which is anchored to the cell membrane from the extracellular side, and the extracellular $\alpha 2$ subunit. Both subunits (together 125kDa) are linked by disulfide-bonds forming the $\alpha 2\delta$ subunit complex. In skeletal muscle, the voltage-gated calcium channels contain an additional γ subunit (25kDa), a transmembrane protein. (Fig. 1.3)

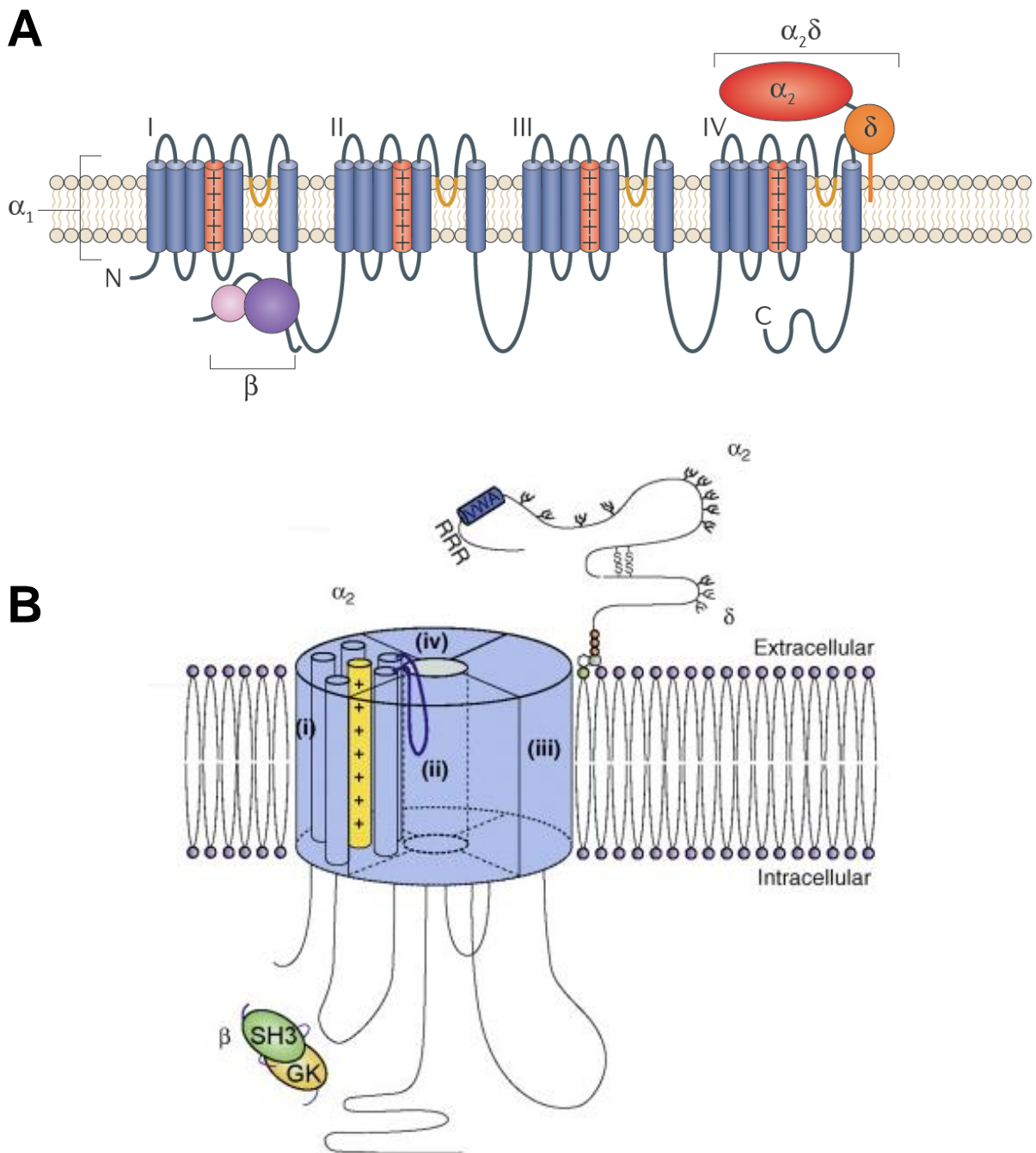


Figure 1.3 – The topology of calcium channel subunits. **(A)** The topology of calcium channel subunits in two dimensions. Voltage-gated calcium channel α_1 subunits have 24 transmembrane α -helices, organized into four homologous repeats (I–IV). The fourth transmembrane segment of each repeat (S4; shown in red) is the voltage-sensing domain of the channel. The yellow segments represent the pore loops. β subunit consists of a Src homology (SH3) domain (pink circle) and a guanylate kinase domain (purple circle), connected by a linker region. The β subunit binds to the intracellular linker between domains I and II of the α_1 subunit (AID). The $\alpha_2\delta$ subunit consists of α_2 (red), which is an extracellular subunit, disulphide-bonded to the δ subunit (orange), which anchors to the cell membrane (Dolphin, 2012). **(B)** Diagram of calcium channel heteromeric structure with all the LTCC subunits, showing potential organization in relation to the cell membrane (Bauer et al., 2010).

1.2 L-type calcium channel

L-type calcium channels (LTCCs) have been extensively studied. They can be found in a wide range of tissues while different isoforms are often expressed together in single cells or tissues.

Like all HVA, the LTCC are activated at a high membrane potential (more than -30mV), and reach their excitation maximum between 0 to +10 mV. The class of L-type calcium channels can be further subdivided into $Ca_v1.1$ to $Ca_v1.4$. The L-type calcium channels have different functions depending on the site of expression (Table 1B).

The $Ca_v1.1$ is critically involved in the electromechanical coupling in skeletal muscle (Rios et al., 1992; Tuluc et al., 2009). The $Ca_v1.2$ is responsible for the maintenance of vascular tone in vascular smooth muscle cells (Moosmang et al., 2003). In the heart, the $Ca_v1.2$ and $Ca_v1.3$ L-type calcium channels play a role both in the formation of electrical pulses as well as the contraction of the heart muscle (Bohn et al., 2000; Zhang et al., 2005). $Ca_v1.2$ can be also detected in the pancreas (Schulla et al., 2003), adrenal glands (Marcantoni et al., 2007) and the brain (Hell et al., 1993). $Ca_v1.3$ is expressed especially in the brain, though in a lesser amount than the $Ca_v1.2$ channel (Hell et al., 1993). Additionally, $Ca_v1.3$ could be identified in ovaries, kidneys, pancreas (Yang and Berggren, 2006), cochlea (Kollmar et al., 1997) and in cardiac tissue (Wyatt et al., 1997), including the sinoatrial node (Bohn et al., 2000; Platzer et al., 2000; Zhang et al., 2011). $Ca_v1.4$ has been discovered mainly in the retina (Baumann et al., 2004; Bech-Hansen et al., 1998; Strom et al., 1998), but at the moment the properties of $Ca_v1.4$ are not yet fully well known.

The LTCC members can be identified by taking in consideration several hallmark parameters: sensitivity to dihydropyridines, activation kinetics including facilitation, channel conductance and the presence of calcium dependent inactivation (CDI) and/or voltage dependent inactivation (VDI).

INTRODUCTION

Name	Primary tissues	Physiological function	Mutations and pathophysiology
Ca_v1.1	skeletal muscle	excitation-contraction coupling, Ca ²⁺ homeostasis	Malignant hyperthermia
Ca_v1.2	heart	prolongation of action potential duration and increased calcium transients	Timothy syndrome Brugada syndrome
	smooth muscle		Ca _v 1.2 deficient mice show multiple phenotypes
	brain		
Ca_v1.3	brain, pancreas kidney, heart, Ovary	hormone release, regulation of transcription, synaptic integration	Congenital cardiac (sinoatrial node arrhythmia) and auditory (deafness) phenotype
Ca_v1.4	mainly retina	neurotransmitter release	CSNB2 CORDX3 ÅIED

Table 1B – Overview on the tissue distribution and physiology / pathophysiology of L-type calcium channels (Bech-Hansen et al., 1998; Catterall et al., 2005; Doering et al., 2007; Firth et al., 2001; Jalkanen et al., 2007; Jalkanen et al., 2006; Liao et al., 2005; Mansergh et al., 2005; Platzer et al., 2000; Schulla et al., 2003; Seisenberger et al., 2000; Splawski et al., 2005; Splawski et al., 2004; Stockner and Koschak, 2013; Striessnig et al., 2010; Striessnig et al., 2004; Zhang et al., 2005)

1.2.1 Regulation by voltage and Ca²⁺ ions

The flux of ions through the calcium channel into the cell is influenced by inactivation of the channel. In LTCC inactivation is primarily voltage dependent (voltage dependent inactivation, VDI). In addition, VGCC are characterized by another type of inactivation called calcium dependent inactivation (CDI). CDI is a negative feedback by which Ca²⁺ ions are able to limit their own influx (Christel and Lee, 2012). In most cell types, this auto-inhibition property is essential to prevent exaggerated Ca²⁺ levels, which may lead to toxicity.

INTRODUCTION

At present, the inactivation mechanism is not fully understood. Most of the recent knowledge is mainly based on the experiments and recordings on Ca_v1.2 or Ca_v1.3 subtype (Tadross et al., 2010). These channels have a strong VDI and CDI which are tied together on a molecular level.

On structural level, the cytoplasmic linker between domain I and II seems to play an important role in the inactivation. This linker is supposed to form a blocking particle (Fig. 1.4, red linker) that closes the pore and causes the inactivation of channel (Cens et al., 1999; Stotz et al., 2000; Tadross et al., 2010). Another crucial structural determinant for inactivation is the cytosolic proximal carboxy tail of the L-type calcium channel which contains several motifs: an EF-hand motif, an IQ motif and the Pre-IQ motif, which corresponds to the sequence stretch between the EF-hand and the IQ motif. This proximal C-terminus is highly conserved among all HVA calcium channels.

The IQ motif is localized 148 amino acids downstream of the last transmembrane segment IV S6 (Zuhlke et al., 1999) and consists of 12 conserved amino acids. To this region binds Calmodulin (CaM), a 17kDa protein, which belongs to the family of EF-hand proteins and serves in eukaryotic cells as a calcium sensor, which by calcium-binding changes its conformation (Halling et al., 2006; Halling et al., 2009; Liang et al., 2003; Pate et al., 2000; Peterson et al., 1999; Pitt et al., 2001; Romanin et al., 2000; Zhou et al., 1997; Zuhlke et al., 1999; Zuhlke and Reuter, 1998). Binding of CaM to the IQ motif has an important function for auto-regulation of LTCC (Zuhlke et al., 2000) and may play a role in regulation of signal transduction pathways in the cell nucleus to enable the transcription of genes (Dolmetsch et al., 2001).

During the rest state, in the absence of Ca²⁺ ions, Ca²⁺-free calmodulin (apocalmodulin) is pre-bound to the A-region (Fig. 1.4) between the EF-hand motif, and the IQ-domain of the carboxy tail of the L-type calcium channel. The channel is closed and there is no calcium influx. Apocalmodulin (ApoCaM) is a calcium sensor containing four EF-hands; two in the N-lobe with low affinity for binding Ca²⁺ ions and two in the C-lobe with high affinity (Chin and Means, 2000).

Upon depolarization (= active state) the channel opens and calcium flows into the cell, and the Ca²⁺ concentration at the intracellular side increases (Liang et al., 2003).

INTRODUCTION

During sustained depolarization, calcium binds with high affinity to CaM. Upon calcium binding, CaM changes its conformation and interacts with the IQ motif. As a consequence, the channel goes to the inactive state and closes (Zuhlke and Reuter, 1998).

Point mutation studies indicate that the isoleucine, in the IQ motif, is required for interaction with CaM. Moreover, the EF-hand motif, which is located between domain IV and the IQ motif, was also reported to be important for the inactivation (de Leon et al., 1995; Zuhlke and Reuter, 1998).

The facilitation is a positive feedback mechanism. This mechanism is characterized by increase in calcium influx through L-type calcium channels after increase the basal calcium concentration (Gurney et al., 1989) or after consecutive pulses (Noble and Shimoni, 1981a, b). The voltage-dependent facilitation is based on a calmodulin kinase II-dependent phosphorylation at positions S1512 and S1570 (Blaich et al., 2010).

The two forms of self-regulation, facilitation and inactivation exist in parallel. In both mechanisms plays calmodulin, which is bound to the IQ motif, an important role (DeMaria et al., 2001; Peterson et al., 1999; Zuhlke et al., 1999; Zuhlke et al., 2000). Due to calcium binding to its C-lobe, CaM interacts with the IQ motif on the channel which leads to facilitation, on the other hand calcium binding to the N-lobe of CaM causes inactivation of the channel (Budde et al., 2002). Facilitation and inactivation have different kinetics and a different start point after depolarization. The facilitation is caused by a fast response of CaM's c-lobe to increase concentration of calcium, while the n-lobe responds slowly to concentration changes of calcium and initiates the channel inactivation. In addition, when both mechanisms are switched on simultaneously, the inactivation of the channel is becoming dominant over the facilitation (Zuhlke et al., 2000) which can not been seen. By point mutation and replacing the isoleucine to alanine in the IQ motif the CDI disappears whereas the facilitation remains unaffected (Zuhlke et al., 1999; Zuhlke et al., 2000).

INTRODUCTION

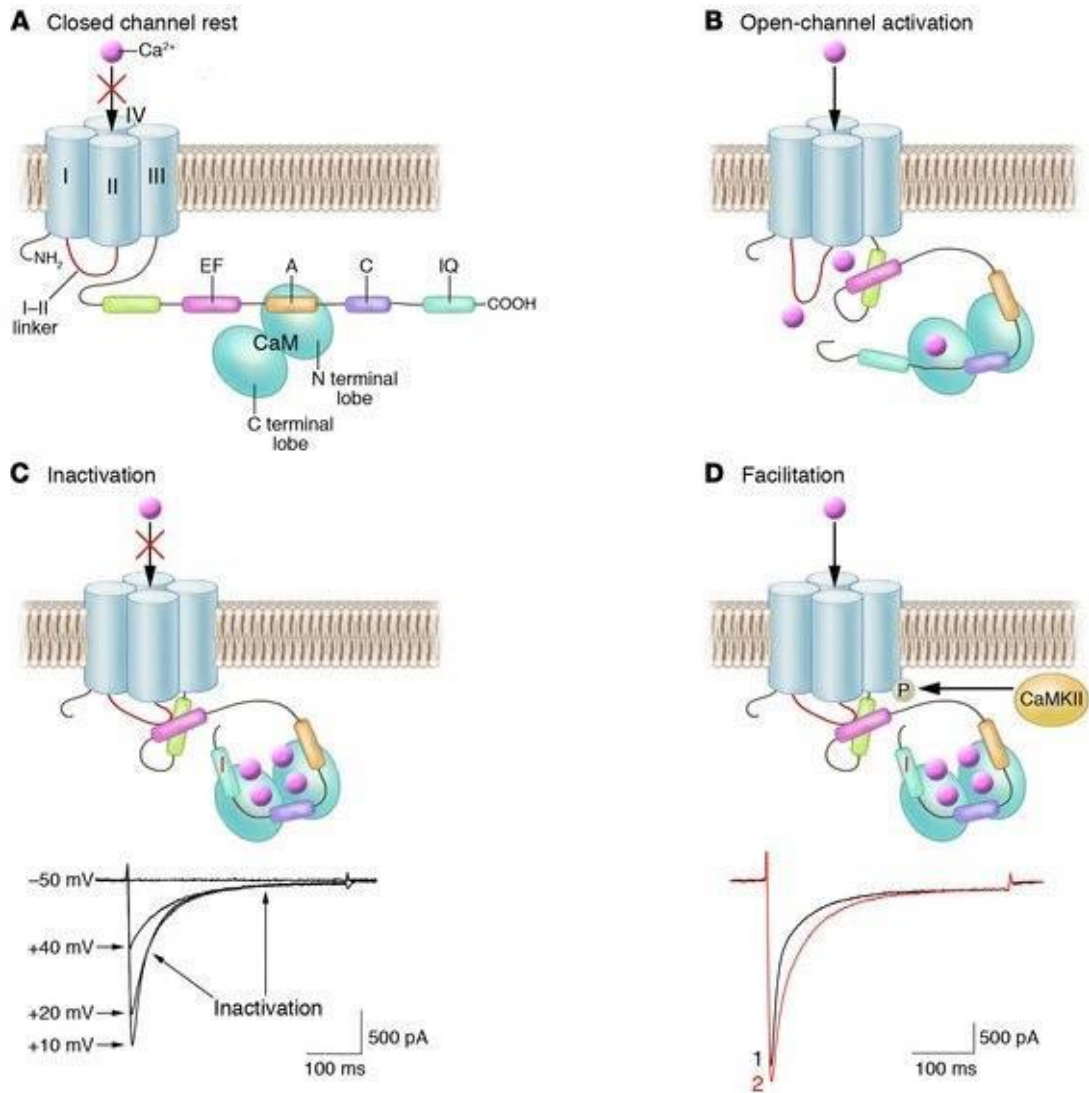


Figure 1.4 – Model for CDI and VDI in LTCC. **(A)** In the ideal state, the channel is closed and there is no Ca²⁺ influx. The CaM binds to peptide A, located between the EF hand and the IQ motif of the C terminus of the LTCC. **(B)** In response to a depolarizing stimulus, Ca²⁺ flows through the LTCC into the intracellular space and binds to CaM. In the open Ca²⁺ channel state, the EF hand prevents structural conformation of the I–II loop required to block Ca²⁺ entry through the channel pore. **(C)** Upon elevation of [Ca²⁺]_i (depolarization), the Ca²⁺/CaM complex undergoes the Ca²⁺-dependent conformational change that relieves the inhibition of EF hand, permitting the I–II loop to interact with the pore and accelerate the fast inactivation process. The graph shows representative I_{Ca} traces evoked by depolarization from –50mV to +40mV, as labeled, using –60mV as holding potential. **(D)** Involvement of CaM and CaMKII in the facilitation process. CaMKII enhances the I_{Ca} through phosphorylation of LTCC. We show murine whole-cell I_{Ca} generated from paired depolarizing pulses (–60mV ± 10mV at 0.5Hz) representing Ca²⁺-dependent facilitation (graph). (Bodi et al., 2005)

1.3 The L-type Calcium Channel $Ca_v1.4$

The $Ca_v1.4$ channels play a key role in synaptic transmission by providing a long-lasting presynaptic Ca^{2+} influx into the cell which is the trigger for glutamate release.

$Ca_v1.4$ channels are tailored for their function due to two facts: First, they have relatively low activation threshold and the very rapid activation kinetics. Second and the most striking feature of $Ca_v1.4$ is slow inactivation of the channel.

The $Ca_v1.4$ differs in important biophysical properties from other HVA channels. $Ca_v1.4$ channels are lacking Ca^{2+} -dependent inactivation (CDI) and have very slow voltage-dependent inactivation (VDI) (Baumann et al., 2004; Griessmeier et al., 2009; Koschak et al., 2003; McRory et al., 2004; Singh et al., 2006; Wahl-Schott et al., 2006). These properties increase dramatically the current window of the $Ca_v1.4$ compared to other HVA channels, a fact that ensures in the dark to a permanent glutamate release at depolarized voltages. (Fig. 1.5)

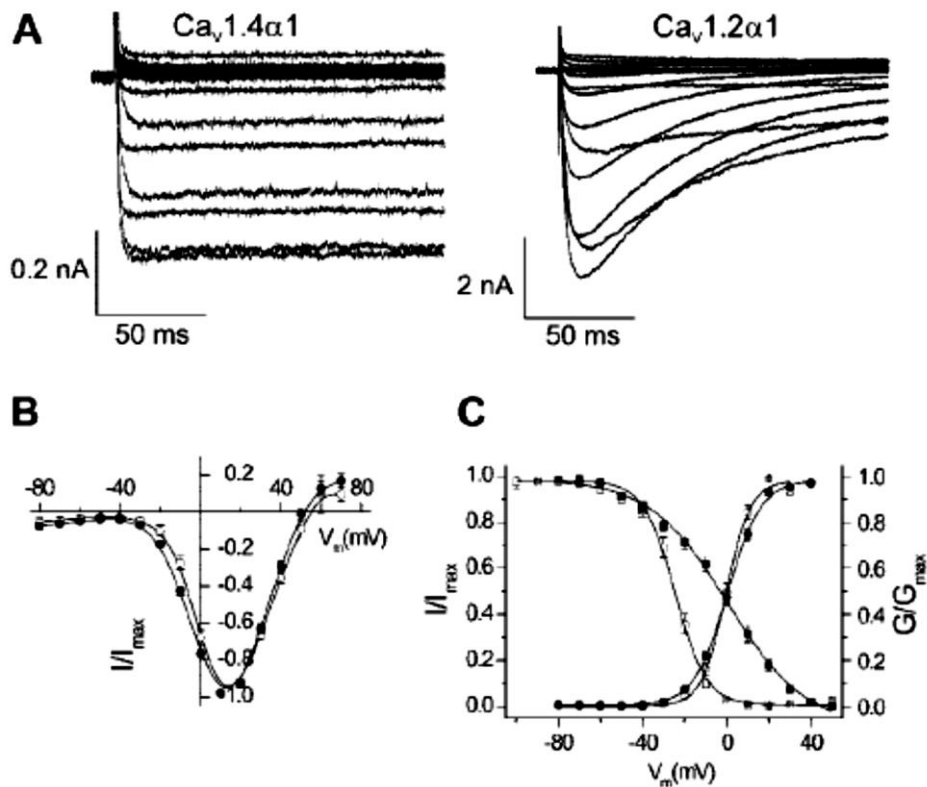


Figure 1.5 – The electrophysiological properties of the $Ca_v1.4$ compare to the $Ca_v1.2$. **(A)** Whole cell recording from cells expressing either $Ca_v1.4$ (left) or $Ca_v1.2$ (right). **(B)** I/V relationship for $Ca_v1.4$ channels (solid cycle) and $Ca_v1.2$ (open cycle). **(C)** Conductance-voltage relationships for $Ca_v1.4$ channels (solid cycle) and $Ca_v1.2$ (open cycle). (Baumann et al., 2004)

It was recently discovered that the $Ca_v1.4$ contains an inhibitory domain (ICDI: inhibitor of CDI) located at the distal C-terminus and is approximately 100 amino acids long (Baumann et al., 2004; Singh et al., 2006; Wahl-Schott et al., 2006). This domain binds to upstream C-terminal regulatory domains and switches off the CDI of the channel. (Detailed sequence of the murine $Ca_v1.4\alpha1$ cDNA can be found at appendix 8.1).

Two experiments support the key role of the ICDI in the $Ca_v1.4$ regulation as auto-inhibitory unit on the channel. First, deletion of the ICDI domain from the wild type $Ca_v1.4$ channel restores the property of Ca^{2+} /CaM-induced CDI, like we see in the other HVA channels. Second, co-expression of truncated channel lacking the ICDI ($Ca_v1.4\Delta$ ICDI) together with the ICDI domain abolishes the CDI.

1.4 Calcium binding proteins (CaBPs)

Many voltage-sensitive or ligand-gated ion channels, which regulate the pre- and post-synaptic calcium influx, are regulated by families of small calcium sensing proteins. These proteins exhibit characteristic calcium binding properties together with specific patterns of cellular expression and subcellular distribution, and by that permit fine tuning of the calcium signaling mainly in the mammalian CNS (Burgoyne and Weiss, 2001; Haynes et al., 2012)

The Calcium Binding Proteins (CaBPs) represent one such family, which belongs to the largest class of calcium sensing proteins in mammals. The CaBPs are part of the calmodulin (CaM) superfamily (Fig. 1.6).

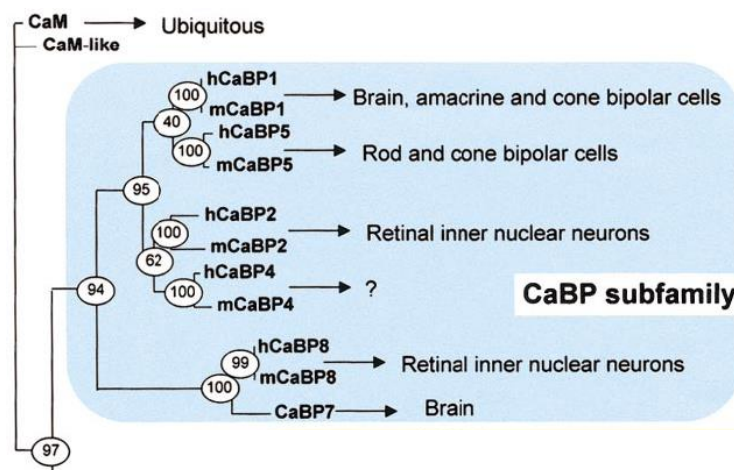


Figure 1.6 – A phylogenetic tree of CaBPs sequences. (Haeseleer et al., 2002)

INTRODUCTION

The CaBPs share a similar molecular architecture as CaM. They are defined as CaM-related calcium sensors with four EF-hand motifs. However, The CaBPs contain significant sequence divergence from their common ancestor – CaM, which may give rise to unique structural and functional properties (Haeseleer et al., 2000; Mikhaylova et al., 2011).

The CaBP family, in humans, comprises six proteins: CaBP1, 2, 4, 5, 7 and 8. The CaBP3 that was originally identified is most likely a pseudogene, while no CaBP6 gene exists. It should be mentioned that CaBP7 and CaBP8 are also known under the alternative names Calneuron-II and Calneuron-I, respectively.

All CaBPs members share a core domain comprised of four EF-hand motifs, like CaM, although some of the EF-hands may not necessarily be functional (Haeseleer and Palczewski, 2002). The EF-hand motif represents a conserved sequence of 30–35 amino acids with greatest similarity to CaM. The EF motif is the residue which can bind Ca^{2+} ions, and each EF-hand has its own distinct Ca^{2+} binding affinity (Gariepy and Hodges, 1983; Yap et al., 1999). The CaBPs members differ also in unique regions located at the N-or C-terminus (McCue et al., 2010). (Fig. 1.7)

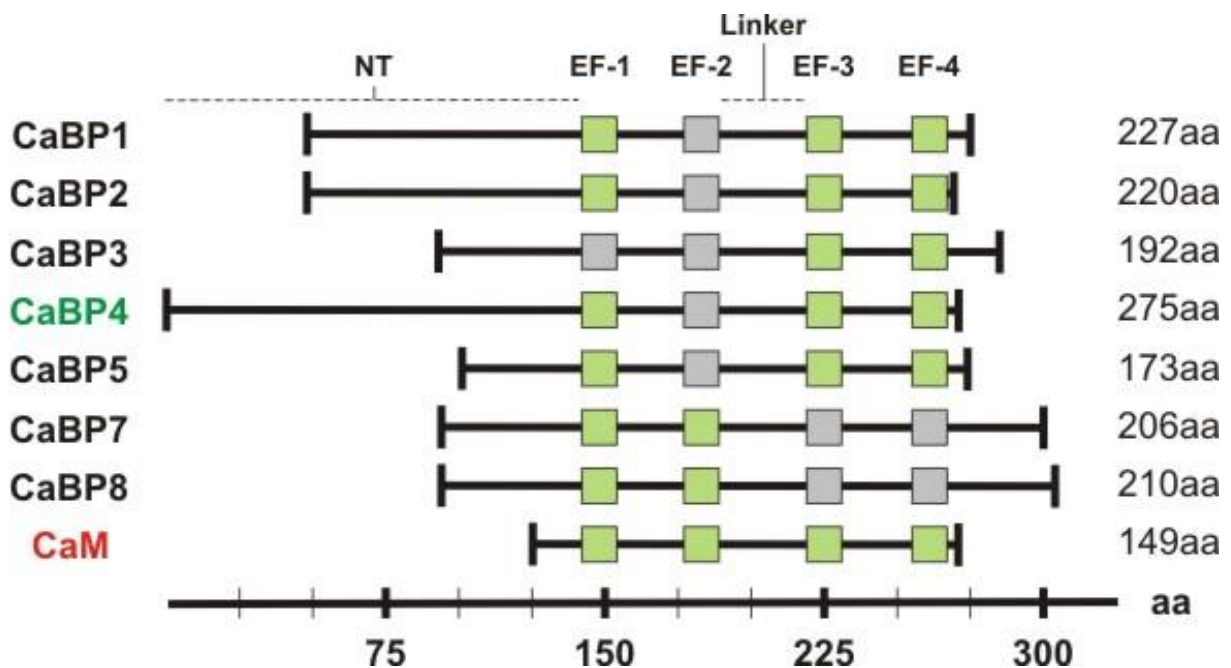


Figure 1.7 – Schematics of the EF motifs organization in a human CaM, CaBP1-5 and CaBP7-8. EF-hand motifs (numbered above) are shown as a functional (green square) and nonfunctional (gray square). The scale in amino acids (aa). (Detailed multiple sequence alignment of the CaBPs can be found at appendix 8.2)

INTRODUCTION

Unlike CaM, which is ubiquitously expressed in all plants and animals and has essential functions in many aspects of normal cellular physiology, the CaBPs are enriched in neuronal tissues where they have been shown to act as important regulators of key calcium influx channels.

Calcium binding proteins have an important role in regulation of the Ca²⁺ influx via the VGCCs in Ca²⁺-dependent feedback mechanisms and mediate Ca²⁺-dependent signal transduction pathways (Cui et al., 2007; Dick et al., 2008; Few et al., 2011; Lee et al., 2002; Liang et al., 2003; Pitt et al., 2001; Zuhlke et al., 2000).

Many EF-hand Ca²⁺-binding proteins achieve their effects by direct regulation of VGCC properties (Dick et al., 2008; Liang et al., 2003; Pitt et al., 2001; Zuhlke et al., 2000). However, it seems that the CaBPs and CaM have the capacity to differentially regulate the VGCC. This suggests that dysfunctions in Ca²⁺-binding protein mediated VGCC regulation may lead to some common human diseases.

In contrast to CaM, CaBPs regulate L-type channels in a Ca²⁺-independent manner (Haeseleer et al., 2004; Lee et al., 2002; Zhou et al., 2004; Zhou et al., 2005).

For example, CaBP1 and CaBP4 compete with CaM for binding to the IQ motif in the LTCC α 1 C-terminal subunit and act as regulators of these channels (Cui et al., 2007; Zhou et al., 2004; Zhou et al., 2005).

CaBP1 is located at the presynaptic ribbon synapse of adult inner hair cells, and is suggested to mediate an inhibitory effect on Ca²⁺-dependent inactivation of Ca_v1.3 in auditory transmission (Cui et al., 2007). Unlike CaBP4, CaBP1 interacts also with the N-terminal domain of Ca_v1.2 to prolong channel activation, independently of the CaM effect (Oz et al., 2011). CaBP2 is also physiologically relevant in the auditory system. It is identified that mutations in CaBP2 cause moderate-to-severe hearing loss (Schrauwen et al., 2012).

CaBP5 (Rieke et al., 2008) are localized at the photoreceptor synaptic terminals in the retina, and are important for developing and sustaining synaptic transmission to bipolar cells.

Both CaBP7 and CaBP8 were found to influence the phosphatidylinositol 4-phosphate (PI4P) levels and trafficking of specific secretory cargo to the plasma membrane by interaction with and inhibition of the activity of PI4K β (PI4P kinase) in mammalian cells (Mikhaylova et al., 2009). Moreover, CaBP8 was reported to inhibit Ca²⁺ currents generated through N-, L- and P/Q- type calcium channels, but not by

direct interaction with the channel rather by restricting trafficking of the channel to the plasma membrane (Shih et al., 2009).

1.4.1 CaBP4

CaBP4 is a neuronal Ca^{2+} sensor protein with structural homology to CaM. Like CaM, CaBP4 contains two globular domains, the N- and the C-lobe, each containing a pair of EF-hand motifs connected by a central helix (Haeseleer et al., 2002; Haeseleer et al., 2000) (Fig. 1.8). It has been shown that CaBP4 is part of the $\text{Ca}_v1.4$ channel complex in the retina (Haeseleer et al., 2004).

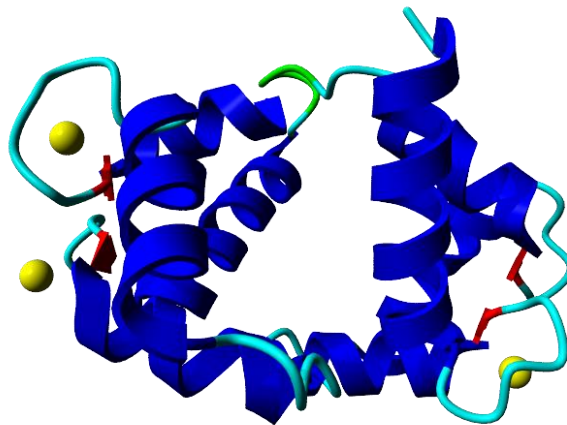


Figure 1.8 – Model based on a secondary structure function of the CaBP4 domains: blue=helix, red=strand, green=turn, cyan=loop. The calcium atoms are shown as yellow balls. http://www.cmbi.ru.nl/~hvensela/CABP4/CABP4_2.html

CaBP4 regulates the $\text{Ca}_v1.4$ channels in the retina (Haeseleer et al., 2004) and the $\text{Ca}_v1.3$ channels in the auditory system (Cui et al., 2007). CaBP4 shifts the activation of $\text{Ca}_v1.4$ to more hyperpolarized potentials through direct interaction with the C-terminal domain of the $\text{Ca}_v1.4$ channel protein.

Phosphorylation of S37 on CaBP4 in the retina is critical for tuning presynaptic Ca^{2+} signals required for light induced neurotransmitter release (Lee et al., 2007).

CaBP4 was linked to several human diseases, since mutations in the gene lead to rod and cone dysfunction and visual impairments (Aldahmesh et al., 2010; Littink et al., 2009; Zeitz et al., 2006). In line with these findings, deletion of CaBP4 in the mouse leads to dysfunction of $\text{Ca}_v1.4$ channels and a CSNB2 like phenotype (Haeseleer et al., 2004). Sequence alignments of the CaBP4 protein variants, which have been investigated in this work, can be found in appendix 8.3.

2. Objective of the study

Despite extensive research in this field, there is still an uncertainty as to why the CaBP4 is an important regulator of Ca_v1.4 channels and how does CaBP4 bind and regulate the channel despite the fact that CaM is also expressed in the cells?

The following objectives have been addressed in this study:

1. The first aim of this study was to examine in detail the mechanism by which CaBP4 regulates the Ca_v1.4 channel. To clarify this question, HEK293 cells which stably express Ca_v1.4 α 1, Ca_v1.4 α 1 Δ ICDI or the Ca_v1.4/5A L-type calcium channel subunit were generated and transiently transfected with the additional subunits β 2a and α 2 δ . Afterwards, the basic biophysical properties, like voltage dependent activation and inactivation as well as CDI, were determined in electrophysiological experiments using whole cell measurements. Additionally, two mutations in CaBP4, which are associated with human retinal disease, were also analyzed in order to give an explanation as to why patients carrying these mutations suffer from a congenital variant of human night blindness (CSNB2).
2. The second objective was to characterize the Ca_v1.4 deficient mouse phenotype in vivo; in particular the Ca_v1.4 channelopathies in aged heterozygote Ca_v1.4 female mice. For this propose, genetically modified mice that are either homozygous or heterozygous for the CACNA1F deletion were analyzed. In order to characterize the effect on retinal function, changes in the morphology and retinal architecture of these mice were correlated with functional alterations as assessed by electroretinography (ERG) and behavioral tests.

3. Materials and Methods

All Buffer and solutions were generated using desalted high purity water and high purity standard chemicals (for molecular biology purposes). Additionally, some of the solutions were autoclaved for long term use.

3.1 Chemicals, Solutions and Equipment

Detailed information on the materials and equipment, which have been used during this research study, can be found in the appendix No. 8.5.

3.2 Molecular biology methods

3.2.1 Plasmids

Plasmids are circular, double-stranded DNA molecules which are used in molecular biology methods to amplify or express DNA in autonomously replicable manner in bacteria. Plasmids work as DNA vectors and contain some essential components like: an origin of replication, an antibiotic resistance sequence for selection and a multiple cloning site (MCS), with variety recognition sites of different restriction enzymes.

pcDNA3 (5.4 kb, Invitrogen)

The pcDNA3 vector was used to heterologously express the L-type calcium channel Ca_v1.4 and Ca_v1.2 subunits for electrophysiology, as well as different fragments for FRET measurements. Because of its cytomegalovirus promoter (CMV promoter) the vector ensures strong constitutive expression in eukaryotic cells. The vector carries an ampicillin resistance gene for positive selection of bacteria after transformation with the vector.

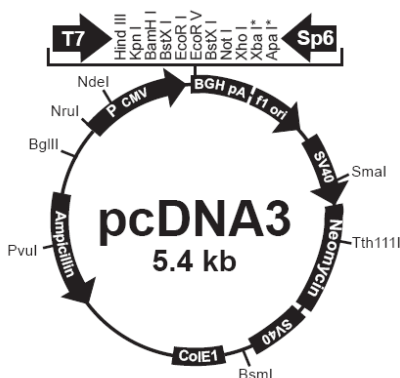


Figure 3.1 – The plasmid map of pcDNA3 (Invitrogen)

pcDNA5 (5.1 kb, Invitrogen)

This plasmid vector was used to generate the stable HEK cell lines based on the Flp-In™ System (Invitrogen), and according to manufacturer's protocol.

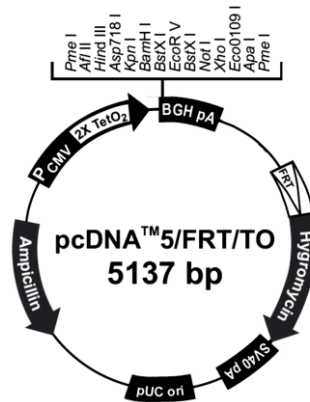


Figure 3.2 – The plasmid map of pcDNA5 (Invitrogen)

pIRES2-EGFP (5.3 kb, Clontech)

The pIRES2-EGFP vector has an internal Ribosome Entry Site (IRES) sequence in addition to its CMV promoter. This sequence is located between the MCS and a coding sequence for EGFP (enhanced green fluorescent protein) and enables simultaneous expression of the inserted gene and the green fluorescent protein. Using this vector makes it possible to identify the transfection efficiency. Vector pIRES2-EGFP was utilized to express all CaBP4 and CaM variants for the patch-clamp measurements. The vector has a kanamycin resistance gene for positive selection of bacteria after transformation with the vector.

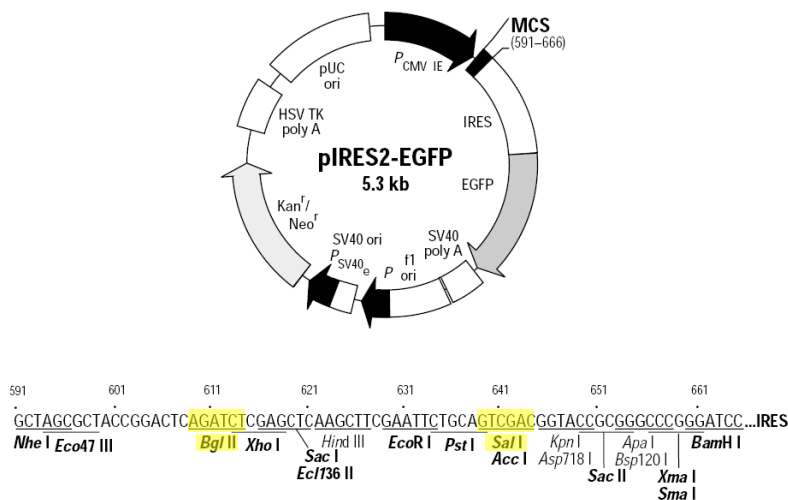


Figure 3.3 – The plasmid map of pIRES2-EGFP (Clontech). The marked restriction sites (*Bgl*II and *Sal*I) were used for cloning.

pEGFP-N3 (4.7 kb, Clontech)

This vector also carries the EGFP gene (red-shifted variant of wild-type GFP). This vector was used in experiments that did not include the use of pIRES2-EGFP, as an empty vector which expresses the EGFP only and serves as a control for positive transfected cells. The vector has a kanamycin resistance as the pIRES2-EGFP vector.

3.2.2 Generated constructs

3.2.2.1 Constructs for electrophysiology

3.2.2.1.1 *Ca_v1.4 subunits constructs*

For stable expression of the wild type murine Ca_v1.4 LTCC α subunit channel (Baumann et al., 2004) (accession number: AJ579852) or other variants of the subunit, namely Ca_v1.4 Δ ICDI and Ca_v1.4/5A (Griessmeier et al., 2009), HEK293 cell lines were generated using the Flp-In™ System (Invitrogen) according to the manufacturer's protocol.

To clone the cDNA of the subunits, the restriction enzymes BamH-I and Xho-I were used in two cloning steps.

The two other subunits of the Ca_v1.4 LTCC, β 2a (accession number: X64297) and α 2 δ 1 (accession number: M21948) were cloned into the pcDNA3 expression vector (Invitrogen) and transiently transfected into the HEK stable lines cells to express the functional calcium channel.

3.2.2.1.2 *CaBP4 constructs*

Wild type CaBP4 (accession no. NM144532: CaBP4 of mus musculus, corresponds to NM145200: CaBP4 of homo sapiens) was cloned into pIRES2-EGFP (Clontech) expression vector, by using the restriction sites: Bgl-II and Sal-I. Consequently, both the CaBP4 and the EGFP are expressed as separate proteins. Transfected cells were easily identified by checking for green fluorescence before patch clamp.

In addition to murine wild type CaBP4, two mutant variants of CaBP4 which are associated with autosomal recessive forms of human congenital retinal disease CSNB2 were cloned. In CaBP4-R216X, a single nucleotide exchange (C646T) replaces an arginine residue at position 216 by a premature stop codon (Littink et al., 2009). This mutation leads to a truncated CaBP4 protein lacking the C-lobe containing EF hand 3 and 4.

MATERIALS AND METHODS

In the second mutation (CaBP4-E267fs) a deletion of two nucleotides causes a frame shift at the last residue of EF hand 4 which elongates the protein by 91 novel amino acid residues (Zeitz et al., 2006). The mutations were introduced into the mouse CaBP4 sequence to keep in line with the findings in genetic mouse models. The human protein sequence of CaBP4-R216X and CaBP4-E267fs corresponds to murine CaBP4-R212X and CaBP4-E263fs, respectively.

3.2.3 Culture and transformation of bacteria

3.2.3.1 Bacteria strains

Different strains of *Escherichia coli* (*E. coli*) were used as host organisms for cloning steps and transformation experiments. The stains with their properties and their origins are shown in Table 2.1.

Strain	Description	Source
<i>Escherichia coli</i> XL1-Blue MRF	Δ (mcrA)183 Δ (mcrCB-hsdSMR-mrr)173endA1supE44 thi-1 recA1 gyrA96 relA lac [F'proAB lacq Z Δ M15 Tn10 (TetR)]	Stratagene
<i>Escherichia coli</i> XL10-Gold[®]	TetR Δ (mcrA)183 Δ (mcrCB-hsdSMR-mrr)173 endA1 supE44 thi-1 recA1 gyrA96 relA1 lac Hte [F'proAB lacq Z Δ M15 Tn10 (TetR)Amy CamR]a	Stratagene

Table 2.1 – The *E. coli* bacteria strains

3.2.3.2 Culture media and antibiotics

Competent *E. coli* bacteria were cultivated in an autoclaved Luria-Bertani (LB) medium with glucose (LB+ medium).

In case of cultivation on petri dishes, solid medium was used. The medium was produced by adding an additional 15g per liter of agarose to liquid LB+ medium.

Bacteria selection medium for selection after transformation were made by addition of the appropriate antibiotic at a final concentration of 100 μ g/mL to an autoclaved LB+ medium.

In agar plates, the appropriate antibiotic was added to the final concentration of 50 μ g/mL after the LB+ and the agar solution was autoclaved and cooled down to 50°C. The medium was then poured into sterile Petri dishes with a diameter of 92mm (Sarstedt). The cooled plates were stored at 4°C

MATERIALS AND METHODS

Both of the manufactured antibiotic stock solutions (Ampicillin 50µg/mL, Roth; Kanamycin 30µg/mL, Roth) were stored at -20°C.

LB medium + Glucose	
Agar (Roth)	15 g
LB+ medium	5 g

LB medium + Glucose	
Peptone (Roth)	10 g
Yeast extract (Roth)	5 g
NaCl (Roth)	5 g
Glucose (Roth)	1 g
H ₂ O	ad 1000 mL
pH 7.2-7.5	

3.2.3.3 Bacteria culture

The cultivation of *E. coli* bacteria was carried out in LB medium under aerobic condition. For small scale plasmid DNA isolation (2.2.4.1), the bacteria were grown in 5mL liquid LB+ medium in plastic 15mL tubes, or in case of large scale isolation (2.2.4.2) in Erlenmeyer flasks with 100mL LB+ medium. The cultivations were incubated at 37°C and 225rpm overnight. The cultures always contained the appropriate antibiotic (Ampicillin or Kanamycin) at a concentration of 50mg/mL, for a positive selection.

In a transformation procedure, the individual colonies were incubated overnight on agar plates, and afterwards were stored at 4°C under selection pressure.

3.2.3.4 Creation of competent bacterial cells stocks

Chemically competent bacterial cells were allowed to grow until they reached optical density (OD₆₀₀) values of 0.3; afterwards they were immediately centrifuged off. The bacterial pellet was then resuspended in TSS solution and stored in 400µL aliquots at -80°C.

TSS (Transformation-Storage-Solution)	
PEG 3350 40%	50 mL
MgCl ₂ 1M	10 mL
DMSO	10 mL
LB+ medium	ad 200 mL

3.2.3.5 DNA Transformation into E. coli cells

Transformation is defined as the introduction of foreign DNA into bacterial cells.

In this work, different plasmids were transfected into chemically competent cells (Table 2.1), using the heat shock method.

The cells were cultured with antibiotic medium in respect to the plasmids selection cassette to obtain a stable transformation of the plasmid in the competent cells.

DNA transfer into E. coli by heat shock

The ligation mixture (5-10 μ L) was added and gently mixed into 100 μ L chemically competent cells which had been thawed on ice. The cells were then incubated for 30min on ice, followed by heat shock for 45sec in a 42°C water bath. By this heat shock, the recombinant DNA was introduced into the cells.

Right after the heat shock step, the cells were returned to additional 2min incubation on ice for recovery. Thereafter, the competent cells were incubated in 900 μ L of SOC(+) medium for one hour at 37°C and 225rpm.

Finally, the cells were seeded on two agar plates: one in low concentration (150 μ L directly from the cell mixture) and the second in high concentration (150 μ L after centrifugation step for 5min at 3500rpm). The two plates were incubated overnight at 37°C.

SOC(+) medium	
Peptone (Roth)	20 g
Yeast extract (Roth)	5 g
NaCl (Roth)	10 mM
KCl (Roth)	2.5 mM
MgCl ₂	10 mM
MgSO ₄	20 mM
Glucose (Roth)	20 mM
H ₂ O	ad 1000 mL
pH 7.2-7.5	

3.2.4 Isolation of plasmid DNA

Isolation of plasmid DNA from E. coli cells was performed by NaOH/SDS lysis, as described in (Birnboim and Doly, 1979). For the small analytical scale, a mini-preparation was performed; on the other hand, maxi-preparation was made for the larger preparative approach.

MATERIALS AND METHODS

3.2.4.1 Mini-preparation (Miniprep)

Miniprep DNA isolation was performed after transformation of plasmids into bacterial cells to check which colony contains the correct plasmid. One by one, colonies were picked from the agar plate after the transformation and cultured in 7mL of LB medium containing 14 μ L antibiotic (Ampicillin or Kanamycin) in a concentration of 50 μ g/mL. The Falcon tube was incubated at 37°C and 225rpm overnight. The next morning, the culture was spun down by centrifugation (5min, 6000xg, 4°C). The pellet was resuspended on ice with 250 μ L MP1. MP2 solution was added to the suspension, causing alkaline lysis of the cells. This step takes 5min while the cells suspension is incubated at room temperature. Next, 250 μ L of MP3 is added and incubated 20min on ice. After a centrifugation step (15min, 20000g, 4°C), the plasmid DNA is now in the supernatant. The next step was to precipitate the plasmid DNA with cold 100% ethanol, centrifuge at 4°C and then wash with cold ethanol 70%. At the end, the washed pellet was dried for 10min in a vacuum centrifuge, and resuspended with a desired amount of H₂O at 37°C.

MP1	
Tris	6.06 g
EDTA·2H ₂ O	3.72 g
RNAse A	100 mg
H ₂ O	ad 1000 mL
pH 8.0	

MP2	
NaOH	8.0 g
SDS 10%	100 mL
H ₂ O	ad 1000 mL

MP3	
KOAc	8.0 g
SDS 10%	100 mL
pH 5.5	

3.2.4.2 Maxi-preparation (Maxiprep)

Maxi-preparation is performed to isolate plasmid DNA at a large scale. For this purpose, bacteria expressing the plasmid were incubated overnight in 500mL Erlenmeyer flasks with 100mL LB+ medium containing antibiotic (for example 150 μ L ampicillin in concentration of 50mg/mL) at 37°C and 225 rpm. After incubation, a glycerol stock from part of the bacteria was made, and in parallel an isolation of the plasmid by using the PureYield™ Midiprep system (Promega), according to the manufacturer protocol was done. This kit is based on the method of alkaline lysis, in combination with purification by a silica membrane column.

3.2.4.3 Determination of the DNA concentration

Quantification of the plasmid DNA can be obtained by their specific absorption at a wavelength of 260nm, using an Eppendorf Bio-Photometer. This photometer can also indicate protein and RNA contaminations of the sample. For this the absorption ratio between OD260 to OD280 (for protein), and OD260 to OD230 (for RNA) were measured. The ratio OD260/OD280 should be approximately between 1.7 and 2, the ratio OD260/OD230 should be greater than 2.

3.2.5 Polymerase chain reaction (PCR)

The Polymerase Chain Reaction (PCR) is an enzymatic method to amplify in-vitro specific DNA fragments from a mixture of nucleic acids (Mullis and Faloona, 1987). The PCR reaction contains 3 consequential steps: denaturation, annealing of the primers and elongation.

A double-stranded DNA template is separated into two single strands at 94°C, in a process called denaturation. By reducing the temperature, specific primers can bind to the single stranded DNA, this is the annealing step. Starting from the specific locus where the primers bind, the polymerases are able to synthesize the complementary lacking single strand. The polymerases fill the nucleotides from the 5' to 3' end. This step is the elongation, and usually it is carries out at 72°C.

The PCR is programmed to be a cycle of denaturation, annealing and elongation which repeats several times. Ideally, after each cycle the amplified DNA fragment is multiplied exponentially. In theory, at n cycles there are only 2^{n-1} amplified DNA fragments.

The annealing temperature in the PCR reaction is dependent on the primers. This temperature is roughly 5°C below the melting temperature of the specific primer, which can be easily calculated based on the nucleotides the primer contains.

The elongation duration and temperature depend on the polymerase type and the length of the target fragment to be amplified.

The PCR method was used at this work in different ways: cloning certain DNA sequence into expressing plasmid, insert point mutations and genotype mice litters.

3.2.5.1 Primers

Primer refers to a DNA fragment with a length of 18-30 base pairs, which is usually used in pair to amplify DNA by PCR. The primers used in this study were ordered all from MWG-Biotech. Some rules need to be considered when designing primers:

- Guanine (G) and Cytosine (C) nucleosides should be less than 50% of the primer.
- There should never be four identical bases in a row.
- The melting temperature should be between 50 to 65°C.
- At the 3'-end should be located a guanine or cytosine residue.
- The primer should only bind specifically to a locus within the target DNA.
- Secondary structures within the primer (like hairpin structures) should be avoided.
- Two pair primers should not be able to hybridize to themselves, in order to avoid formation of a dimer.

The computer program "DNA-Man 5.0" (Lynnon BioSoft) was used to design the primers. The lyophilized primer DNA was dissolved with H₂O to a concentration of 10pmol/L. For detailed primers list used in the study, check appendix 8.4.

3.2.5.2 Standard genotyping PCR

The thermo-stable Taq polymerase is characterized by fast DNA synthesis, but at a relatively high failure rate (0.1% - 1 in 1000 bases is wrong). Therefore, Taq polymerase or REDTaq[®] ReadyMix (Sigma-Aldrich) was only used for genotyping

MATERIALS AND METHODS

Standard-PCR-reaction	
DNA template	30 – 150 ng
10x Taq-Buffer	2.5 µL
dNTP's (1,25mM)	4 µL
Primer forward (10µM)	1.25 µL
Primer reverse (10µM)	1.25 µL
Taq-Polymerase	0.25 µL
H ₂ O	ad 25 µL

REDTaq [®] -PCR-reaction	
DNA template	4 µL
Primer forward (10µM)	1 µL
Primer reverse (10µM)	1 µL
REDTaq ready-mix Buffer	9 µL

Standard-PCR -program	
94°C	5 min
94°C	30 sec
56°C	30 sec
72°C	60 sec \ 1kb
72°C	10 min

} **X30**

3.2.5.3 High Fidelity PCR for cloning

The Phusion High Fidelity polymerase is also a thermostable enzyme with a high synthesis capacity and the ability of proof-reading. This enzyme is able to detect and correct errors in DNA synthesis. Additionally, it also has a very high synthesis rate (30-60 bases/sec). PCR with Phusion polymerase (Finnzymes) was used with the appropriate reaction buffer (HF buffer) for cloning.

Each reaction conditions had to be adapted specifically in two important points before using this PCR protocol: First, the annealing temperature of the primers, which depends on the melting temperature of each primer. Second, the elongation time depending on the size of the amplified DNA fragment.

The dNTP mixture was made of dATP, dCTP, dTTP, dGTP, manufactured by NEB, with a final concentration of 10mM of each nucleotide.

MATERIALS AND METHODS

Phusion -PCR-reaction		Phusion -PCR -program		
DNA template	15 - 30 ng	98°C	5 min	
5xHF-Puffer	10 µL	98°C	30 sec	} X10
dNTP's (1,25mM)	8 µL	65°C	30 sec (-1°C)	
Primer forward (10µM)	2.5 µL	72°C	30 sec \ 1kb	
Primer reverse (10µM)	2.5 µL	98°C	30 sec	
Taq-Polymerase	0.5 µL	45-60°C	30 sec	} X35
H ₂ O	ad 50 µL	72°C	30 sec \ 1kb	
		72°C	7 min	

3.2.5.4 Overlap-PCR

PCR is a suitable method to introduce point mutations into a target fragment. This can be done by using overlap PCR. In this case, primers carrying a substitution of one or more base(s) in their sequences were used. The new base may create new recognition sites for restriction enzymes or change amino acid sequences and by that the functional properties of the protein.

To introduce a mutation by using the overlap PCR in a DNA fragment, two steps are required. First, two fragments are amplified; each one carries the mutation in question, one at the 3' end and the second at the 5' end. The two fragments have a common overhanging end. Then these two sub-fragments can be brought together to form the desired mutated fragment by using primers which are complementary to the ends of the fragment.

This technique was used to generate the chimera constructs between CaBP4 and CaM.

3.2.5.5 Quikchange-PCR

For the introduction of the point mutations in the CaBP4 sequence the QuickChange Site-Directed Mutagenesis kit from Stratagene was used.

This mutagenesis kit allows introducing mutations directly on double-stranded DNA plasmids. Therefore, sub-cloning of the mutated DNA fragment is no longer necessary. In Figure 3.4, the principle of this mutagenesis kit is illustrated.

MATERIALS AND METHODS

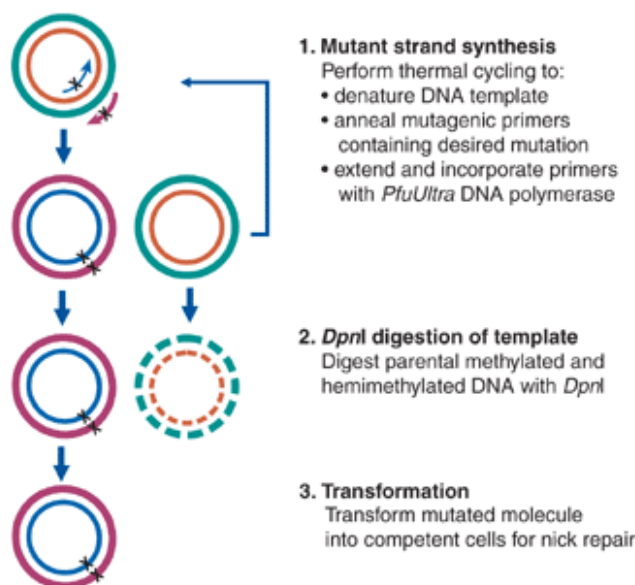


Figure 3.4 – The QuikChange II site-directed mutagenesis method. (Stratagene).

This mutagenesis approach requires 2 anneal mutagenic primers which introduce the point mutation, by amplification the whole DNA plasmid using a predetermined program in a thermocycler. The polymerase is *PfuUltra HF* DNA.

At the end of the amplification step, there are 2 plasmids in the reaction cup, one is the template plasmid and the other is the plasmid with the introduced point mutation.

QuikChange-PCR -program	
95°C	30 sec
95°C	30 sec
55°C	30 sec
68°C	60 sec \ 1kb

} X12

In order to eliminate the template plasmid, the restriction enzyme *DpnI* (10U/μL) was added to the solution for a digestion step (1h at 37°C). The *DpnI* enzyme digests only methylated plasmid DNA. Therefore the newly synthesized and modified plasmid remains intact and could be transformed into chemically competent cells. Some of the EF hands mutations in the CaBP4 have been introduced with this technique.

MATERIALS AND METHODS

QuikChange-PCR-reaction	
DNA template	100 ng
10x Buffer	5 μ L
dNTP's mix	1 μ L
Primer forward (10 μ M)	1.5 μ L
Primer reverse (10 μ M)	1.5 μ L
PfuUltra HF polymerase	1 μ L
H ₂ O	ad 50 μ L

3.2.6 Isolation, purification and quantification of DNA

DNA fragments from PCR or restriction digestion can be separated by agarose or PAGE gels. In both, the DNA fragments are separated by gel electrophoresis. The negatively charged nucleic acids migrate to the positive pole under electric field. The DNA is separated as a function of the applied voltage, the concentration of the gel as well as the conformation and size of the DNA fragments. The migration rate increases with decreasing DNA mass.

The DNA samples were loaded on the gel with gel-loading buffer (6x Dye) which contains the dyes bromophenol blue & xylene cyanol to track electrophoresis progress. The bromophenol blue dye runs at the same level like DNA fragments with a size of 10-100bp, while the xylene cyanol dye can be seen at the level of DNA fragments with a size of 5kb. A universal size standard for DNA fragments (1kb DNA Ladder, Invitrogen) was used next to the samples. 1x Tris/Borate/EDTA buffer (TBE) was used as electrophoresis running buffer.

6x Dye	
Ficoll	18 g
0.5 M EDTA (pH=8)	24 mL
10x TBE	60 mL
Bromophenol blue (50 μ g/mL)	3 mL
Xylene cyanol (50 μ g/mL)	3 mL
H ₂ O	ad 100 mL

10x TBE	
Tris HCl	540 g
Boric acid	275 g
0.5 M EDTA (pH=8)	200 mL
H ₂ O	ad 1000 mL
Electrophoresis running buffer	
10x TBE	1 L
H ₂ O	9 L

The concentration of agarose or acrylamide (PAGE) in the gel is depended on the size of the DNA fragments which need to be separated.

MATERIALS AND METHODS

3.2.6.1 Agarose gel

Separation of DNA on an agarose gel by electrophoresis was the standard procedure. Depending on the fragment size, gels with different agarose (peqGOLD universal agarose Peqlab) concentration were used. Gels with 0.7% for fragments bigger than 1000bp and 2% for fragments between 200-1000bp. The agarose was added to 1x TBE solution and set to boil in the microwave. Afterwards, the solution was cooled to about 60°C and 0.8µg/mL ethidium bromide solution was added to it. The ethidium bromide is a DNA intercalator which makes the DNA visible under UV light. After the gel solidified, it was placed in a horizontal electrophoresis chamber, overlaid with 1x TBE. The samples were mixed in the ratio 1:6 with 6x loading buffer and carefully pipetted into the gel pockets. The electrophoresis was carried out at 100 to 135V. Following the procedure, the gel was photographed in a gel documentation system (Gel Doc 2000, Bio-Rad). In case of a preparative gels, the desired band was excised with a scalpel from the gel, in order to isolate the DNA from the gel (2.2.6.3).

3.2.6.2 Polyacrylamide gel electrophoresis (PAGE)

For the separation of very small DNA fragments (<400bp) 5% polyacrylamide gels (PAGE) without ethidium bromide were used. These are vertical gels with thickness only of 0.75mm for analytical purposes or 1.5mm thick gels for preparative purposes. The samples are mixed with 6x loading buffer and applied to the vertical electrophoresis PAGE gel filled with 1x TBE buffer. The gel was running for 10min at 100V, followed by 50min at 260V.

Subsequently, the gel was stained for 10min in ethidium bromide (final concentration 0.8µg /mL), followed by a washing step with double distilled H₂O to remove the rest of the ethidium bromide. At the end, the gel was photographed with Gel Doc system.

PAGE-Gel	
Rotiphorese Gel 40 (Acrylamid / N,N'-Bisacrylamid = 29:1, 40% aqueous solution)	3.8 mL
1x TBE	ad 30 mL
TEMED (N,N,N',N' - Tetramethylethylendiamin)	20 µL
APS	70 µL

3.2.6.3 Isolation of DNA from a gel

The band of interest was excised under UV-light with a scalpel from the gel. Isolation and purification of DNA from agarose gel was performed with a kit according to the manufacturer's instructions (QIAquick Gel Extraction Kit, Qiagen). Alternatively, the DNA band was excised from the gel and inserted into a dialysis tube (Sigma) with 300 μ L 1x TBE solution with no air bubbles. The dialysis tube was placed in a horizontal electrophoresis (containing 1x TBE running buffer) for 2-3 hours at 145mA of electro-elution. The buffer inside the dialysis tube, which contains after the elution the DNA, was transferred into a reaction vessel, to proceed with the DNA precipitation protocol.

3.2.6.4 Precipitation of DNA

Purification or concentration of DNA by ethanol precipitation was performed from aqueous solutions. The precipitation was done by adding 2 solutions successively: First, 1/10 times volume of 5M NaCl fraction (pH 5.2) was added to the DNA solution. Second, 2.5 times the volume of 100% ethanol (-20°C). The reaction cup was then mixed and set for 15min at -80°C to let precipitate the DNA.

Centrifugation at 14,000rpm for 15min at 4°C followed, to discard the supernatant. The pellet was washed with 100mL of 70% ethanol and centrifuged again for 5min (14,000rpm, 4°C). Finally, the DNA was dried in a vacuum centrifuge (SpeedVac, Heraeus) for 3-5 minutes and dissolved in the desired amount of water.

3.2.6.5 Isolation of genomic DNA from mouse tissues

Due to the large size of the genomic DNA molecules and the fact that it can easily be damaged by shear forces, it is impossible to isolate DNA from mouse tissues (toes) for genotyping like in the procedure to isolate a plasmid DNA. The lysis of the cell membranes was done by incubating the mouse tissue in 100 μ L lysis buffer containing 10 μ L proteinase K buffer and 1 μ L proteinase K, to solubilize the cell membrane. This mixture was incubated overnight at 55°C and 650rpm. The following day, the mixture was heated to 95°C K for 10min to inactivate the proteinase K, and stored at 4°C. The DNA is then used for genotyping analysis.

For Southern blot, 5mm mouse tail tissue was incubated with 500 μ L lysis buffer at 56°C and 300rpm overnight.

3.2.6.6 Phenol-chloroform extraction

By phenol-chloroform extraction, proteins can be separated from an aqueous solution of DNA to obtain particularly pure DNA. The extraction procedure was done in the following steps:

First, the DNA-protein mixture was increased with autoclaved H₂O to a minimum volume of 500µL. Afterwards, the solution was mixed with an equal volume of phenol-chloroform-isoamyl alcohol mixture (25:24:1, Roth), and centrifuged for 5 min at 14,000rpm and 4°C. As a result, two phases formed, the lower organic phase containing the protein and the upper aqueous phase, in which the DNA is dissolved.

The upper phase was removed and mixed with 500µL chloroform and centrifuged again. The DNA in the upper phase was collected and could be precipitated (like 2.2.6.4).

The phenol-chloroform extraction was used also as intermediate step to purify the DNA while pre-overlap PCR application.

3.2.6.7 Sequencing of DNA

The DNA fragments were analyzed by restriction digestion and also by sequencing. The DNA fragment (genomic or plasmid) was sent with forward and/or reverse primer(s) to Eurofins MWG Operon, Ebersberg Germany for sequencing. The sequencing was done according to company's instructions and protocols.

(<http://www.eurofinsdna.com>)

3.2.7 Enzymatic modification of DNA

Cloning of DNA fragments after the amplification and purification steps and/or linearization of the DNA vector require using enzymatic modifications steps like restriction digestion. The enzymes that were used in this work were purchased from New England Biolabs (NEB) and Fermentas.

3.2.7.1 Restriction digestion

Restriction enzymes are bacterial endonucleases that recognize and cut specific sequences in double-stranded DNA (Sambrook and Russell, 2001). In this work, restriction endonucleases type II, which digest the DNA within their specific palindromic recognition sequence, were used. Characteristically, the enzyme can create either blunt ends ("blunt ends") or as complementary 5'-and 3'-protruding cohesive ends ("sticky ends").

The recognition sequences, reaction buffer and incubation conditions of each enzyme were taken from the manufacturer's specifications.

When using two restriction enzymes with different optimal buffers, one reaction buffer was chosen in which each enzyme activity did not decrease below 75%. For detailed restriction enzymes list used in the study please check appendix 8.4.

3.2.7.2 Dephosphorylation

To prevent religation of the restricted, linearized vector during the ligation, the vector DNA was dephosphorylated at the 5' ends. The 5'-phosphate group was removed by treatment with CIP (calf intestinal phosphatase).

After the restriction digestion of the vector, the vector was treated with 1 μ L CIP (corresponding to 1 unit) with the appropriate buffer at 37°C for 15min, followed with heat inactivation step (65°C, 5min). Before and after the dephosphorylation step, the restriction mixture was purified a phenol-chloroform extraction followed by DNA precipitation (2.2.6.6, 2.2.6.4). Lastly, the vector DNA was used for ligation (2.2.7.3).

3.2.7.3 Ligation

The T4 DNA ligase was used to link the compatible ends of the linearized vector and the DNA insert fragment. This enzyme is ATP-dependent, ligating two ends of double stranded DNA by catalyzing the formation of a phosphodiester bond between a 5'-phosphate and a 3'-hydroxyl group. T4 DNA ligase can be used for DNA with sticky ends as well as with blunt ends.

MATERIALS AND METHODS

Ligations were performed, using the 1 μ L Quick T4 DNA ligase (NEB), in a volume of 20 μ L with the buffer system (contains ATP) provided by the manufacturer. The ligation mixture was incubated for 5 min at RT or alternatively overnight at 16°C in a water bath.

For ligation, vector and insert were used in a mass ratio of 1:3, respectively. The vector DNA was being approximately 10ng. The amount of insert DNA was calculated using the following equation:

$$\text{Insert amount [ng]} = \frac{3 \times \text{vector quantity [ng]} \times \text{insert length [bp]}}{\text{vector length [bp]}}$$

As a result of the ligation, circular plasmid was created containing the desired DNA insert sequence. This recombinant plasmid could be later introduced by transformation in *E. coli* (2.2.3.5).

3.2.8 Southern-Blot

The Southern blot method makes it possible to identify single-stranded DNA fragments from total genomic DNA (Southern, 1975). Briefly, The DNA fragments are separated on an electrophoresis gel, which are then blotted onto a membrane and immobilized. By hybridization with a radioactively labeled probe which is complementary to region of interest, the specific DNA fragment can be detected.

This technique was used once in this study to confirm that the mice we used as our animal model are indeed $Ca_v1.4$ knockout mice.

MATERIALS AND METHODS

3.2.8.1 Buffers and solutions for Southern blot

5M NaCl		0.4M HCl		10x TE	
NaCl	29.2 g	HCl _{conc.}	40mL	Tris 1M pH 8.0	50 mL
H ₂ O	ad 100 mL	H ₂ O	ad 1000 mL	EDTA 0.5M pH 8.0	10 mL
0.5M EDTA pH 8.0		ssDNA 10mg/mL		H ₂ O	ad 500 mL
Na ₂ EDTA*2 H ₂ O	93.05 g	ssDNA _{from herring sperm}	0.5 g	2x wash buffer	
H ₂ O	ad 500 mL	H ₂ O	ad 50 mL	20x SSC	200 mL
1M Tris pH 8.0		20x SSC pH 7.0		20% SDS	10 mL
Tris	60.5 g	NaCl	175 g	H ₂ O	ad 2000 mL
H ₂ O	ad 500 mL	Na ₃ Citrat*2 H ₂ O	88 g	0.4x wash buffer	
20% SDS		H ₂ O	ad 1000 mL	20x SSC	40 mL
SDS	100 g	0.5M NaOH / 1.5M NaCl		20% SDS	10 mL
H ₂ O	ad 500 mL	NaOH	40 g	H ₂ O	ad 2000 mL
1M NaH₂PO₄		NaCl	175.3 g	Church buffer	
NaH ₂ PO ₄ *2 H ₂ O	156 g	H ₂ O	ad 2000 mL	BSA	5 g
H ₂ O	ad 1000 mL	0,5M Tris / 3M NaCl pH 7.0		1M Na ₂ HPO ₄	193.5 mL
1M Na₂HPO₄		Tris	121 g	1M NaH ₂ PO ₄	56.5 mL
Na ₂ HPO ₄ *2 H ₂ O	178 g	NaCl	351 g	20% SDS	175 mL
H ₂ O	ad 1000 mL	H ₂ O	ad 2000 mL	0.5M EDTA	1 mL
				ssDNA 10mg/mL	5 mL
				H ₂ O	50 mL

3.2.8.2 Extraction of genomic DNA from mouse tissue

In order to isolate the genomic DNA, a short piece from the mouse tail was incubated at 60°C overnight in 500µL lysis buffer contains proteinase K. The next morning, the DNA was precipitated ethanol-NaCl mixture followed by phenol/chloroform extraction.

3.2.8.3 Restriction digestion of genomic DNA

The extracted genomic DNA was incubated in 50µL restriction mix with the enzyme Bgl-II according to the enzyme's manufacturer requirements at 37°C for 2-3 hours.

After inactivation of the restriction enzyme, the DNA mix was applied on 0.8% agarose gel for separation.

3.2.8.4 Separation of genomic DNA on agarose gel

The digested DNA was loaded on a 0.8% agarose gel and separated at 150V. Subsequently, the gels were photographed under UV light with an applied ruler to determine the size of the band after blotting.

3.2.8.5 Depurination of genomic DNA

Depurination of the genomic DNA increases the effectiveness of relatively large DNA fragments to be transferred from the agarose gel to the membrane. Before the blotting step, the agarose gel was treated in 3 washing steps: first with 0.4M HCl for 15min to break the DNA strands. Second, with 0.5M NaOH/1.5M NaCl for 15 min to separate the two DNA strands. And finally, with 0.5M Tris/ 3M NaCl (pH 7.5) for 20min for neutralization.

3.2.8.6 Blotting

The DNA fragments from the gel are transferred by capillary force to a Hybond-N membrane. The agarose gel is placed over 3 layers of filter paper on soaked sponges with 10x SSC buffer in half-filled with 10x SSC buffer metal dishes. The membrane was placed over the agarose gel with another 3 layers of filter paper and a big stack of paper towels on top. Great care was taken that no liquid bridges between paper towels and buffer stocks formed, so that the entire liquid could travel through the gel and the membrane towards the paper towels, whereby the DNA fragments are transferred to the membrane.

On the following day, the membrane was removed after marking the gel pockets and the ladder marker with a pencil. The DNA on the membrane was then immobilized with UV light (cross-linking), and dried for 1-2 hours at 80°C.

3.2.8.7 Amplification of the ³²P-labeled probe

The probe for the Southern blot was amplified by PCR from genomic DNA and sub-cloned using restriction enzymes. Before the labeling reaction, the probe was excised from the vector by restriction digestion and purified. Radioactive labeling was performed using the "random-primed DNA labeling kit" from Roche. About 100ng DNA fragment served as a template after 10 minutes denaturation at 95°C. The Klenow enzyme optimally synthesizes new labeled DNA strands with dNTP mix (with

MATERIALS AND METHODS

radioactive α -³²P-dCTP) at 37°C. After 1.5 hour of labeling reaction the labeled probe was purified on a NickTM Column (GE Healthcare). The activity of the probe was determined using a scintillation counter.

3.2.8.8 Hybridization

The membrane with the immobilized DNA fragments was first prehybridized for 2 hours at 60°C with Church buffer in a water bath, to block nonspecific binding sites. For hybridization, the radioactive labeled probe, which was previously denatured at 95°C for 5 minutes, was added to pre-warmed Church buffer. The membrane was then incubated overnight at 60°C, in a water bath.

3.2.8.9 Washing and analyzing the membrane

The next day, the membrane was washed briefly with pre-heated to 60°C 2xSSC washing buffer, and then treated along the following washing steps in order to remove excess and non-specifically bound probe:

- | | | | |
|----|-------|-------------------|------|
| 1. | 15min | 2.0xSSC / 0.1%SDS | 60°C |
| 2. | 30min | 0.4xSSC / 0.1%SDS | 65°C |
| 3. | 30min | 0.4xSSC / 0.1%SDS | 67°C |
| 4. | 30min | 0.4xSSC / 0.1%SDS | 72°C |

The membrane was washed until the point that its activity was between 20-50cpm, by Geiger counter. The membrane was then air-dried at room temperature on filter paper, and placed overnight to several days with a Phospho-imager plate (BAS MP2025P, Fujifilm) in exposure case. The signals on this plate were detected by BAS 1000 Phospho imager (Fujix Company).

3.3 Biochemical methods

Protease inhibitors were added to the solutions, in all the steps described below, according to the manufacturer's instructions. Moreover, the steps were performed at 4°C, in order to prevent denaturation or degradation of the proteins.

3.3.1 Protein extraction from HEK293 cells

HEK293 cells were transfected using a calcium phosphate protocol (as described in 2.4.3.2). The medium was exchanged 16-20 hours after transfection, and the HEK293 cells were harvested 3 days after transfection. For lysing the cells, first the culture medium was aspirated; the cells washed once with 10mL of PBS and lysed with 0.5mL of cell lysis buffer containing protease inhibitors (Complete® EDTA-free, Roche).

To detach the cells, the culture dishes were placed on a shaker for 15min at 4°C and 100rpm. The lysed cells were subsequently transferred by pipetting up and down several times in a 1.5mL reaction tube. After 15 minutes of centrifugation at 4°C (13,000 rpm), the supernatant containing the solubilized protein was transferred into a new reaction tube. The pellet was discarded and the supernatant was frozen at -80°C for further use.

Cell lysis buffer	
Tris HCl pH 7.4	50 mM
NaCl	150 mM
EDTA	1 mM
Triton X-100	1 %

3.3.2 Quantification of protein concentration

The overall protein concentration of lysates was quantified with photometrical method – Bradford assay (Bradford, 1976), using the BioPhotometer (Eppendorf).

For this purpose, 5µL from the protein solution were mixed with 95µL 0.15M NaCl and subsequently with 1mL of Coomassie solution. The mixed solution was incubated for 2 min at room temperature.

The Coomassie solution contains the dye Brilliant Blue G250 which forms complexes with proteins in acidic conditions. The complex shifts the absorption maximum from

MATERIALS AND METHODS

465nm to 595nm. Therefore, the protein concentration in the solution is quantified by absorbance at 595nm.

Coomassie solution	
Coomassie brilliant blue G250	50 mg
EtOH 95%	25 mL
H ₃ PO ₄ 85%	50 mL
H ₂ O	ad 500 mL

3.3.3 Electrophoretic separation of proteins by SDS-PAGE

The separation of proteins according to their molecular weight was carried out by SDS – polyacrylamide gel electrophoresis, as described in (Laemmli, 1970).

By heating the sample in 6xLaemmli sample buffer to denaturing conditions, proteins become unfolded and coated with sodium dodecyl sulfate (SDS) detergent molecules, acquiring a high net negative charge that is proportional to the length of the polypeptide chain. By this modification the separation depends only on the size and not on the net charge of the proteins. Before application to the gel, the samples were denatured by addition of Laemmli buffer for 5min at 98°C.

To prepare the gel, all components of the stacking gel and the separating gel were initially mixed without ammonium peroxodisulphate (APS) and TEMED. After adding these two components, the liquid separating gel was first poured into the prepared glass plates (Biorad) with thickness of 1.5mm. 100% ethanol was added on top to ensure a smooth surface of the gel. The gel polymerized within about 30 minutes, then the ethanol layer was removed and the ready mixed stacking gel was set onto the separation gel with the gel comb. The concentration of acrylamid/bisacrylamid solution (Rotiphorese Gel 30, 37.5:1, Roth) in the separation gel is depended on the size of the protein to be analyzed. For electrophoresis, the Mini-Protean 3 electrophoresis system (Biorad) was used. The electrophoresis was done at 100V with the protein standard Kaleidoscope Protein Ladder (Biorad).

MATERIALS AND METHODS

4xTris-HCl/SDS pH6.8 (0.5M Tris, 0.4% SDS)	
Tris Base	6.04 g
SDS	0.4 g
H ₂ O	ad 100 mL
4xTris-HCl/SDS pH8.8 (1.5M Tris, 0.4% SDS)	
Tris Base	18.2g
SDS	0.4 g
H ₂ O	ad 100 mL

Stacking gel	
Rotiphorese Gel 30	0.65 mL
4xTris-HCl/SDS pH6.8	1.25 mL
H ₂ O	3.05 mL
APS	25 µL
TEMED	5 µL
Separation gel (7%-15%)	
Rotiphorese Gel 30	3.5-7.5 mL
4xTris-HCl/SDS pH8.8	3.75 mL
H ₂ O	7.75-3.75 mL
APS	30 µL
TEMED	10 µL

6xLaemmli sample buffer (Storage at -20°C)	
4xTris-HCl/SDS pH6.8	7 mL
Glycerol	3 mL
SDS	1 g
Bromphenol blue	0.004%
DTT	0.9 g
H ₂ O	ad 10 mL

10xElectrophoresis buffer	
Tris Base	30.2 g
Glycine	144 g
SDS	10 g
H ₂ O	ad 1000 mL

3.3.4 Western Blot

Recombinant CFP-tagged human CaBP4 mutations (CaBP4 R216X and CaBP4 E267fs) and wild type CaBP4 were expressed in HEK293 cells using the calcium phosphate transfection method (2.4.3.2). Western Blot protocol was performed as published previously (Schieder et al., 2010), using an antibody against GFP (Clontech).

Briefly, after electrophoretic separation was carried out, the proteins were transferred to an Immun-Blot PVDF membrane (Polyvinylidene difluoride, Immobilon, pore size 0.45 microns, Millipore). The transfer process was done in a tank-blot system (Mini Trans-Blot, Bio-Rad) with ice cooling at 100mA for 1 hour. The duration of the blotting was determined by the size of the transferred proteins.

MATERIALS AND METHODS

After blotting, the PVDF membrane was dried for 1h at 37°C and blocked with tris buffered saline (TBST) containing 5% milk powder for 1 hour at room temperature. Incubation with primary anti-GFP antibody (mouse monoclonal, IgG) was done overnight at 4°C. The blot was then incubated (1h, RT) in the secondary anti-mouse IgG antibody conjugated with horseradish peroxidase, which was diluted 1:5000 in TBST containing 3% milk powder. Between and after the incubation steps the membrane was washed three times for 5min with TBST. At the end, protein was detected by enhanced chemiluminescence using the ECL Western Blotting Analysis System (Amersham Biosciences or Roche) and a light sensitive film (Hyperfilm ECL, Amersham Biosciences).

10x TBS (pH 8.2)	
Tris Base	12.1 g
NaCl	80.2 g
H ₂ O	ad 1000 mL
1x TBST	
10 x TBS	100 mL
Tween 20	1 mL
H ₂ O	ad 1000 mL

Transfer buffer	
10x Electrophoresis buffer	100 mL
Methanol	200 mL
H ₂ O	ad 1000 mL
Blocking buffer	
5% powdered milk in 1x TBST	

3.4 Culture and transfection of eukaryotic cells

All work described in this section was carried out under sterile conditions (laminar air flow, HERAsafe HS18, Heraeus). All media and solutions were heated in a 37°C water bath before use.

3.4.1 HEK293 cells culture

HEK293 (human embryonic kidney) cells were treated to overexpress the human wild type CaBP4 and/or the CaBP4 mutations before proceeding with the western blot. The cells were cultured in 100mm Petri dishes (Sarstedt) in an incubator (Heraeus) at 37°C and 10% CO₂. Dulbecco's modified Eagle medium (DMEM) containing 1g/L D-glucose and pyruvate supported with 10% fetal bovine serum (FBS), 100U/mL Penicillin G and 100µg/mL Streptomycin was used as the culture medium.

3.4.2 Establish of HEK293 stable cell lines

Murine Ca_v1.4 α1 subunits (wild type, ΔICDI and 5A) were expressed in stable HEK293 cell lines generated by using the Flp-In™ System (Invitrogen).

The Flp-In system is based on using the FLP recombinase and FLP site - a specific recombination sequence in order to integrate a gene of interest at a defined position in the target cell genome. The target cell line HEK-Flp™ is a genetically modified cell line which contains a singular FRT site (FLP recombination target site) in the genome and a zeocin resistance gene. In parallel, the plasmid vector pcDNA5/FRT also contains an FRT site, combined with a hygromycin resistance gene. The Ca_v1.4 α1 subunits of the calcium channel were cloned in two steps into the vectors MCS, under control of the CMV promoter.

Co-transfection of the targeting vector with the gene of interest and the FLP recombinase expression vector (pOG44) causes integration of the gene into the genome. The result of the integration is a change of resistance cassette from zeocin to hygromycin. Therefore, only cells that can grow under hygromycin selection are cells carrying the gene of interest.

Cells were seeded in 35mm diameter culture dishes and grown overnight, without antibiotic selection. The next day, cells were transfected with 1.5µg Ca_v1.4α1 pcDNA5/FRT-Plasmid and 2.5µg pOG44 plasmid. After 4 hours, the transfection medium was removed, the cells washed with PBS and received fresh medium without antibiotic. 24 hours after transfection, the cells were trypsinized and

MATERIALS AND METHODS

transferred to a new culture dish using hygromycin to select for the positive, resistant cells. The positive cells were frozen and stored in liquid nitrogen.

During routine work, the cells were cultured in 25cm² cell culture flask in an incubator at 37°C and 10% CO₂, using DMEM containing 4.5g/L D-glucose and pyruvate with addition to 10% FBS and antibiotics (Penicillin and Streptomycin).

Once the cells had grown close to 100% confluence, they were split. The cells were washed once with phosphate buffered saline (PBS) to remove leftover of the culture medium and subsequently disaggregated with EDTA-trypsin. After inactivation of trypsin by adding DMEM medium to the flask, the cells were resuspended by mechanic force.

5% of the cells were seeded into a new 25cm² culture flask and another 5% were seeded into 12 wells plate for transfection. After transfection, the cells were seeded in 24-well plates with and poly-L-lysine coated coverslips, in a final volume of 1mL.

PBS (pH 7.4)	
NaCl	40.0 g
KCl	1.0 g
Na ₂ HPO ₄ *12H ₂ O	14.5 g
KH ₂ PO ₄	1.2 g
H ₂ O	ad 5000 mL
EDTA-trypsin solution	
Stock solution (0.5% trypsin/0.2% EDTA)	10 mL
PBS (pH 7.4)	ad 100 mL

3.4.3 Transfections

3.4.3.1 Transient transfection with Fugene

The transient transfection of HEK293 cells was performed both for electrophysiology as well as for the FRET measurements using Fugene 6 transfection reagent (Roche), according to the manufacturer's instructions. The ratio of DNA (micrograms) to Fugene (μL) was typically 3:1, the ratio of Fugene (μL) to the reaction medium (μL, DMEM without additives) 1:10. Cells with 90% confluent in 12 well plates were

MATERIALS AND METHODS

transfected 48 to 62 hours before preform the whole-cell patch clamp measurements on them. The transfection rate and right time window to patch the cells was estimated base on the eGFP expression in the transfected cells.

3.4.3.2 Transient transfection with calcium phosphate

HEK cells were grown on 100mm culture dishes in 10mL medium to approximately 75% confluency before being transfected with the calcium phosphate method.

The DNA was diluted to final volume of 400 μ L with H₂O, and then 100 μ L 2.5M CaCl₂ and 500 μ L 2xBBS were added. The mixture was incubated for 12min at room temperature before it was distributed drop-wise on the 100mm culture dish. The cells were incubated for approximately 16h overnight at 37°C incubator with 3% CO₂. The next morning, the medium was changed and the cells were incubated at 37°C and 10% CO₂ for 2-3 days, and then lysed. For each dish, 30 μ g of plasmid DNA was used.

2x BBS (pH=7)	
BES	0.533 g
NaCl	0.818 g
Na ₂ HPO ₄ *2H ₂ O	0.013 g
HEPES	5 mM
H ₂ O	ad 50 mL

2.5 M CaCl ₂	
CaCl ₂ * 2H ₂ O	7.35 g
H ₂ O	ad 20 mL

3.4.4 Harvesting of HEK293 cells

Cells were harvested 72 hours after transfection. They were washed twice with PBS and scraped from the bottom of the culture dish with a cell scraper. The cells were collected in a reaction tube and stored at -80°C, after short centrifugation step of 5 minutes at 1000rpm, until further use.

3.4.5 Freezing of HEK293 cells

The HEK cells can also be stored to a longer period at -180°C. For that purpose, the HEK cells must be first trypsinized and centrifuged at 1000rpm for 5 minutes. The pellet is then resuspended in 1mL of freezing medium, and stored for a few weeks at -80°C or at -180°C for longer time.

3.5 Investigation of Ca_v1.4 knockout mice

All experiments were conducted in accordance with animal welfare guidelines and approved by the government of Upper Bavaria.

The animals were kept under a 12:12 hour's light/dark cycle and received food and water ad libitum. The offspring of breedings were genotyped 7-10 days after birth by a PCR analysis. At the age of 3-4 weeks the pups were separated from their mothers.

3.5.1 The Ca_v1.4 knockout mice

In the second part of the study, Ca_v1.4 specific KO mice were used. The Ca_v1.4 deficient mice were generated by deletion of exons 14-17 and disruption of Ca_v1.4 gene (Fig. 3.5) through homologous recombination using a Cre/loxP site strategy (Specht et al., 2009).

All test mice were descendent from heterogeneous breeding mates, after several generations of cross-breeding with C57-BI6/N mouse strain.



Figure 3.5 – The targeting locus of Ca_v1.4 (Cacn1f) with the 48 exons. The targeting vector contains two recombination arms: 5' with exons 9-13 and 3' with exons 18-27. In addition the targeting locus, where exons 14-17 are floxed with the NeoR selection cassette. Green triangles: loxP sites, Blue triangles: FRT sites, B: Bgl-II. The Southern blot probe is marked in Orange and the sizes of the fragments are mentioned.

3.5.2 Immunohistochemical methods

Immunohistochemical staining was performed at 3, 6 and 12 months according to the procedures described previously (Michalakis et al., 2005).

Briefly, the eyes were removed completely from a mouse that was sacrificed with diethyl ether, and pierced with a needle so the 4% PFA fixative could penetrate the eye during pre-fixation (5 min). After pre-fixation, the area above the *ora serrata* was cut and removed along the glass lens body.

MATERIALS AND METHODS

The remaining eye cup with the retina inside was fixed for 45 minutes in 4% PFA, then washed three times in 0.1M PB and incubated overnight in 30% sucrose. Finally, the eye cup was embedded in tissue freezing medium, Tissue-Tek O.C.T Compound (Sakura Finetech). 10 μ m thick sections of the eye cup were cut by using a cryotome. The retina slices were rehydrated with 0.1M PB and then fixed for 10min with 4% PFA. After three washing steps with 0.1M PB the slices were incubated with the primary antibody overnight at 4°C in a solution of 0.1M PB, 5% ChemiBLOCKER™ and 0.3% Triton X. The next morning, the slices were washed again three times with 0.1M PB before proceeding to the incubation with the secondary antibodies. The secondary antibodies were diluted in 0.1M PB with 3% ChemiBLOCKER™ and slices incubated for 90 minutes, followed by washing step. The cell Nuclei were treated with the cell nucleus stained marker Höchst 33342 for five minutes. Finally, the sections were washed with 0.1M PB and covered with coverslips.

The following primary antibodies were used:

Rabbit anti-Ca_v1.4 (Ca_v1.4 Pep3; 1:1000; (Specht et al., 2009)), rabbit anti-Calbindin (Swant, Bellinzona, Switzerland; 1:2000; (Michalakis et al., 2012)), mouse anti-PKC α (anti-Protein Kinase C-Biotin, Leinco Technologies Inc.; 1:50; (Young et al., 1988)), mouse anti-NF200 (anti-Neurofilament 200; Sigma; 1:300; (Franke et al., 1991)), Cy3-coupled anti-GFAP (Sigma, Germany; 1:1000; (Michalakis et al., 2005)), mouse anti-Rhodopsin (anti-Rhodopsin Clone 1D4; Thermo Scientific; 1:150; (Michalakis et al., 2010)), FITC-peanut agglutinin (PNA, Sigma-Aldrich, 1:100, (Michalakis et al., 2010)) was used as a cone marker, guinea pig anti-glycogen phosphorylase (GlyPho, 1:1000 (Pfeiffer-Guglielmi et al., 2003)), rabbit anti-cone arrestin (kindly provided by Cheryl Craft, 1:300, (Koch et al., 2012)), rabbit anti-complexin 3 (kindly provided by Kerstin Reim (Reim et al., 2005), 1:1000, (Koch et al., 2012)), rabbit anti-complexin 4 (kindly provided by Kerstin Reim (Reim et al., 2005), 1:20000, (Koch et al., 2012)). Laser scanning confocal micrographs were made using a LSM 510 meta microscope (Carl Zeiss, Germany) and images presented as collapsed confocal z-stacks. The fluorescence images were taken with a confocal laser scanning microscope Zeiss LSM 510 Meta microscope (Carl Zeiss, Germany) and images are presented as collapsed confocal z-stacks. The stainings were reproduced in ≥ 3 independent experiments.

3.5.3 Electroretinography (ERG)

ERG analysis was performed using 3 months old mice according to the procedures described previously (Seeliger et al., 2001; Tanimoto et al., 2009), in the lab of Prof. Mathias Seeliger at Division of Experimental Ophthalmology, Institute for Ophthalmic Research, Centre for Ophthalmology, Eberhard Karls Universität Tübingen, Germany.

3.5.4 Behavior test - Water maze

A modified version of the Morris water maze was used to test Rod visual function and vision-guided behavior (Pang et al., 2006). Mice were housed separately in an inverse 12h light/dark cycle. The experiment was performed in dark in the first 3 days.

Mice were trained for 3 days (8 trials a day) to locate a stable platform (10cm in diameter) at dim light conditions of 0.32cd/m^2 to ensure that vision is totally dependent on the rod system. The platform was placed in a circular swimming pool (120cm in diameter, 70cm high, white plastic) filled with water up to a depth of 30cm. The location of the platform was marked with black triangle attached to the maze wall next to the platform. The starting position of the mouse was changed from trial to trial in a pseudorandom order to avoid distal spatial cues, whereas the platform was kept in a constant location.

Trials were terminated if the mouse climbed onto the platform or when it swam for 2 min without finding the platform. In cases when a mouse did not find the platform it was gently placed on the stable platform. After each trial, the mouse was left on the platform for 30s undisturbed before the mice were towel-dried, transferred to their home cage, and warmed using a heating lamp. On Days 4 and 5, the experiment was performed under light conditions (29.04cd/m^2) to test cone vision-mediated behavior.

The platform was cleaned thoroughly between all trials and the water in the maze was mixed to remove potential proximal cues (e.g., urine). Every day, after finishing all trails, the water in the maze was exchanged with fresh water.

The experiment was performed and analyzed blind to the animal genotype. In total, 11-KO, 9-HZ and 9-WT mice were tested.

3.6 Electrophysiology

3.6.1 Experimental implementation

HEK293 cells stably expressing $Ca_v1.4 \alpha$ (wild type, $Ca_v1.4/5A$ or $Ca_v1.4\Delta ICDI$) were transiently transfected with expression vectors encoding the other subunits of the calcium channel $\beta 2\alpha$ (accession number: X64297) and $\alpha 2\delta 1$ (accession number: M21948). In some cases wild type CaBP4 or CaBP4 variants were also transfected in equal amount - 1.5 μ g from each construct.

Depending on the transfection conditions (details in 3.4.3.1), the transfected cells were taken on coverslips coated with poly-L-lysine to be patched after 2-3 days. The electrophysiological measurements were carried out at room temperature in the whole-cell configuration. For data acquisition an Axopatch 200B amplifier and the computer program Clampex 10.2 (Axon Instruments) were used. In addition Clampfit 10.2 (Axon Instruments) and Origin 7.5 (Microcal, Originlab Corporation) software to analyze acquired patch-clamp data.

Patch pipettes were made from borosilicate glass capillaries with an outer diameter of 1.5mm and an inner diameter of 1.17mm (GC150TF-8, Harvard Apparatus). The pipettes were pulled in a horizontal pipette puller (DMZ-Universal Puller). The pipette resistance varied from 2.0 to 3.0M Ω , and the cell sizes ranged between 10 and 100pF. I_{Ca} and I_{Ba} were measured from the same cell.

The following bath and pipette solutions were used for the whole-cell measurements:

Bath solution 10mM Ca	
NaCl	102 mM
CaCl₂	10 mM
CsCl ₂	5.4 mM
MgCl ₂	1 mM
TEA	20 mM
HEPES	5 mM
Glucose	10 mM
adjusted to pH 7.4 with NaOH	

Bath solution 10mM Ba	
NaCl	102 mM
BaCl₂	10 mM
CsCl ₂	5.4 mM
MgCl ₂	1 mM
TEA	20 mM
HEPES	5 mM
Glucose	10 mM
adjusted to pH 7.4 with NaOH	

MATERIALS AND METHODS

Pipette solution	
CsCl	112 mM
MgCl ₂	3 mM
MgATP	3 mM
EGTA	10 mM
HEPES	5 mM
adjusted to pH 7.4 with CsOH	

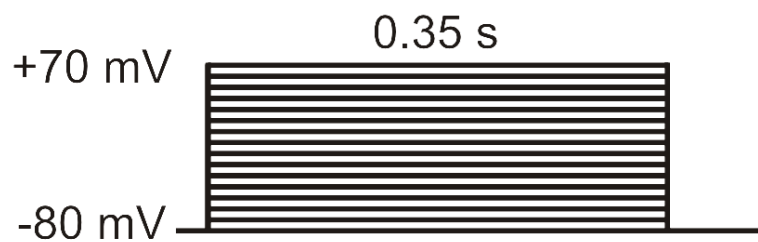
For experiments carried out in low (2mM) Ca²⁺ in the extracellular solution, the omitted Ca²⁺ was equimolarly replaced by Na⁺. Bath solutions were changed during experimentation using a local solution exchanger.

3.6.2 Patch-clamp protocols

The peak I/V-relationship was measured by two different voltage protocols:

Protocol for determining the half-maximum activation voltage ($V_{0.5}$)

The I/V curves were measured by applying 350ms voltage pulses to potentials between -80 and 70mV in 10mV increments at 0.2Hz. The holding potential was -80mV.



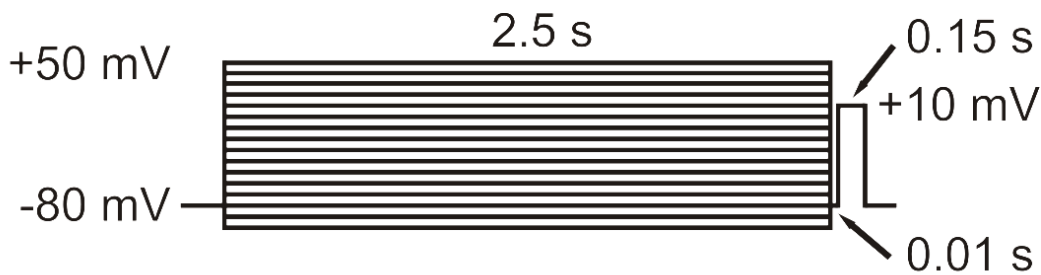
Protocol for determining the half-maximum inactivation voltage ($V_{0.5,inact}$)

In order to efficiently record the inactivation property of the Ca_v1.4 channel, the $V_{0.5,inact}$ was determined using a pseudo-steady state inactivation protocol, rather than true steady state inactivation. In this protocol, a prepulse duration of 2.5s was

MATERIALS AND METHODS

sufficient to induce considerable open state inactivation which was comparable to values achieved by a 5s prepulse in past publications (Baumann et al., 2004). Moreover, the time interval between trials (10s) was sufficient to recover the majority of inactivated channels. Ultra-slow inactivation of $Ca_v1.4$, which needs more than 10 minutes to recover (Peloquin et al., 2008) was not addressed in the present research. The protocol was adjusted and the prepulse lengths and inter-trial intervals were decreased as follows:

From a holding potential of -80mV a series of 2.5s conditioning pre-pulses to various voltages between -100mV and +50mV were used. The conditioning pulse was followed by a 10ms long return to the holding potential and a 150ms test pulse to +10mV (the maximum activation voltage (V_{max})). The individual trials of the protocol were applied at a time interval of 10s.



Additionally, $Ca_v1.4$ channel inactivation was quantified by calculating the fraction of peak Ba^{2+} and Ca^{2+} currents remaining after 350ms of depolarization (R350) as described. R350 is used to quantify CDI.

3.6.3 Data analysis

For determination of half-maximum activation voltage ($V_{0.5,act}$), I/V curves were recorded and the chord conductance (G) was calculated from the current voltage curves by dividing the peak current amplitude by its driving force at that respective potential, where V_{rev} is the interpolated reversal potential, V_m is the membrane potential, and I is the peak current.

$$G = \frac{I}{(V_m - V_{rev})}$$

The reversal potential is the voltage at which no net current flows through the channel. It is determined also as the intersection of the IV curve with the x-axis ($I = 0\text{pA}$).

Conductivity curves were calculated by nonlinear curve fitting using the Boltzmann equation:

$$G = \frac{G_{max}}{\left(1 + \exp\left(\frac{V_{0.5,act} - V_m}{K_{act}}\right)\right)}$$

Where G_{max} is the maximum conductance, $V_{0.5}$ is the half-maximum activation voltage, V_m is the membrane potential, and k_{act} is the slope factor of the activation curve.

The current density was obtained by normalizing the maximum current amplitude at maximum activation voltage (V_{max}) to the cell membrane capacitance (C_m). The activation threshold is defined and determined from I/V curves as the potential at which 5% of the maximum current is elicited.

Families of current traces obtained by applying the pseudo steady state inactivation protocol were analyzed by normalizing tail currents immediately after the test pulse to +10mV to the maximum current amplitude and plotted as a function of the membrane potential of the conditioning pulse. The data points were fitted with the Boltzmann function:

$$I = \frac{1}{\left(1 + \exp\left(\frac{V_m - V_{0.5,inact}}{K_{inact}}\right)\right)}$$

Where V_m is the test potential, $V_{0.5,inact}$ is the half-maximum voltage for pseudo-steady state inactivation, and k_{inact} is the slope factor of the curve.

As a measure for overall channel availability, the window conductance was determined. Window conductance exists at potentials whereby ion channels are already activated but not yet fully inactivated. This condition is present within the overlapping region under the intersection of activation and inactivation curves of $\text{Ca}_v1.4$ channels. For the quantification of window conductance, $V_{0.5}$ for activation and $V_{0.5,inact}$ for inactivation was corrected for the liquid junction potential. Window conductance was then calculated by multiplying the activation curve by the inactivation curve (Chemin et al., 2000; Liao et al., 2007).

To estimate the window conductance at physiological Ca^{2+} concentrations, the shift of $V_{0.5}$ of voltage dependent activation and inactivation was determined upon lowering Ca^{2+} concentration from 10mM to 2mM. The $V_{0.5}$ for activation was shifted by 5.3mV, $V_{0.5,\text{inact}}$ for inactivation by 2.0mV both to more hyperpolarized potentials. These shifts were used to correct window conductance for surface potential effects in all measurements using extracellular solution containing 10mM extracellular Ca^{2+} .

3.6.4 Calculation of the liquid junction potential (LJP)

The composition of the extracellular solution (bath solution) and the intracellular solution (Pipette solution) differs in whole-cell patch-clamp experiments considerably. The different ions, present at the interface between different solutions, form an interfacial potentials (=Liquid junction potential (LJP, V_{LJP})), due to their mobility. This potential is dependent on the mobility, charge and concentration of the ions.

The LJP were calculated using the software JPCalc (Barry, 1994).

During a patch clamp experiment, the amplifier adjusts command voltage V_{cmd} , but nevertheless, due to the offset potential this value is too large and must be corrected after the measurement.

$$V_m = V_{\text{cmd}} - V_{\text{LJP}}$$

The calculated liquid junction potential for calcium extracellular solutions is: 5.4mV for extracellular solution containing 10mM Ca^{2+} and 5.0mV for extracellular solutions containing 2mM Ca^{2+} .

Unless stated otherwise, the liquid junction potential was not corrected.

3.7 Statistical analysis

Data analysis, plotting, curve fitting, and statistical analysis were performed using Origin 7.5 (Microcal). All values are presented as mean \pm SEM for the indicated number "n" of experiments. An unpaired t test was performed for the comparison between two groups. Significance was tested by ANOVA followed by Dunett's test if multiple comparisons were made. P-values of less than 0.05 were considered significant. Significance levels are indicated as * ($p < 0.05$), ** ($p < 0.01$) and *** ($p < 0.001$).

4. Results

4.1 The regulation properties of retinal Ca_v1.4 channel by CaBP4

4.1.1 Ca_v1.4 channels are regulated by CaBP4

The Ca_v1.4 channels show relatively small amplitude compared with other LTCC, which makes it difficult to investigate and discover how different proteins regulate the channel. In order to overcome this problem, we established a new approach by using a stable HEK293 cells line expressing the pore subunit Ca_v1.4 α 1 (WT, 5A or Δ ICDI). Those stable cells show a high expression of the Cav1.4 pore subunit and do not express the CaBP4 endogenously (Fig. 4.1). In whole cell recordings, a robust Ca_v1.4 specific Ca²⁺ current could be observed, which made it possible to unravel how CaBP4 regulates the Ca_v1.4 channel.

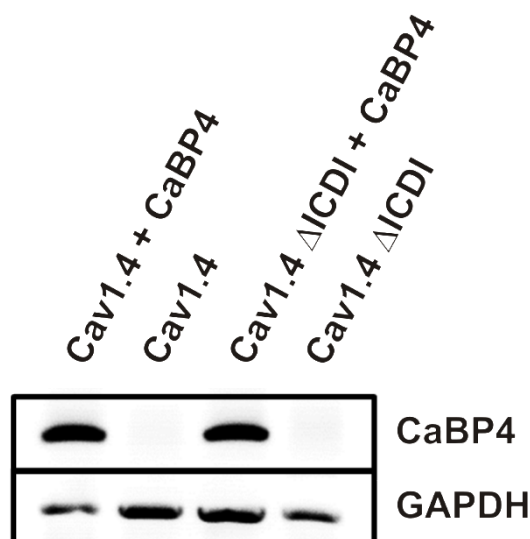


Figure 4.1 – CaBP4 is not expressed in HEK Ca_v1.4 stable cells. RT-PCR of CaBP4 from the two stable HEK cell lines, which were used in electrophysiological experiments. GAPDH serves as loading control.

4.1.1.1 The calcium dependent inactivation (CDI) in truncated Ca_v1.4 variants

The CaBP4 affects strongly the calcium dependent inactivation (CDI) in other LTCC, like in Ca_v1.2 and Ca_v1.3 (Cui et al., 2007; Yang et al., 2006). However, Ca²⁺ and Ba²⁺ currents recorded from Ca_v1.4 stable cell lines display no difference in time course of activation or inactivation irrespective of the absence or presence of CaBP4 (Fig. 4.2A and B, respectively). Under both conditions, no CDI could be observed.

RESULTS

The calcium and barium currents were measured on the same cells by stepping from a holding potential of -80mV to +10mV during a 350ms pulse. Current traces were normalized to peak current, and the Ba²⁺ traces were scaled to match Ca²⁺ traces (scale bar).

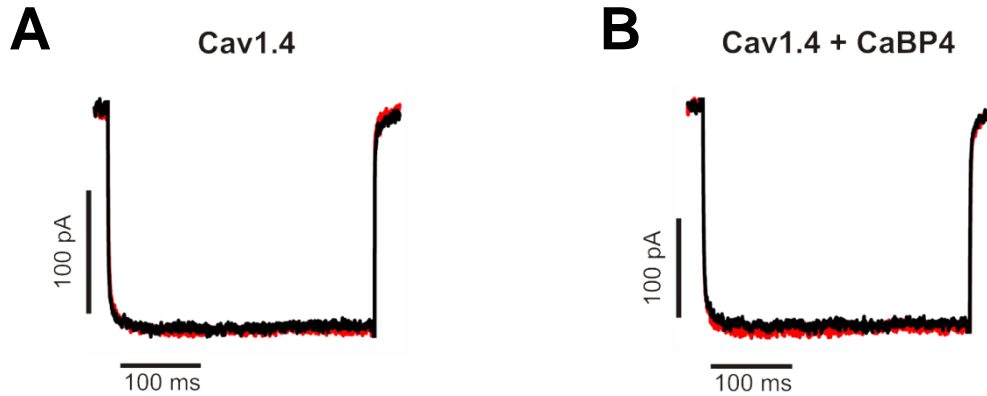


Figure 4.2 – Representative traces of I_{Ca} (red traces) and I_{Ba} (black traces) through Ca_v1.4 (A), Ca_v1.4 + CaBP4 (B), recorded in bath solution containing 10mM Ca²⁺ (red trace) or 10mM Ba²⁺ (black trace) as charge carrier.

Truncation of the ICDI domain in the distal C-terminus of Ca_v1.4 unmasked CDI, which is caused by endogenous CaM (Wahl-Schott et al., 2006) (Fig. 4.3A). In contrast, CaBP4 completely abolished CDI in Ca_v1.4 channels lacking the ICDI domain (Fig. 4.3B).

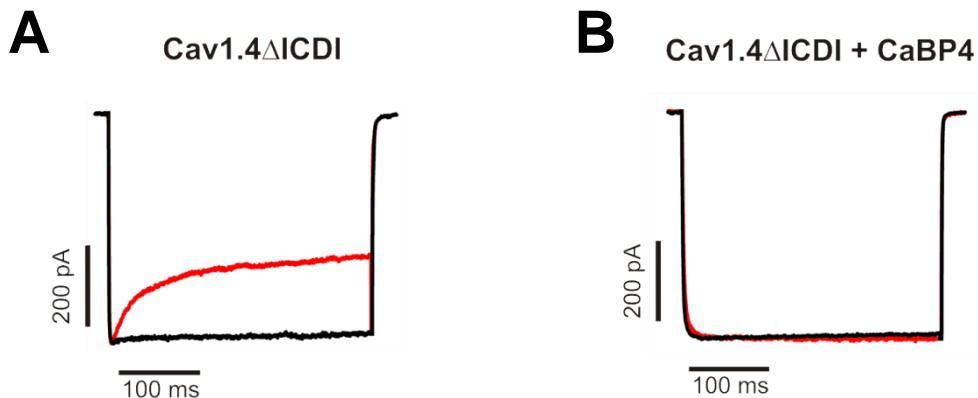


Figure 4.3 – Representative traces of I_{Ca} (red traces) and I_{Ba} (black traces) through Ca_v1.4ΔICDI (A) and Ca_v1.4ΔICDI + CaBP4 (B), recorded in bath solution containing 10mM Ca²⁺ (red trace) or 10mM Ba²⁺ (black trace) as charge carrier.

The CDI can be quantified as the value of R350 which corresponds to the fraction of I_{Ca} or I_{Ba} remaining after 350ms (Fig. 4.4 A and B)

RESULTS

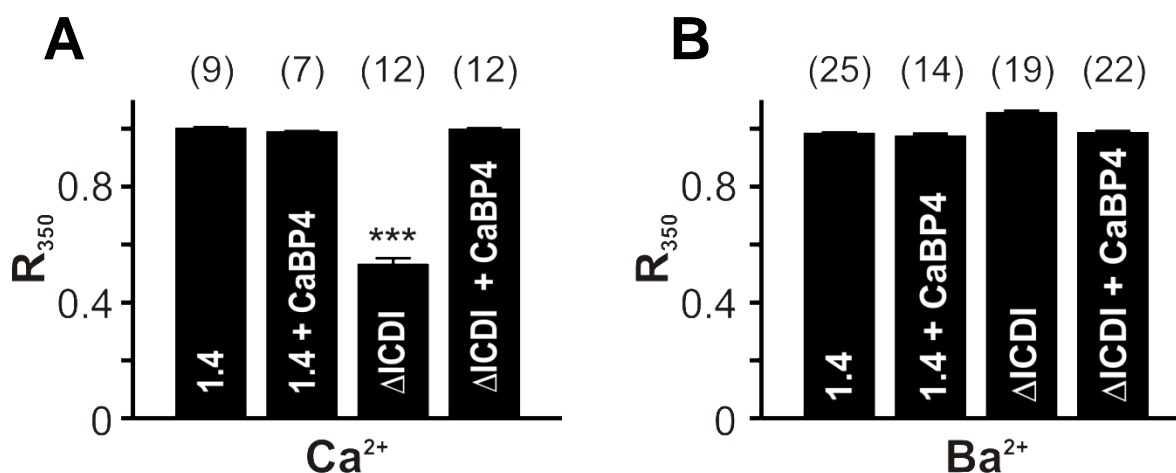


Figure 4.4 – Quantification of the CDI in figures 4.2 and 4.3: Fractional inactivation of I_{Ca} (A) or I_{Ba} (B) during a 350ms test pulse to V_{max} . The number of experiments is given in parentheses. Statistical significance is given in comparison to the other constructs of this panel.

These findings indicate that both CaBP4 and the ICDI domain have equivalent functions with regard to their effect on CDI. Both are able to inhibit the CDI of the $Ca_v1.4$ channel. Furthermore, these observations suggest that CaM and CaBP4 stabilize the channel in a different conformational state that gives rise to the absence of CDI in the case of CaBP4 and to the presence of CDI in the case of CaM.

4.1.1.2 CaBP4 increases $Ca_v1.4$ channel availability by modulating voltage dependent gating of the channel

To analyze the effect of CaBP4 on voltage dependence of $Ca_v1.4$, activation and inactivation curves for Ca^{2+} and Ba^{2+} (10mM) currents were determined in the absence and presence of CaBP4 using activation (Fig. 4.5A) and inactivation (Fig. 4.5B) protocols. The voltage dependent inactivation gating was characterized by using a pseudo-steady-state inactivation protocol, rather than true steady-state inactivation. In order to efficiently record inactivation, the protocol was adjusted and the prepulse lengths and inter-trial interval were shortened. However, induction of complete inactivation requires long prepulse length and long recovery interval between individual trials. Representative families of Ca^{2+} current traces of $Ca_v1.4$ from the protocols are displayed in figure 4.5. For the I/V relationships, peak current amplitudes were plotted against membrane potential (Fig. 4.5E and F).

RESULTS

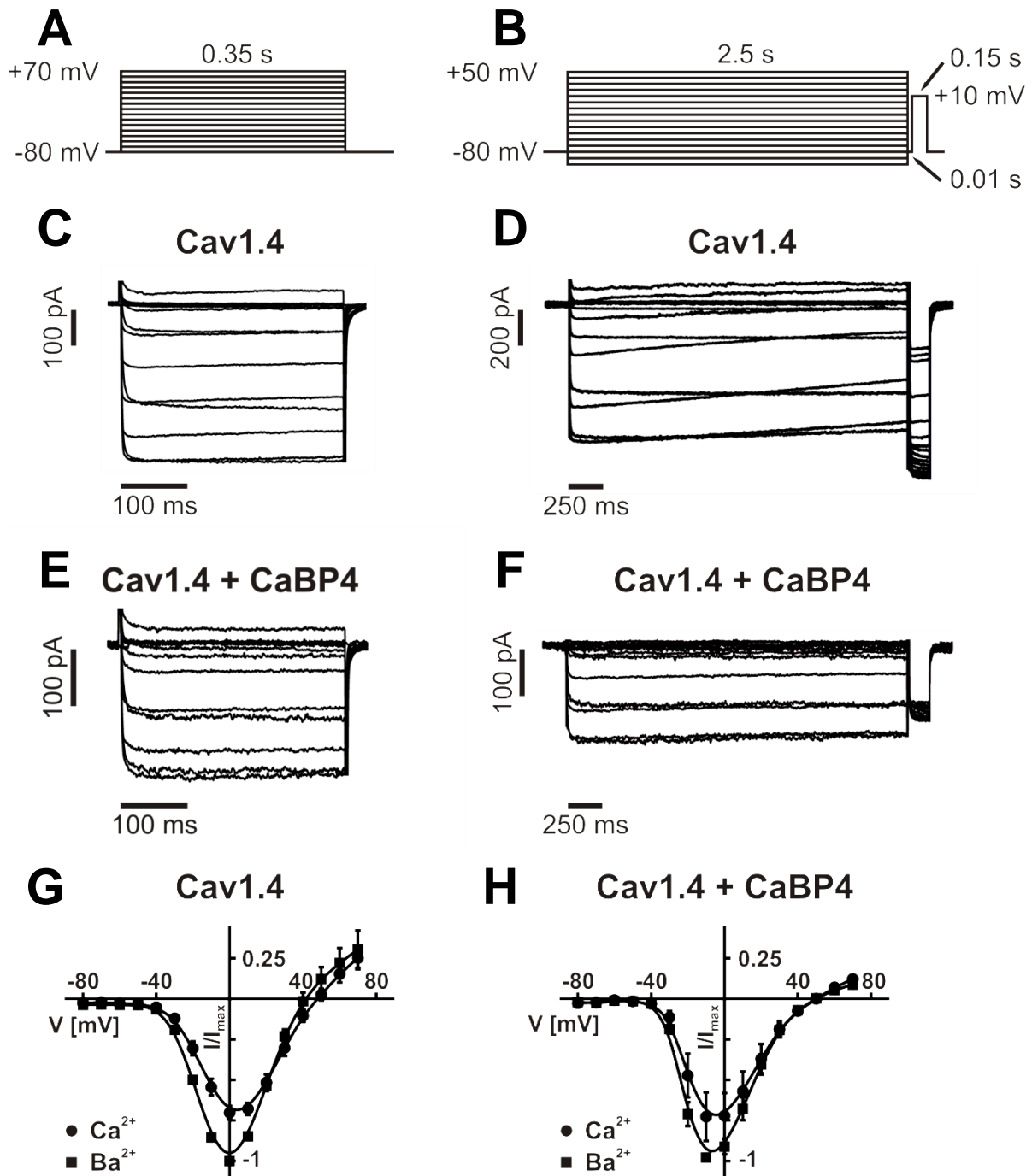


Figure 4.5 – Voltage dependent activation and inactivation of $\text{Ca}_v1.4$ in the absence and presence of CaBP4 . Voltage protocol used for the determination of activation properties (**A**) and of pseudo-steady state inactivation properties (**B**). Representative family of Ca^{2+} current traces for $\text{Ca}_v1.4$ in the absence (**C**), and presence of CaBP4 (**E**), using the activation protocol. Representative family of Ca^{2+} current traces for $\text{Ca}_v1.4$ in the absence (**D**) and presence of CaBP4 (**F**), using the pseudo-steady state inactivation protocol. I/V relationship for $\text{Ca}_v1.4$ in absence of CaBP4 (**G**) or in the presence of CaBP4 (**H**). In (**E**) and (**F**) currents were recorded in bath solution containing 10mM Ca^{2+} (circles) or 10mM Ba^{2+} (squares) as charge carrier. Currents were normalized to the peak Ba^{2+} current.

RESULTS

Using the two protocols for activation and pseudo-steady-state inactivation, the fractional activation and inactivation curves of $\text{Ca}_v1.4$ could be plotted in figure 4.6 as function of the voltage (mV), while Ca^{2+} or Ba^{2+} serve as charge carrier.

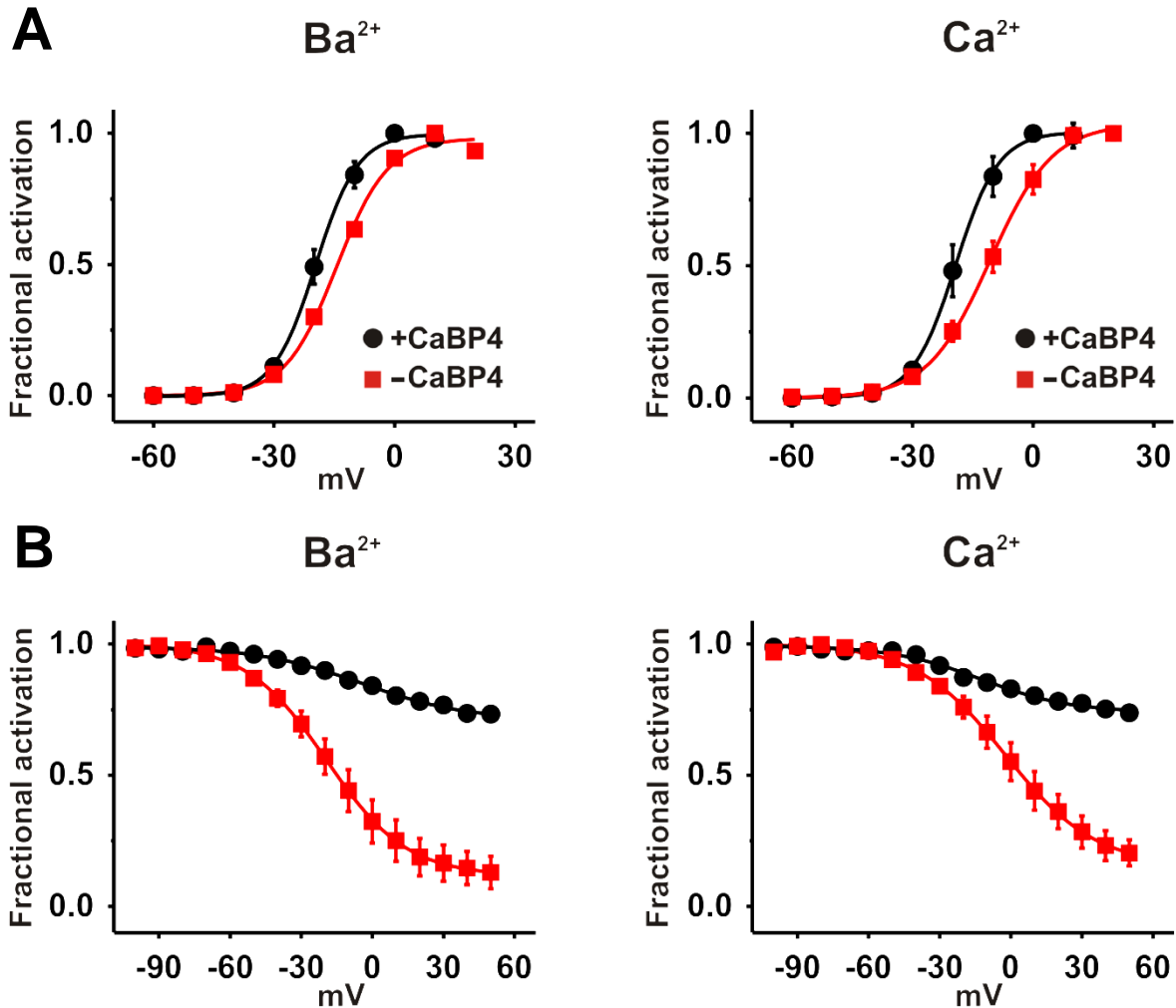


Figure 4.6 – The voltage dependent gating of $\text{Ca}_v1.4$ properties in the absence and presence of CaBP4. **(A)** Activation curves for $\text{Ca}_v1.4$ in the absence (red) and in the presence of CaBP4 (black). In the left panel Ba^{2+} (10mM) was the charge carrier and in the right panel Ca^{2+} (10mM) was the charge carrier. **(B)** Pseudo-steady state inactivation curve for $\text{Ca}_v1.4$ in the absence (red) and in the presence of CaBP4 (black).

Together the effects of CaBP4 on activation and inactivation lead to a pronounced increase of the window conductance which can be demonstrate by the overlap of the activation and the inactivation curve (Fig. 4.7).

RESULTS

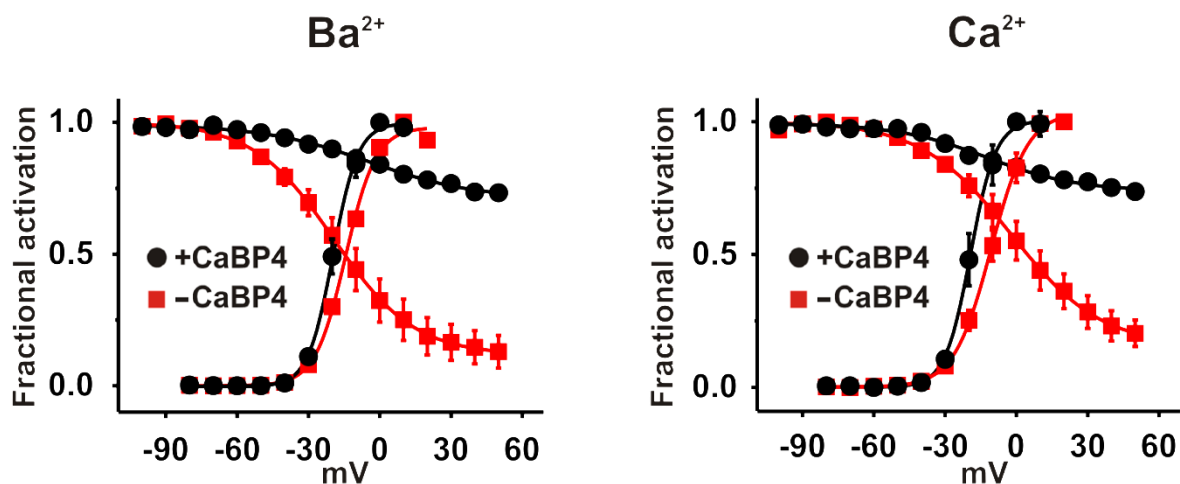


Figure 4.7 – CaBP4 increases dramatically the $\text{Ca}_v1.4$ channel availability. The overlay of activation curves presented in (Fig. 4.5A) and pseudo-steady state inactivation curves presented in (Fig. 4.5B) demonstrate an increase in availability of $\text{Ca}_v1.4$ in the presence of CaBP4.

The increase in the channel availability and window conductance are caused by three major facts: 1. The CaBP4 shifts the activation curve of $\text{Ca}_v1.4$ to more hyperpolarized potentials; 2. The CaBP4 increases the steepness of the activation curve (Table 8.6.1 – appendix 8.6); 3. The CaBP4 dramatically reduces pseudo-steady-state inactivation of the channel (Table 8.6.2 – appendix 8.6).

Similar experiments were carried out for $\text{Ca}_v1.4\Delta\text{ICDI}$ channels. Surprisingly, in the absence of the ICDI domain CaBP4 had no effect on voltage dependent activation and inactivation and window currents (Fig. 4.8). Moreover, voltage dependent activation and inactivation of $\text{Ca}_v1.4\Delta\text{ICDI}$ channels were very similar to that of wild type $\text{Ca}_v1.4$ channels in the presence of CaBP4. In the absence of the ICDI domain the only effect of the CaBP4 on the $\text{Ca}_v1.4$ was the blockade of the CDI (Fig. 4.3).

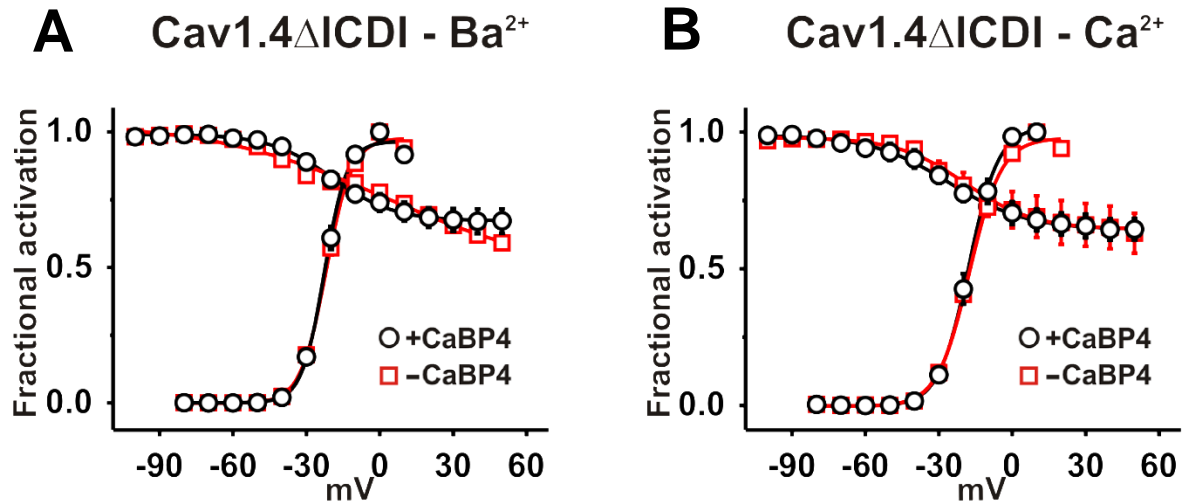


Figure 4.8 – In the absence of the ICDI domain the effect of CaBP4 on voltage dependent gating is abolished. Overlay of activation curves and pseudo-steady-state inactivation curves for Ba²⁺ (10mM; **A**) or Ca²⁺ (10mM; **B**) currents through Ca_v1.4ΔICDI channels in the absence (red) and the presence (black) of CaBP4.

Taking together these observations indicate that CaBP4 and the ICDI domain modulate the Ca_v1.4 in a complex fashion. Regarding to voltage dependent gating of Ca_v1.4 channels, the ICDI domain and CaBP4 have opposing functional effects. The ICDI domain shifts the activation curve of Ca_v1.4 to more depolarized potentials and increases inactivation, while CaBP4 shifts the activation curve of Ca_v1.4 to more hyperpolarized potentials and decreases inactivation. Concerning the inhibition of the CDI, the ICDI domain and CaBP4 have equivalent functional effects.

RESULTS

4.1.2 Functional alterations in two CaBP4 human mutations

So far, four different human mutations in the CaBP4 have been reported in the literature (Aldahmesh et al., 2010; Littink et al., 2009; Zeitz et al., 2006). Since two of the mutations cause either non-functional truncated protein or point mutation without major effect, this study focused to analyze the functional consequences of the other two human mutations which were associated with autosomal recessive forms of human congenital retinal disease CSNB2.

The expression of two CaBP4 mutant proteins was analyzed by Western blot from transfected HEK cells (Fig. 4.9). The first mutation (CaBP4-R216X) results in a truncated CaBP4 protein lacking the C-lobe that contains EF hand 3 and 4 (Littink et al., 2009). In the second CaBP4 mutant (CaBP4-E267fs) the last residue of EF hand 4 (E267) is exchanged to Valine followed by a frame shift elongating the protein (Zeitz et al., 2006).

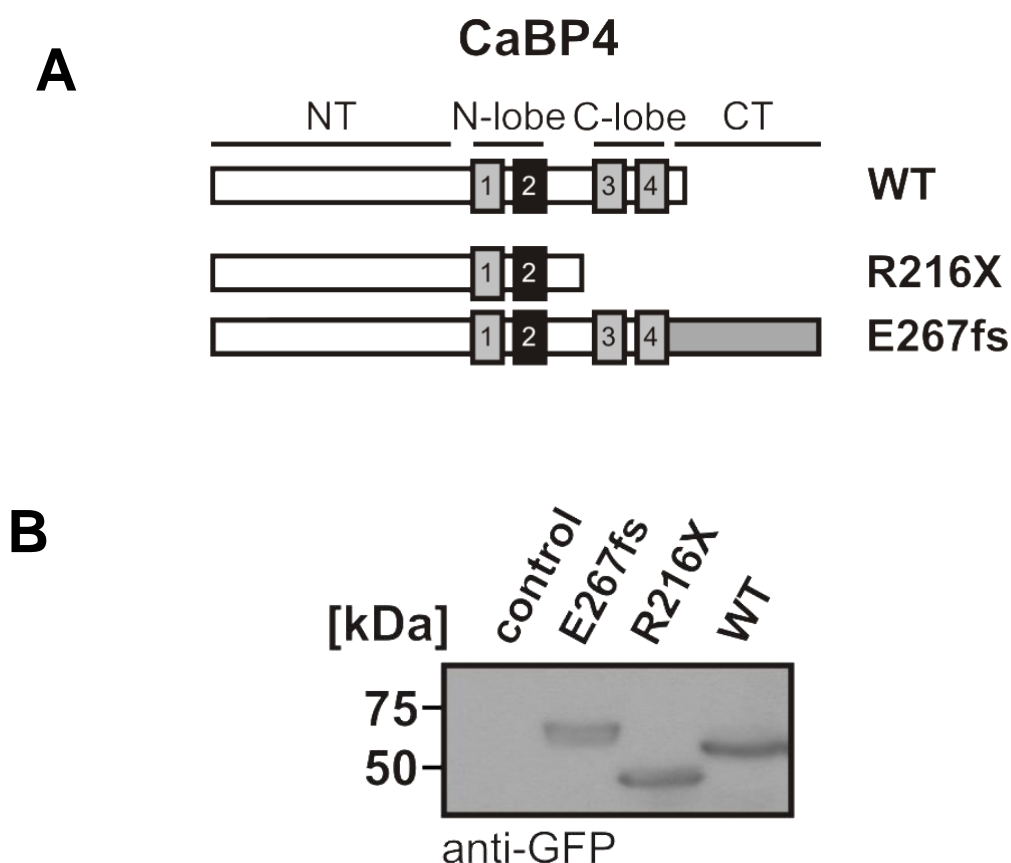


Figure 4.9 – Schematic representation and expression of the human CaBP4 mutants in HEK293 cells **(A)** Schematic description of the CaBP4 mutants compared to the WT. The boxes represent EF hands 1-4. Gray boxes: functional EF hands 1, 3 and 4; black box: nonfunctional EF hand 2. NT: N-terminus of CaBP4; CT: C-terminus of CaBP4. **(B)** Western blot demonstrating the expression of mutant variants and wild type CaBP4 fused to GFP.

RESULTS

In FRET experiments, both of the CaBP4 human mutants CaBP4-E267fs and CaBP4-R216X were shown to interact with the C-terminus of Ca_v1.4 even with higher FRET signal than that of wild type CaBP4 (Shaltiel et al., 2012). (These experiments were performed by Christos Pappas-C.P., data not shown).

The finding that CaBP4-R216X interacts with the C-terminus of Ca_v1.4 is very interesting because it shows that the N-lobe of CaBP4 is sufficient to interact with Ca_v1.4. Furthermore, the presence of CaBP4-E267fs and CaBP4-R216X may partially impair binding of the ICDI domain.

The functional impact of the CaBP4 mutations was analyzed in electrophysiological experiments (Fig. 4.10 and Fig. 4.11). After coexpression of CaBP4-R216X or CaBP4-E267fs together with wild type Ca_v1.4 channels, Ca²⁺ currents did not display CDI. In contrast, in coexpression experiments of mutated CaBP4s together with Ca_v1.4 Δ ICDI, CDI could be indeed observed, which was pronounced for CaBP4-R216X and subtle but detectable for CaBP4-E267fs (Figs. 4.10).

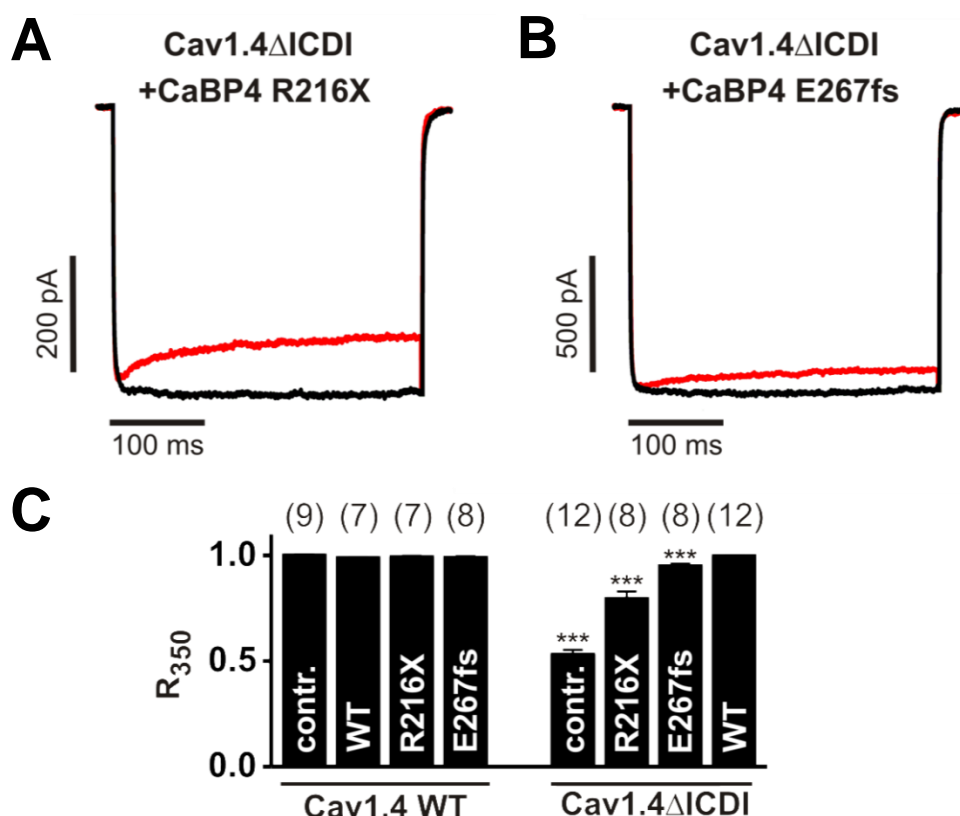


Figure 4.10 – The CaBP4 mutant variants display CDI. Representative traces of I_{Ca} (10mM; red traces) and I_{Ba} (10mM; black traces) through Ca_v1.4 Δ ICDI coexpressed with CaBP4-R216X (A) or CaBP4-E267fs (B). Currents were evoked by stepping from a holding potential of -80 mV to +10 mV (pulse duration: 350ms). Current traces were normalized to peak current. (C) Quantification of CDI as R₃₅₀ values. The number of experiments is given in parentheses. *** p<0.001. Statistical significance is given in comparison to WT.

RESULTS

The appearance of slow CDI in coexpression experiments of $\text{Ca}_v1.4\Delta\text{ICDI}$ channels and mutant CaBP4 suggests that endogenous CaM can access the effector site for CDI at least in some of the channels.

Next, the effect of CaBP4 mutations on voltage dependent gating of $\text{Ca}_v1.4$ was analyzed (Figs. 4.11). In contrast to wild type CaBP4, both CaBP4 mutations did not shift voltage dependent activation to more hyperpolarized potentials. For CaBP4-E267fs the activation curve was even shifted by about 6mV to more depolarized potentials in experiments using Ca^{2+} as charge carrier (Fig. 4.11 B).

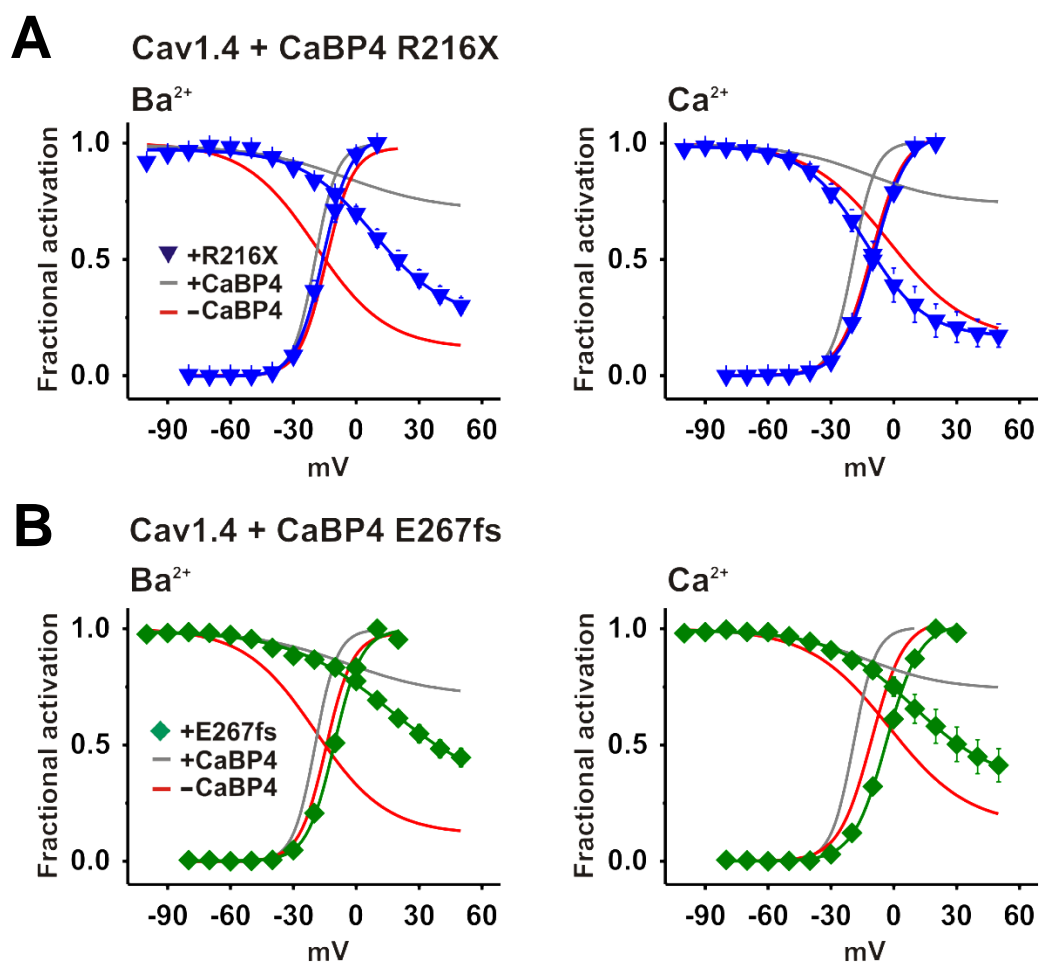


Figure 4.11 – Mutant CaBP4 variants reduce $\text{Ca}_v1.4$ channel availability as compared to WT CaBP4. Overlay of activation and pseudo-steady-state inactivation curves for $\text{Ca}_v1.4$ coexpressed with CaBP4-R216X (**A**) and CaBP4-E267fs (**B**). For comparison activation and pseudo-steady-state inactivation curves for $\text{Ca}_v1.4$ in the absence (red) and presence of CaBP4 (grey) are indicated. Graphs for Ba^{2+} (10mM) are shown on the left, those for Ca^{2+} (10mM) on the right.

RESULTS

Slope factors of both CaBP4 mutations were significantly higher than those observed in the presence of CaBP4 and very similar to that observed in the absence of CaBP4 (Table 8.6.1 – appendix 8.6). CaBP4 mutants like wild type CaBP4 functionally reduce the inactivation process (Table 8.6.2 – appendix 8.6). However, the effect of mutant CaBP4s was significantly less pronounced as compared to wild type CaBP4.

4.1.3 Window conductance and availability of the Ca_v1.4 channel under physiological extracellular Ca²⁺ concentrations

In order to determine the correct window conductance for Ca_v1.4 channels closed to the physiological extracellular Ca²⁺ concentrations, recordings with a extracellular solution containing 2mM Ca²⁺ were performed (Fig. 4.12).

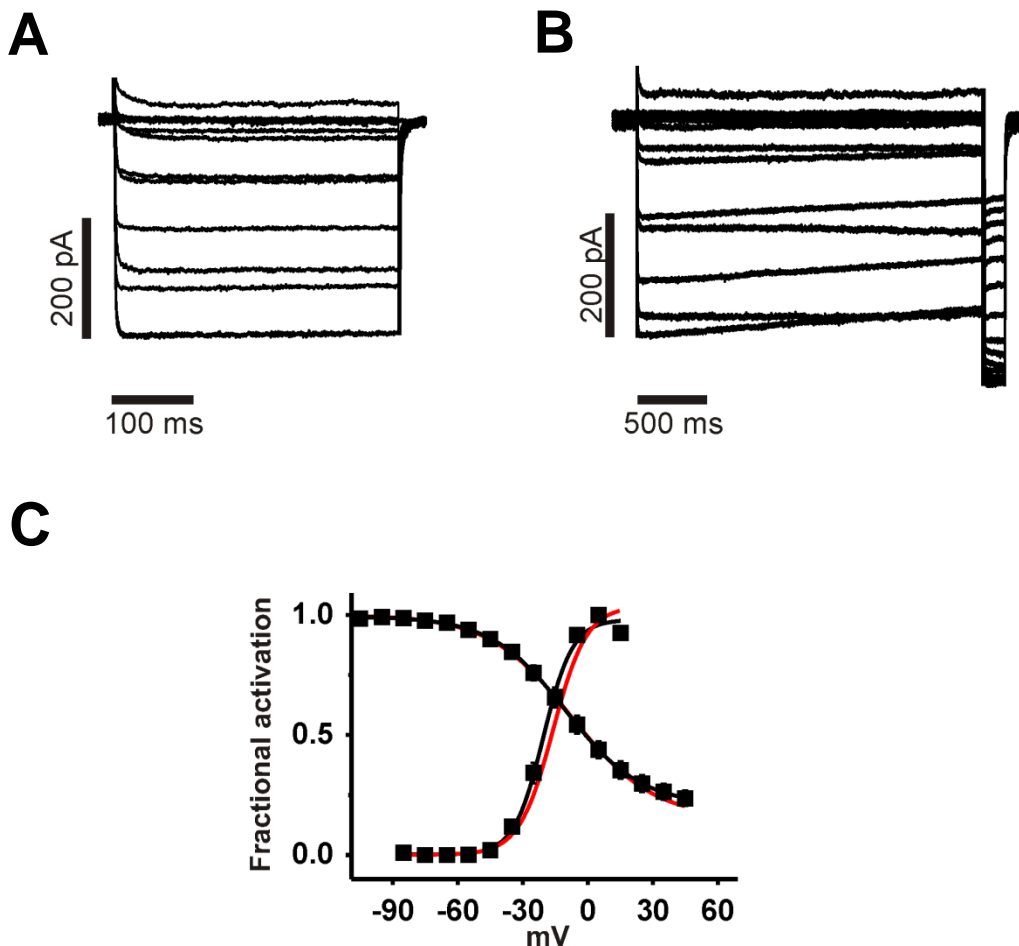


Figure 4.12 – Ca_v1.4 activation and inactivation measured in physiological extracellular Ca²⁺ (2 mM) concentration. **(A-B)** Representative family of Ca²⁺ current traces recorded by applying the activation protocol **(A)** or the pseudo-steady-state inactivation protocol **(B)**. **(C)** Lowering extracellular Ca²⁺ from 10mM (red line) to 2mM (black squares) results in a shift of the voltage dependent activation curve (n=9) and the voltage dependent inactivation (n=12) curve both to more hyperpolarized potentials.

RESULTS

Lowering extracellular Ca^{2+} from 10mM to 2mM results in a shift of the voltage dependent activation curve of 5.3mV and a shift of the voltage dependent pseudo-inactivation curve of 2.0mV, both to more hyperpolarized potentials. Therefore, under more physiological conditions, the window conductance was shifted to more hyperpolarized potentials, Compared to standard extracellular recording solution containing 10mM Ca^{2+} .

Based on the experimentally determined voltage shift in 2mM Ca^{2+} , all the window conductances obtained in experiments using standard recording solutions (10mM extracellular Ca^{2+}) were also corrected (Fig. 4.13).

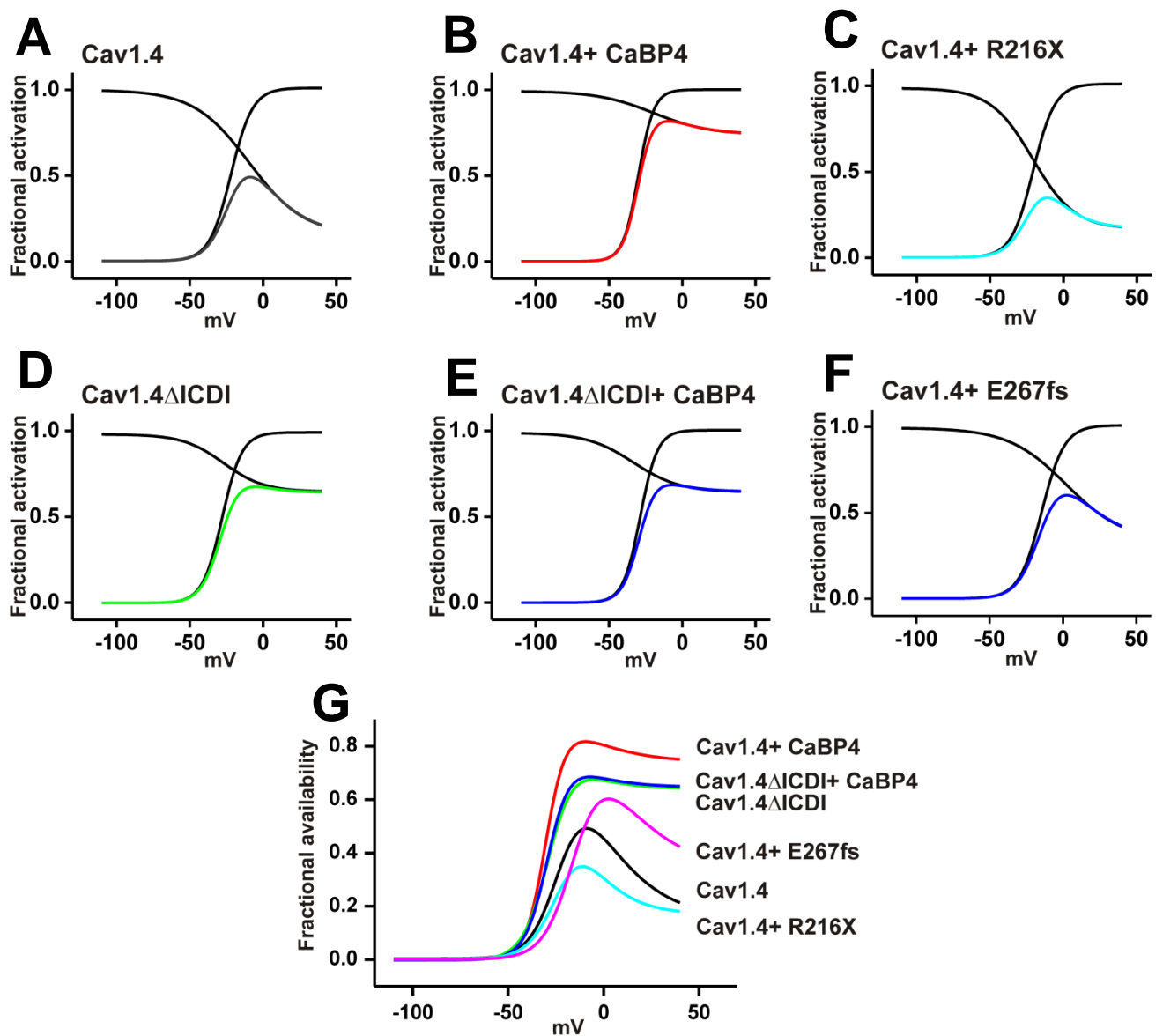


Figure 4.13 – Predicted availability of $\text{Ca}_v1.4$ wild type or $\text{Ca}_v1.4\Delta\text{ICDI}$ channels in the absence or presence of CaBP4 wild type or CaBP4 mutants as indicated (**A-F**). (**G**) Fractional availability for combinations as indicated in A-F. The predicted availabilities are calculated for 2mM extracellular Ca^{2+} .

RESULTS

To calculate the availability of $\text{Ca}_v1.4$ wild type or $\text{Ca}_v1.4\Delta\text{ICDI}$ channels window conductances were determined by multiplying the normalized activation curve with the normalized inactivation curve.

The comparison revealed that in the presence of CaBP4 the predicted window conductance for the physiological conditions of 2mM Ca^{2+} was more than 2-fold larger than in the absence of CaBP4 (Figs. 4.14 A). To reflect more the physiological voltage range observed in photoreceptors (less than -30mV), window conductances at -30mV and -40mV were calculated too (Fig. 4.14B).

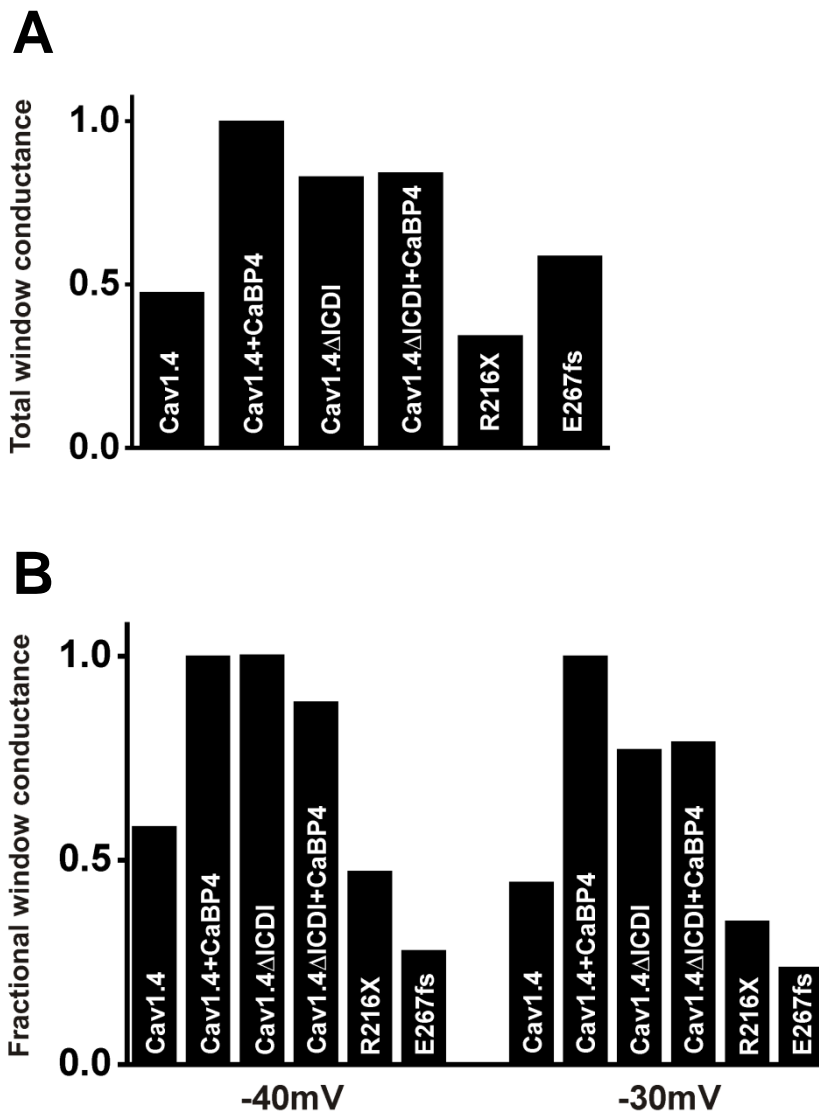


Figure 4.14 – Quantification of total and physiologically relevant window conductance at -30 mV and -40 mV . **(A)** Comparison of total window conductances taken from Fig. 4.13 (A-F). **(B)** Window conductances at -30 mV and -40 mV as indicated. Conductances are normalized to $\text{Ca}_v1.4 + \text{CaBP4}$.

RESULTS

Fig. 4.14 indicates that the window conductance was 2.2-fold or 1.7-fold higher in the presence of CaBP4 at -30 or -40mV, respectively. Moreover, the observed effects in CaBP4 mutants significantly decreased the predicted window conductance as compared to wild type CaBP4; 2-fold or 3-fold for CaBP4-R216X at -40mV or -30mV, respectively and 3-fold or 4-fold for CaBP4-E267fs at -40mV or -30mV, respectively. These observations indicate that CaBP4 markedly increased overall $Ca_v1.4$ channel availability, and changes in $Ca_v1.4$ channel availability are significantly less pronounced in the presence of mutant CaBP4 proteins than in the presence of wild type CaBP4. This effect was equally pronounced for Ca^{2+} and Ba^{2+} currents, indicating that this effect is not Ca^{2+} dependent.

4.1.4 CaBP4 binds to the IQ motif in the C-terminus of $Ca_v1.4$

FRET experiments were carried out by C.P. to further examine the interaction between CaBP4 and $Ca_v1.4$, using YFP-tagged variants of $Ca_v1.4$ C-terminus and CFP-CaBP4. In those experiments, it was found that CaBP4 interacts with the C-terminus of both wild type $Ca_v1.4$ and $Ca_v1.4\Delta ICDI$. Moreover, like other CaBPs and/or CaM, CaBP4 binds to the IQ motif in the C-terminal tail of $Ca_v1.4$. In these experiments, 5 residues within the IQ motif in the CT $Ca_v1.4$ were replaced by 5 alanines (1.4/5A). The CaBP4 was not able to interact with 1.4/5A C-terminus, which indicating that CaBP4 and CaM share the same binding domain on the C-terminus of $Ca_v1.4$.

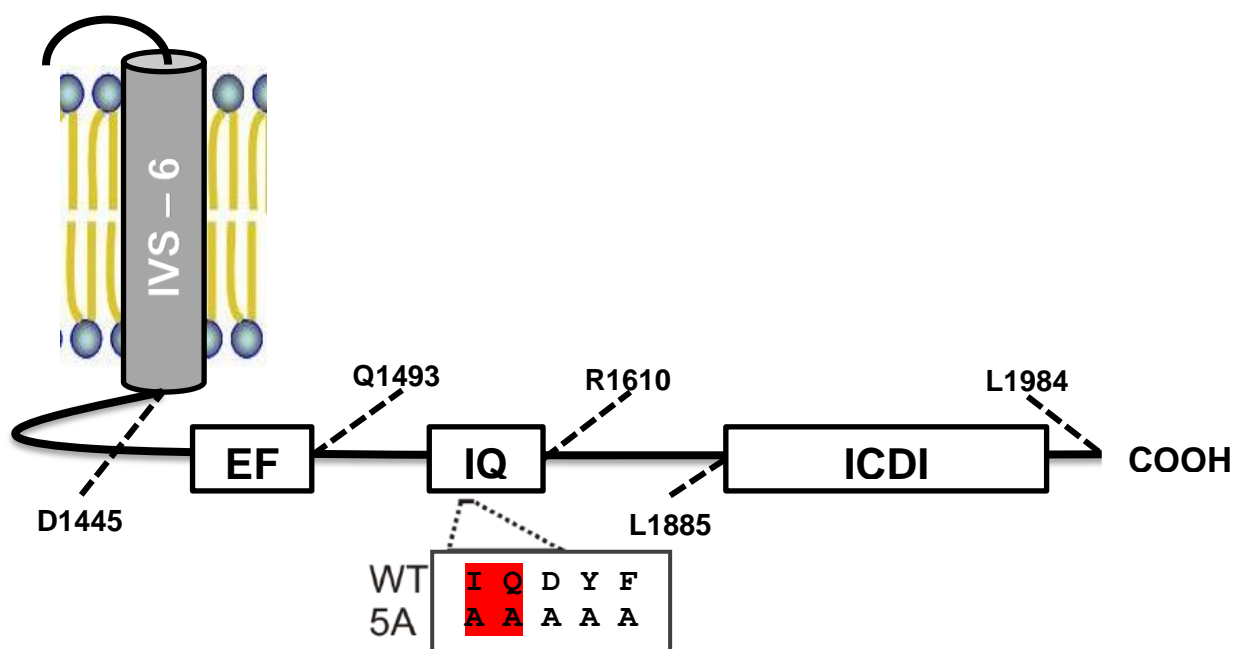


Figure 4.15 – Schematic representation of the $Ca_v1.4/5A$ C-terminus. The highly conserved amino acids are highlighted in red.

RESULTS

Electrophysiological measurements by patch clamp technique of the $\text{Ca}_v1.4/5A$ channel variant may provide further insights how the IQ motif is important to the CaM and CaBP4 regulation of the channel. These experiments may also help us to explain why the activation curve of the human mutant CaBP4-E267fs was even shifted to more depolarized potentials in experiments using Ba^{2+} and Ca^{2+} as charge carrier.

The activation and inactivation curves of $\text{Ca}_v1.4/5A$ as function of the voltage (mV) were plotted using the two protocols for activation and pseudo-steady-state inactivation, where Ca^{2+} or Ba^{2+} served as charge carrier (Fig. 4.16 A and B). The $\text{Ca}_v1.4/5A$ curves were compared to wild type $\text{Ca}_v1.4$ and $\text{Ca}_v1.4\Delta\text{ICDI}$. For both of the charge carriers, the activation curves shift between 5mV to 10mV to more depolarized potential, whereas the inactivation of the $\text{Ca}_v1.4/5A$ were reduced compared to the $\text{Ca}_v1.4$ WT channel. These results also confirm that the endogenous CaM itself, by binding to the $\text{Ca}_v1.4$ in the IQ motif, shifts the activation to more hyperpolarized potential. However, this shift is less pronounced compared to the CaBP4.

In order to find if the CaBP4 is still able to regulate the channel without the ability to bind to the IQ motif, HEK293 cells stably expressing the $\text{Ca}_v1.4/5A$ variant were transfected with CaBP4 (Fig. 4.16 C). Surprisingly, in electrophysiological recordings from these cells, CaBP4 causes an increase in the channel availability and window conductance due to the following effects: 1. The CaBP4 shifts the activation curve of $\text{Ca}_v1.4/5A$ to more hyperpolarized potentials, but less pronounced compared to the shift in $\text{Ca}_v1.4$ WT channel; 2. The CaBP4 increases the steepness of the activation curve; 3. Finally, the CaBP4 is able to reduce the pseudo-steady-state inactivation of the channel. This result suggests that the CaBP4 has a second binding site on the $\text{Ca}_v1.4$ beyond the IQ motif.

RESULTS

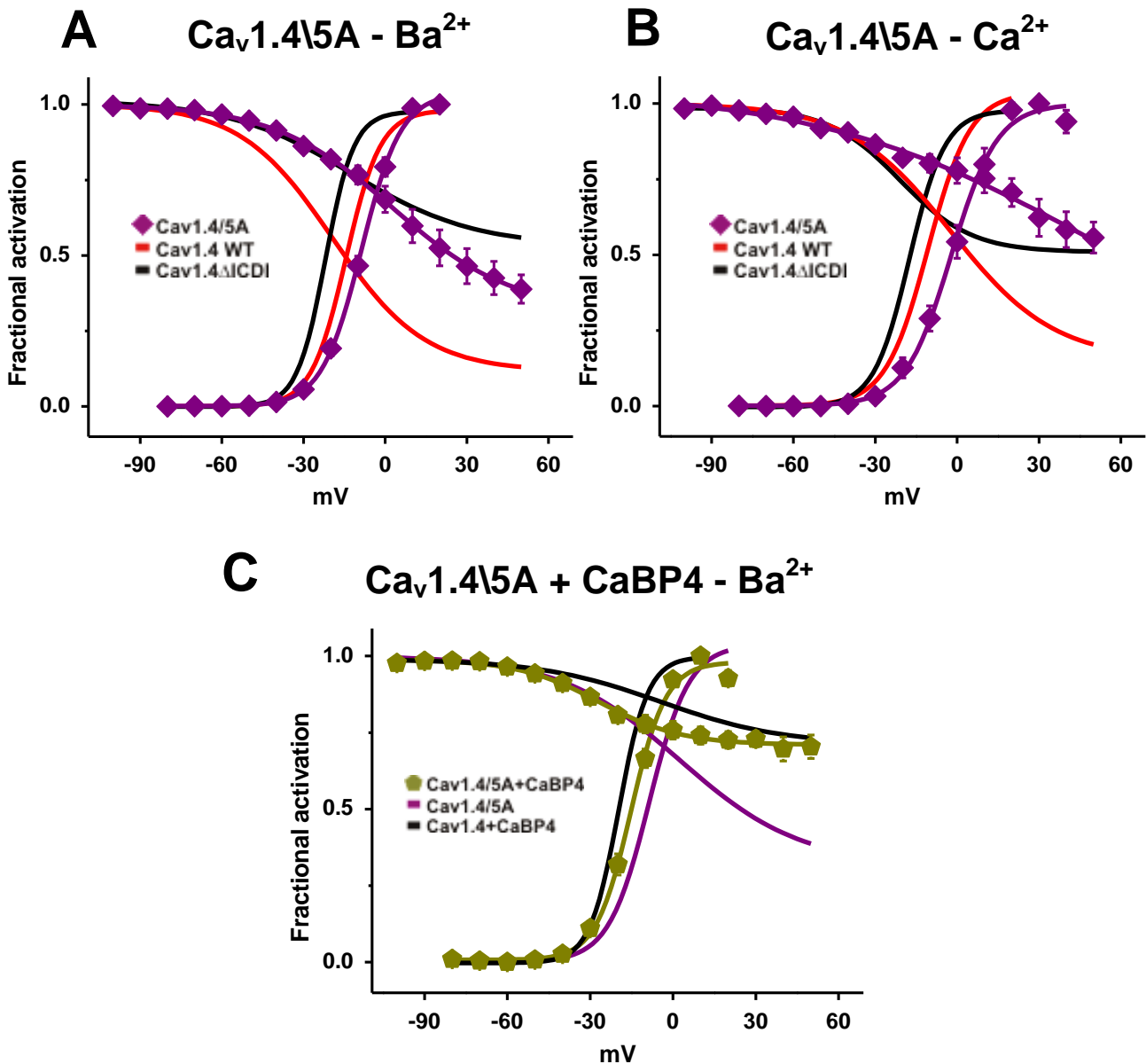


Figure 4.16 – CaBP4 can even change the channel availability of the $\text{Ca}_v1.4/5A$ variant. **(A-B)** Overlay of activation and pseudo-steady-state inactivation curves for the $\text{Ca}_v1.4/5A$ channel variant (purple) compared to the activation and pseudo-steady-state inactivation curves for $\text{Ca}_v1.4$ (red) and $\text{Ca}_v1.4\Delta\text{ICDI}$ (black). Graphs for Ba^{2+} as charge carrier (10mM; activation $n=9$, inactivation $n=8$) are shown on the left **(A)**, those for Ca^{2+} as charge carrier (10mM; activation $n=7$, inactivation $n=5$) on the right **(B)**. **(C)** The overlay of activation curves and pseudo-steady state inactivation curves for the $\text{Ca}_v1.4/5A$ channel variant in presence of CaBP4 (yellow) in bath solution containing 10mM Ba^{2+} (activation $n=13$, inactivation $n=7$) as charge carrier. For comparison activation and pseudo-steady-state inactivation curves for $\text{Ca}_v1.4$ in presence of CaBP4 (black) and the $\text{Ca}_v1.4/5A$ channel variant in the absence of CaBP4 (purple) are shown.

4.2 Characterization of the $Ca_v1.4$ channels function *in-vivo*

In the second part of this study, we have focused to characterize the *in-vivo* the function of $Ca_v1.4$ channels using genetic modified mice lacking $Ca_v1.4$ $\alpha1$ pore subunit ($Ca_v1.4^{-/-}$ - $Ca_v1.4$ KO). The mice were obtained from Dr. Marion Maw, University of Otago, North Dunedin, New Zealand (Specht et al., 2009). In these mice, the *CaCNA1F* locus was globally disrupted through homologous recombination by a Cre/loxP based deletion of exons 14-17, which encode the transmembrane helices 8-12 located in domain 2 of the channel protein (Fig. 4.17 A).

$Ca_v1.4$ deficient mice were born at the expected Mendelian ratio, were fertile and showed no visible behavioral and physical abnormalities. The deletion of exon 14-17 of the $Ca_v1.4$ gene was confirmed at the level of genomic DNA by Southern blot analysis (Fig. 4.17 B).

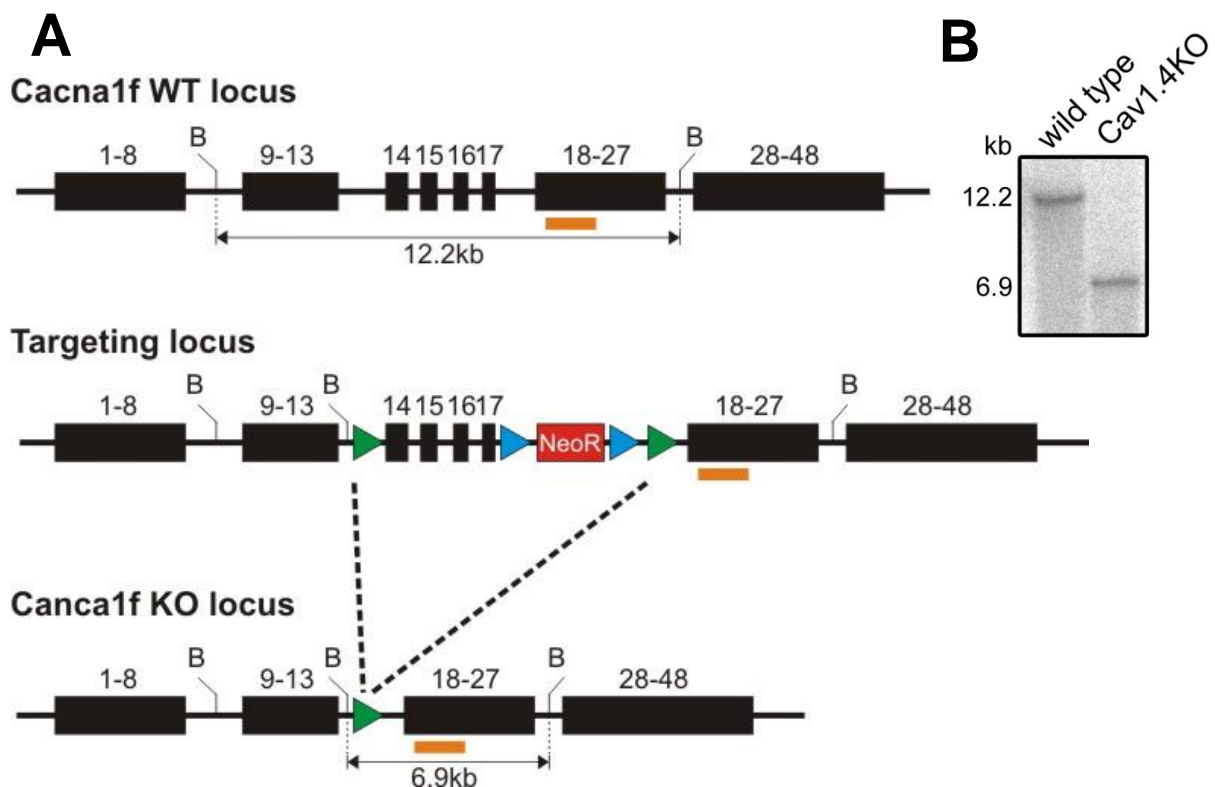


Figure 4.17 – The *Cacna1f* targeting locus. **(A)** Schematic display of the *Cacna1f* wild type (WT) locus (top) the targeting locus (middle) and the knockout (KO) locus (bottom). The targeting locus has a FRT site (blue arrowhead) flanked neomycin resistance selection cassette (NeoR) and two loxP sites (green arrowheads) that flank exons 14-17 and the NeoR cassette. Cre recombinase mediated excision of the loxP flanked sequence results in the KO locus that lacks exons 14-17. B, Bgl-II restriction enzyme recognition site. All exons except 14-17 are shown in a condensed view. The position of the probe used for the southern blot in panel B is marked by an orange line. **(B)** Southern blot on Bgl-II digested genomic DNA from wild type (left lane) and $Ca_v1.4$ KO (right lane) mice.

RESULTS

Furthermore, the protein expression of $Ca_v1.4$ in the $Ca_v1.4$ KO mice was also analyzed, using immunohistochemistry. In the wild type retinae, $Ca_v1.4$ could be detected in the OPL and to a lesser extent in the IPL, while in retinae from $Ca_v1.4$ KO mice the $Ca_v1.4$ immunoreactivity was not present in the OPL and IPL (Fig. 4.18 B). To exclude the possibility that the expression levels of other voltage gated Ca^{2+} channels or auxiliary subunits which are present in the retina are altered in response to the global deletion of $Ca_v1.4$, a quantitative PCR analysis of the retina was performed (Fig. 4.18 A).

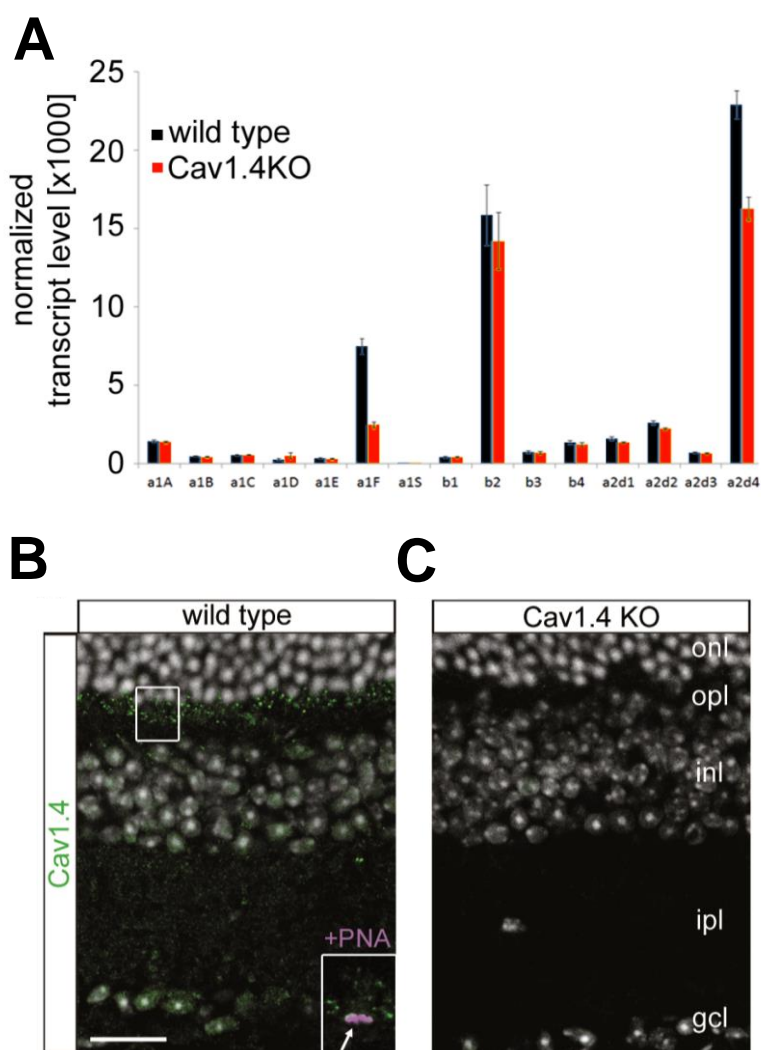


Figure 4.18 – Analysis of the *Cacna1f* KO ($Ca_v1.4$ KO) mice **(A)** Quantitative reverse transcriptase PCR gene expression analysis of all relevant L-type calcium channel subunits from wild type (black bars) and $Ca_v1.4$ KO retina (red bars). **(B-C)** Confocal scans of vertical retinal sections from wild type **(B)** and $Ca_v1.4$ KO mice **(C)** labeled with a $Ca_v1.4$ -specific antibody (green). Cell nuclei were stained with the nuclear dye Hoechst 33342 (grey). Inlay in B: magnification of the outer plexiform layer (opl) region marked with a white rectangle illustrating the partial co-localization of the $Ca_v1.4$ signal with the cone pedicle marker peanut agglutinin (PNA, magenta). The scale bar marks 20 μ m. gcl: ganglion cell layer, inl: inner nuclear layer, ipl: inner plexiform layer, onl: outer nuclear layer.

RESULTS

The data show that the number of transcripts for the major voltage gated Ca^{2+} channels and auxiliary subunits are unchanged in $\text{Ca}_v1.4$ KO mice, excepting for $\alpha2\delta4$ and $\alpha1F$. This finding indicates that compensatory remodeling or changes in gene expression of other Ca_v channels or subunits are not a relevant issue in the $\text{Ca}_v1.4$ -deficient retina.

To evaluate the overall retinal function of $\text{Ca}_v1.4$ KO mice, a Ganzfeld Electroretinograms (ERGs) was carried out using specific stimulation protocols to differentiate between the rod- and cone-driven activities. In the dark-adapted (scotopic) part of the protocol, in which cones are non-responsive, the b-wave component and oscillatory potentials were completely absent in ERG recordings of $\text{Ca}_v1.4$ KO mice as compared to wild-type mice throughout the stimulus range. In $\text{Ca}_v1.4$ KO mouse, the amplitude and the threshold of the a-wave was similar in all mice tested (Fig. 4.19 A). In the light-adapted (photopic) part of the protocol, in which rods are non-responsive due to desensitization, ERG recordings in the b-wave component and oscillatory potentials were completely absent in ERG recordings of $\text{Ca}_v1.4$ KO mice, while the amplitude and the threshold of the a-wave was similar to wild type mice (Fig. 4.19 B). The absence of a scotopic and photopic b-wave in the $\text{Ca}_v1.4$ KO mice is consistent with a defect in neurotransmission between rod and cone photoreceptors and second-order neurons, particularly bipolar cells.

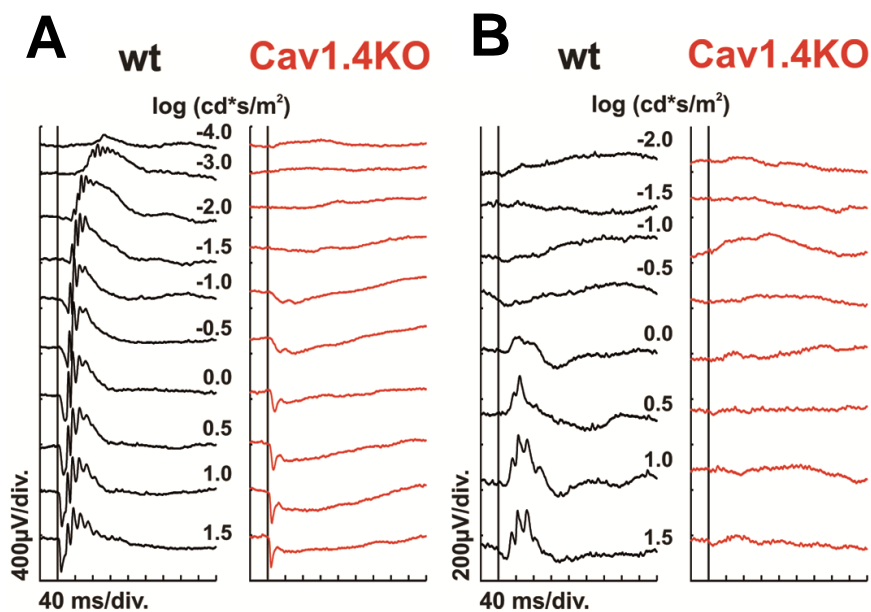


Figure 4.19 – Electroretinographic analysis of retinal function in $\text{Ca}_v1.4$ KO mice. Representative Ganzfeld-ERG intensity series from dark-adapted (**A**) and light-adapted (**B**) wild type (wt, black traces) and $\text{Ca}_v1.4$ KO mice (red traces).

RESULTS

The functional significance of the observed defects in the ERG responses was evaluated by testing the visual performance of $Ca_v1.4$ KO mice in a visual water-maze behavioral task. The latency to locate a visible platform under dark and normal light conditions was significantly increased in $Ca_v1.4$ KO as compared to wild type mice (Fig. 4.20). In more than 30% of the trials in the dark and more than 20% of the trials during light $Ca_v1.4$ KO mice did not manage to find the platform (error of omission). By contrast, there was no error of omission in wild type mice.

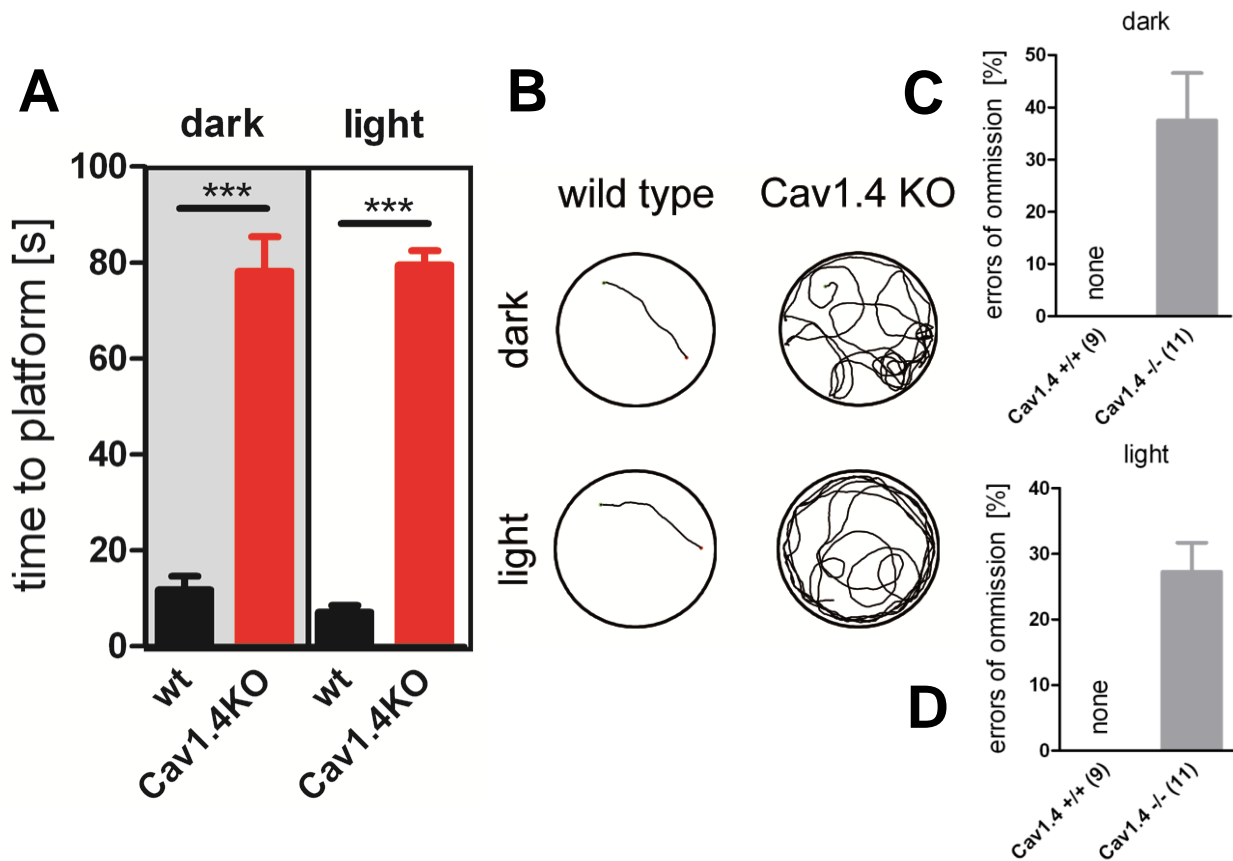


Figure 4.20 – Performance of $Ca_v1.4$ KO mice in a visual water-maze behavioral task. **(A)** Latency to locate a visible platform under dark (left two bars) and normal light conditions (right two bars). **(B)** Example swimming paths under dark (upper part) and normal light conditions (lower part). **(C)** Errors of omission under dark **(D)** and normal light conditions **(D)**.

During a three days training period performed under dark light conditions, wild type mice dramatically improved locating the visible platform, while in $Ca_v1.4$ KO mice no improvement was observed. Furthermore, under normal light conditions (day four) no further improvement was observed in either group (Fig. 4.21).

RESULTS

A similar learning curve was also observed during a three days training period performed under normal light conditions. $Ca_v1.4$ KO mice did not show any improvement during the test period. Consistent with the increased latency the swimming path was much longer (Fig. 4.20 B) and the average and not the maximal swimming speed was reduced in $Ca_v1.4$ KO mice as compared to wild type mice (Fig. 4.21 C and D).

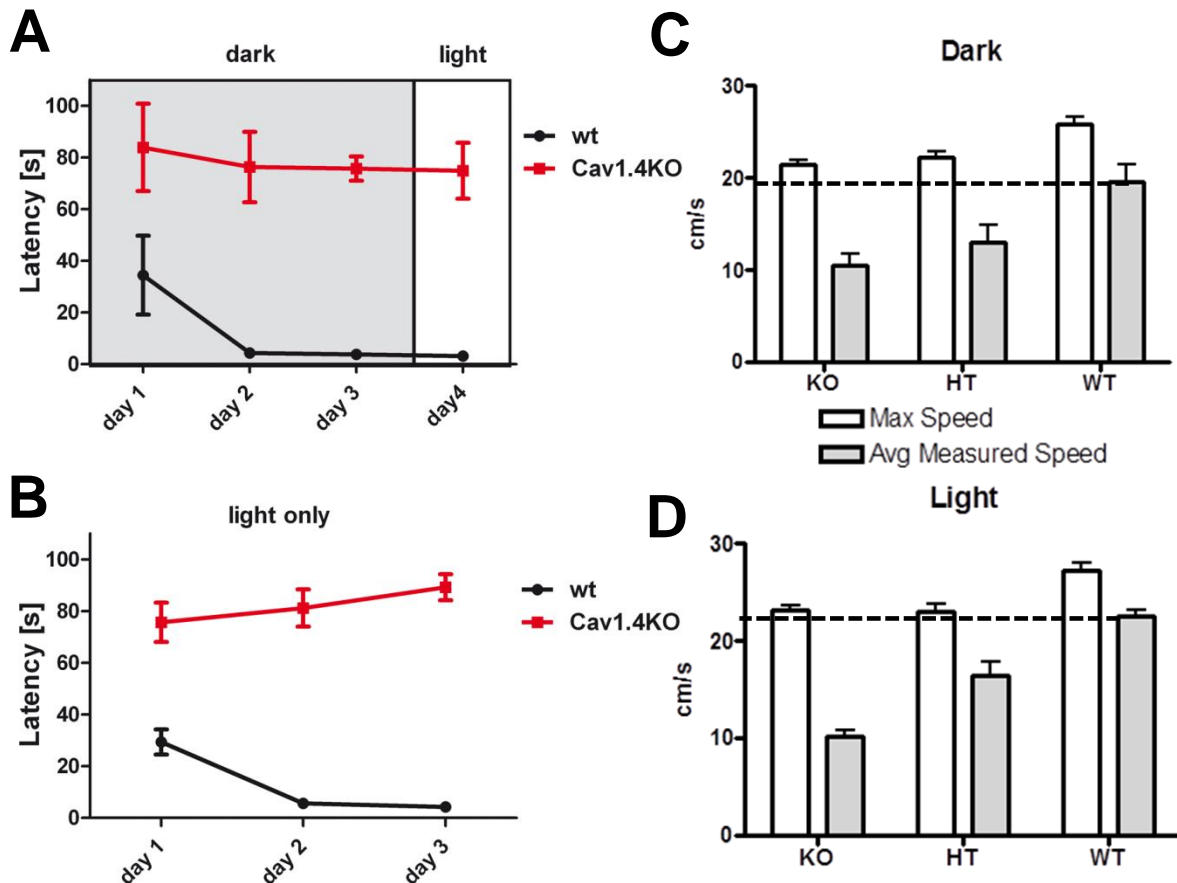


Figure 4.21 – A visual water-maze performance over three days training period. **(A)** Learning curves for wild type (wt) and $Ca_v1.4$ KO mice in the visual water-maze behavioral task under dark (days 1-3) and normal light conditions (day 4). **(B)** Learning curves for wt and $Ca_v1.4$ KO mice in the visual water-maze behavioral task on three consecutive days under normal light conditions. **(C-D)** Maximal swimming speed and the average (Avg) measured speed of $Ca_v1.4$ KO, heterozygote (HT) and wt mice under dark **(C)** and normal light conditions **(D)**.

Synaptic changes in the retinal network architecture caused by $Ca_v1.4$ deletion in *Cacna1f* deficient mice were characterized by immunohistochemistry. These experiments revealed marked changes in second-order neurons in $Ca_v1.4$ KO mice. Stainings of wild-type retinas using the horizontal and amacrine cell marker calbindin showed strong labeling of horizontal cell bodies and a dense plexus of horizontal cell

RESULTS

processes in the *opl* (Fig. 4.22 A). By contrast, in retinas of $Ca_v1.4$ KO mice, calbindin staining was reduced in the *opl*, and horizontal cell processes extended far into the *onl* in young (Fig. 4.22 B) and aged animals (Fig. 4.22 C).

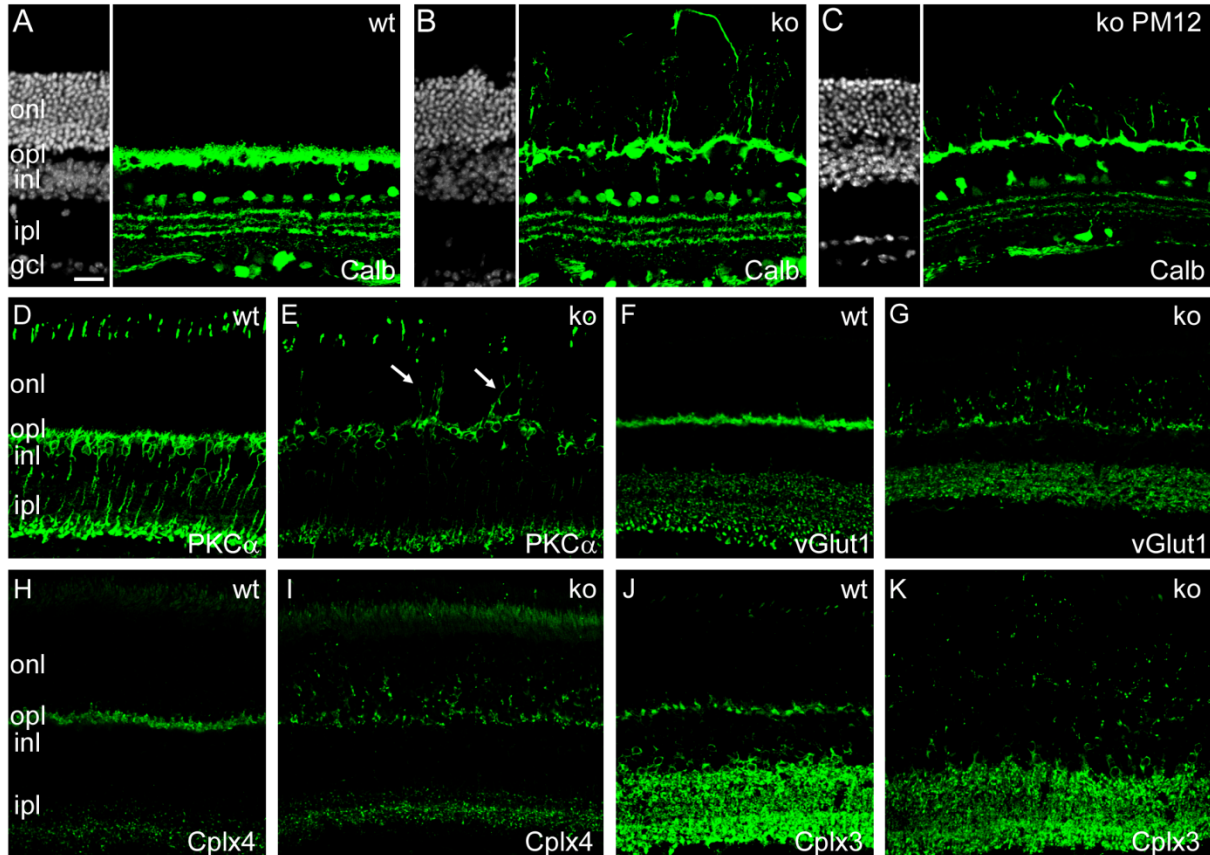


Figure 4.22 – Confocal scans of vertical retinal sections from wild type (wt) (A) and $Ca_v1.4$ KO mice (B-C). Immunolabeling of horizontal and amacrine cells with calbindin (Calb, green, right parts in A-C). The cell nuclei were stained with the dye Hoechst 33342 (grey) to illustrate the retinal layers (left part in A-C). Horizontal cell neurites extent deep into the outer nuclear layer (*onl*) in young (6-week-old) (B) and aged (12-month-old, PM 12) ko mice (C). Retinal sections from 6-week-old wt and ko mice immunolabeled with the rod bipolar cell marker protein kinase C alpha ($PKC\alpha$) (D-E), as well as with the presynaptic markers vesicular glutamate transporter 1 (vGlut1) (F-G), Complexin 4 (Cplx4) (H-I) and complexin 3 (cplx3) (J-K). The scale bar shown in (A) marks 20 μ m.

In wild-type retinas stainings by $PKC\alpha$, a rod bipolar cell marker, showed regular arborisation of bipolar cell dendrites restricted to the *opl* (Fig. 4.22 D). In contrast, $PKC\alpha$ staining in retinas of $Ca_v1.4$ KO mice demonstrates pronounced growth of the rod bipolar cell dendrites extended beyond the *opl*, far into the *onl* (Fig. 4.22 arrows in E). Note that $PKC\alpha$ also labels cone outer segments (upper part in D and E), which appear disorganized in $Ca_v1.4$ KO mice (Fig. 4.22 E).

RESULTS

Evaluation of the overall structure revealed outgrowth of neurites from the *opl* into the *onl* and caused a marked thinning of the *opl* in $Ca_v1.4$ KO retinas as compared to wild type retinas (Fig. 4.22 A-C). Presynaptic markers were used to test whether this outgrowth leads to the formation of ectopic synapses between photoreceptor terminals and aberrant dendrites of rod bipolar and horizontal cells, which were displaced out of the *opl* and into the *onl* stainings. The presynaptic markers reveal a disperse redistribution of rod (vGlut1 and Cplx4) and cone (Cplx3) presynaptic elements from the *opl* to the *onl* in the $Ca_v1.4$ KO mice (Fig. 4.22 G, I and K), compared to the wild type mice (Fig. 4.22 F, H and J). The presynaptic markers confirmed a greatly reduced immunoreactivity in the *opl* and an increased punctuated staining in the *onl* in $Ca_v1.4$ KO mice as compared to wild type mice. These results are consistent with a loss of synaptic contacts in the *opl* and the formation of ectopic synapses in the *onl*. In addition, specific staining of horizontal cell neurites by NF200 demonstrate a pronounced outgrow of neurites into the *onl* (not shown).

Together, these findings indicate both, disturbed photoreceptor to rod bipolar cell and horizontal cell contacts with pronounced outgrow of neurites into the *onl*. In contrast, Calbindin-expressing amacrine and ganglion cells appeared identical in the wild-type and $Ca_v1.4$ KO retinas.

The expression and localization of the rod arrestin, a rod photo-transduction cascade protein, was not affected in outer segments of rod photoreceptors in the $Ca_v1.4$ KO mice (Fig. 4.23 A, B). However, the synaptic fraction of rod arrestin (arrows in A) was lost from the *opl* and was partially found in the *onl* (arrows in B). In addition, staining of cone photoreceptors by cone arrestin was markedly down regulated throughout the cone cells in $Ca_v1.4$ KO mice (Fig. 4.23 C, D). In line with this finding, specific labeling of cone photoreceptor extracellular matrix by peanut lectin revealed a loss of cone pedicle whereas the morphology of the cone inner and outer segments (*is*, *os*) was preserved (Fig. 4.23 E, F). In $Ca_v1.4$ KO retinas, the present GFAP-positive stress fibers are indicating a reactive gliosis. Together, these findings indicate that there is an ongoing rod and cone photoreceptor synaptopathy and reactive gliosis in the $Ca_v1.4$ KO mouse.

RESULTS

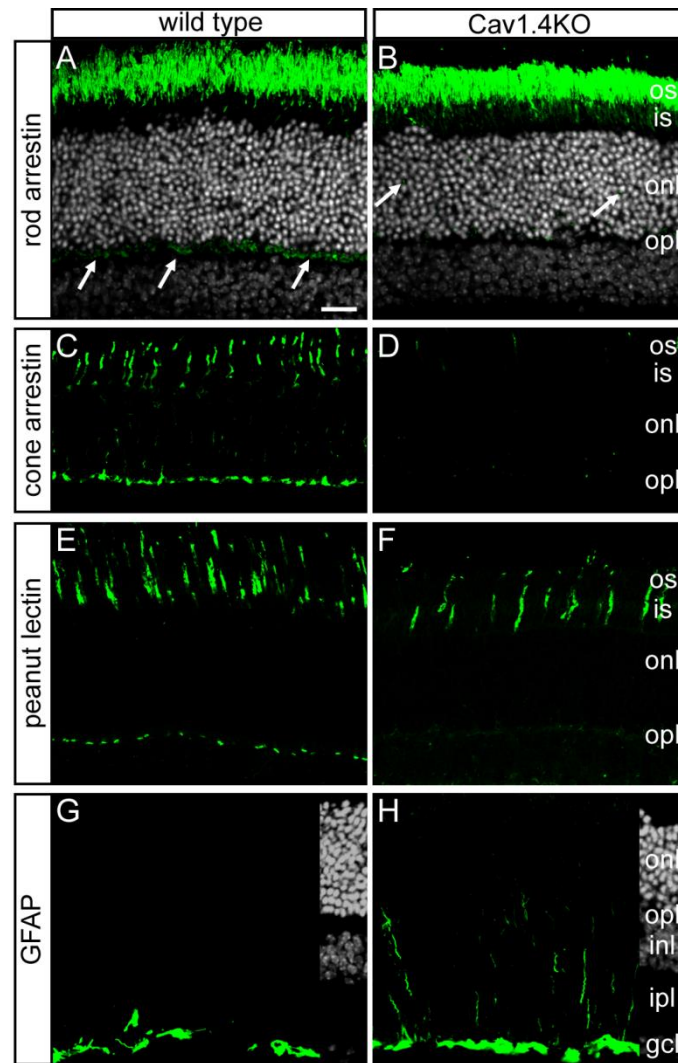


Figure 4.23 – Photoreceptor morphology in $Ca_v1.4$ KO mice. Confocal scans of vertical retinal sections from 6-week-old wild type (wt) and $Ca_v1.4$ KO mice labeled for rod arrestin (**A-B**), cone arrestin (**C-D**), peanut lectin (**E-F**) and GFAP-positive stress fibers (**G-H**). The right part (in panels G-H) represents Hoechst 33342 (grey) nuclear staining of the respective retinal slices. The scale bar marks 20 μ m. *gcl*: ganglion cell layer; *inl*: inner nuclear layer; *ipl*: inner plexiform layer; *onl*: outer nuclear layer; *is*, inner segment and *os*: outer segment.

Next, we were examining whether the changes observed in male $Ca_v1.4$ deficient mice are also present in heterozygous (hz) females ($Ca_v1.4^{+/-}$). Interestingly, the hz mice show a pronounced mosaic (patchy) photoreceptor synaptopathy (Fig. 4.24), which can be characterized by islets of $Ca_v1.4$ immunoreactivity and areas without $Ca_v1.4$ immunoreactivity next to each other (Fig. 4.24 A-C).

RESULTS

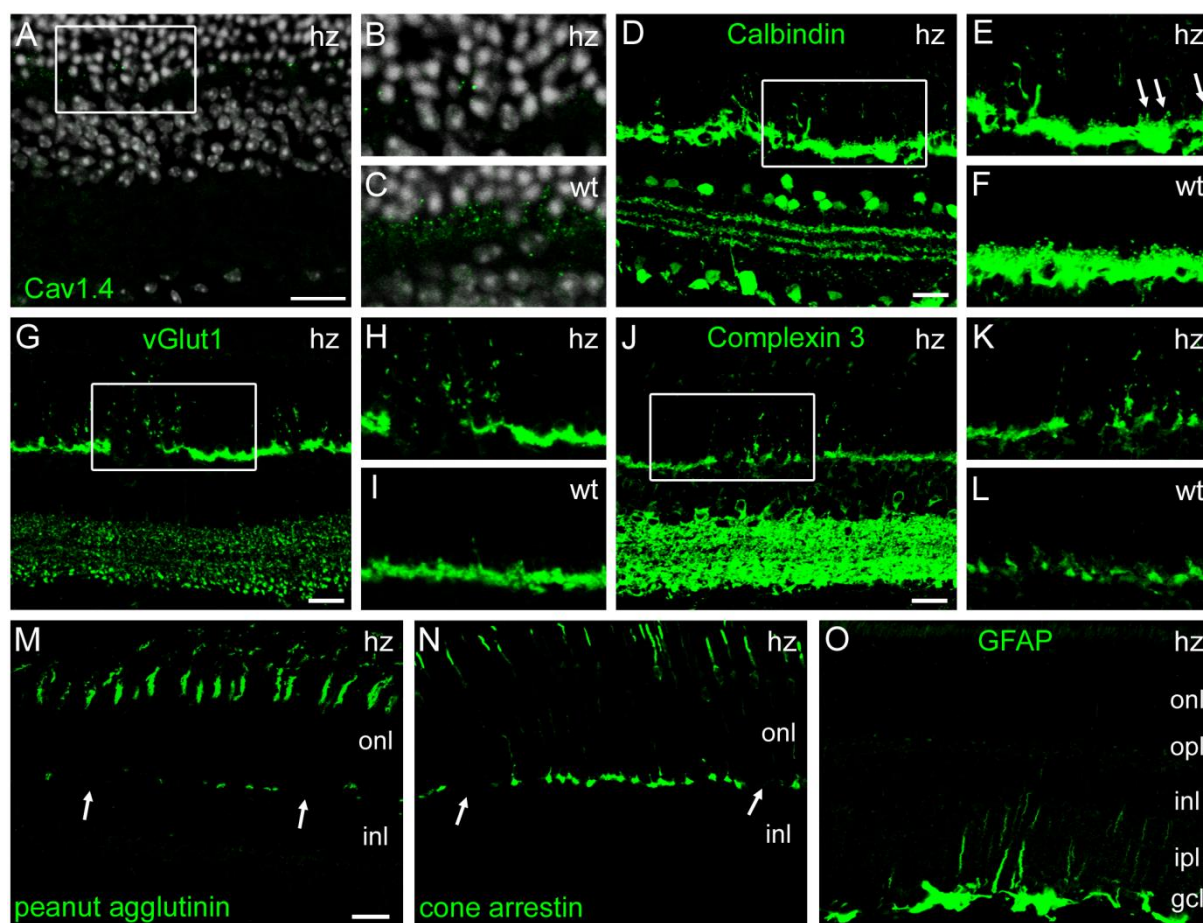


Figure 4.24 – Mosaic synaptopathy in $Ca_v1.4$ hz mice. Confocal scans of vertical retinal sections from $Ca_v1.4$ hz mice. **(A)** Representative image from an hz mouse labeled with a $Ca_v1.4$ -specific antibody (green). **(B)** Magnification view on the outer plexiform layer region marked with a white rectangle in **(A)**. **(C)** Magnification view on the corresponding region from a wild type control mouse labeled with a $Ca_v1.4$ -specific antibody (green). Cell nuclei in **(A-C)** were stained with the nuclear dye Hoechst 33342 (grey). **(D-L)** Retinal sections from hz **(D-E, G-H and J-H)** and wt **(F, I and L)** mice immunolabeled for calbindin (Calb) **(D-F)**, vGlut1 **(G-I)** and complexin 3 (cplx3) **(J-L)**. The regions marked with a white rectangle in panels **(D, G and J)** are shown in **(E, H and K)**, respectively. **(F, I and L)** show corresponding immuno-stainings from wt mice. **(M-O)** Representative image from hz mice labeled for peanut agglutinin **(M)**, cone arrestin **(N)** and GFAP **(O)** reveal a mosaic loss of synaptic cone structures and reactive gliosis in the hz. The scale bar marks 20 μ m. *gcl*: ganglion cell layer; *inl*: inner nuclear layer; *ipl*: inner plexiform layer; *onl*: outer nuclear layer; *opl*: outer plexiform layer.

In line with this finding, stainings for calbindin (Fig. 4.24 D-F), vGlut1 (Fig. 4.24 G-I), and complexin 3 (Fig 4.24 J-L) revealed a similar patchy histology pattern with areas characterized by the KO phenotype and wild type areas close to each other. Specifically, retinal network columns lacking $Ca_v1.4$ consistently showed outgrowths of horizontal cell neurites and bipolar cell dendrites into the *onl* and a reduction of the *opl*. In addition, a pronounced loss of synaptic cone structures and degeneration was

RESULTS

observed in KO-like retinal columns in the $Ca_v1.4$ hz mice (Fig 4.24 M and N), in addition to a reactive gliosis (Fig. 4.24 O).

By co-staining analysis using pre and postsynaptic markers, the formation of ectopic disturbed contacts between the photoreceptor and bipolar or horizontal cells could be observed. The disturbed contacts are characterized by horseshoe shaped wild type-like presynaptic structures synapsing to aberrant rod bipolar and horizontal cell dendrites (Fig 4.25). Together, these findings are consistent with a pronounced mosaic rod and cone photoreceptor synaptopathy.

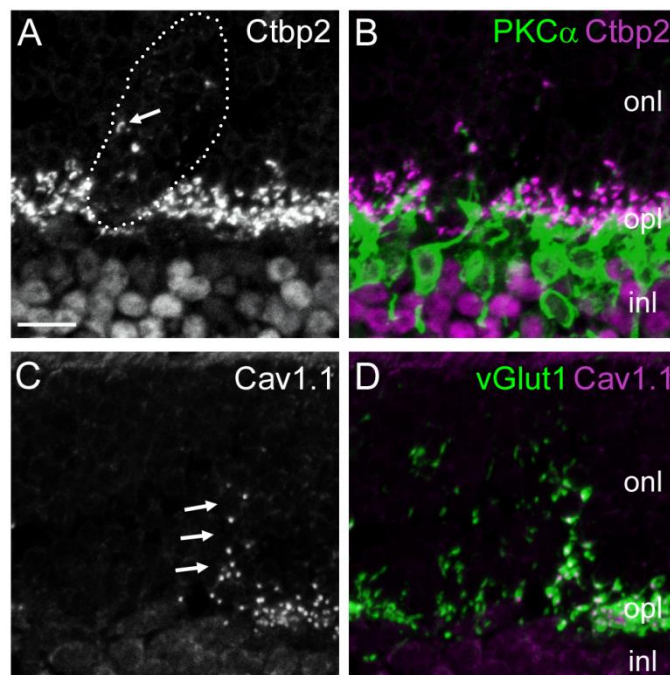


Figure 4.25 – Pre- and postsynaptic changes in $Ca_v1.4$ heterozygous mice. High resolution confocal scans of vertical retinal sections from $Ca_v1.4$ hz mice double-labeled for a combination of pre- a postsynaptic marker proteins. **(A)** Immunostaining for the ribbon synapse marker C-terminal binding protein 2 (Ctbp2). The affected area is encircled with a dotted line. The arrow marks an ectopic wild type-like horseshoe shaped Ctbp2-positive structure at the border of the affected area. **(B)** Merged image for Ctbp2 (magenta) and $PKC\alpha$ (green). **(C)** Immunostaining for the postsynaptic L-type calcium channel subunit 1.1 ($Ca_v1.1$). The arrows point to $Ca_v1.1$ -positive synapse at the border of the affected area. **(D)** Merged image for $Ca_v1.1$ (magenta) and vGlut1 (green). The scale bar marks 10 μm . *inl*: inner nuclear layer; *onl*: outer nuclear layer; *opl*: outer plexiform layer.

The functional consequences of these morphological changes were tested by ERG measurements. In scotopic ERG in heterozygous female mice (Fig 4.26 A) revealed significantly reduced b-wave amplitude (Fig 4.26 A, B) and also reduced oscillatory potentials as compared to wild-type mice throughout the stimulus range. The threshold of the b-wave was normal in $Ca_v1.4^{+/-}$ mice. The amplitude and the

RESULTS

threshold of the a-wave were similar in all mice tested ($n=5$ $Ca_v1.4^{+/-}$; $n=2$ WT). Similar changes were observed for the photopic ERGs (Fig 4.26 C, D).

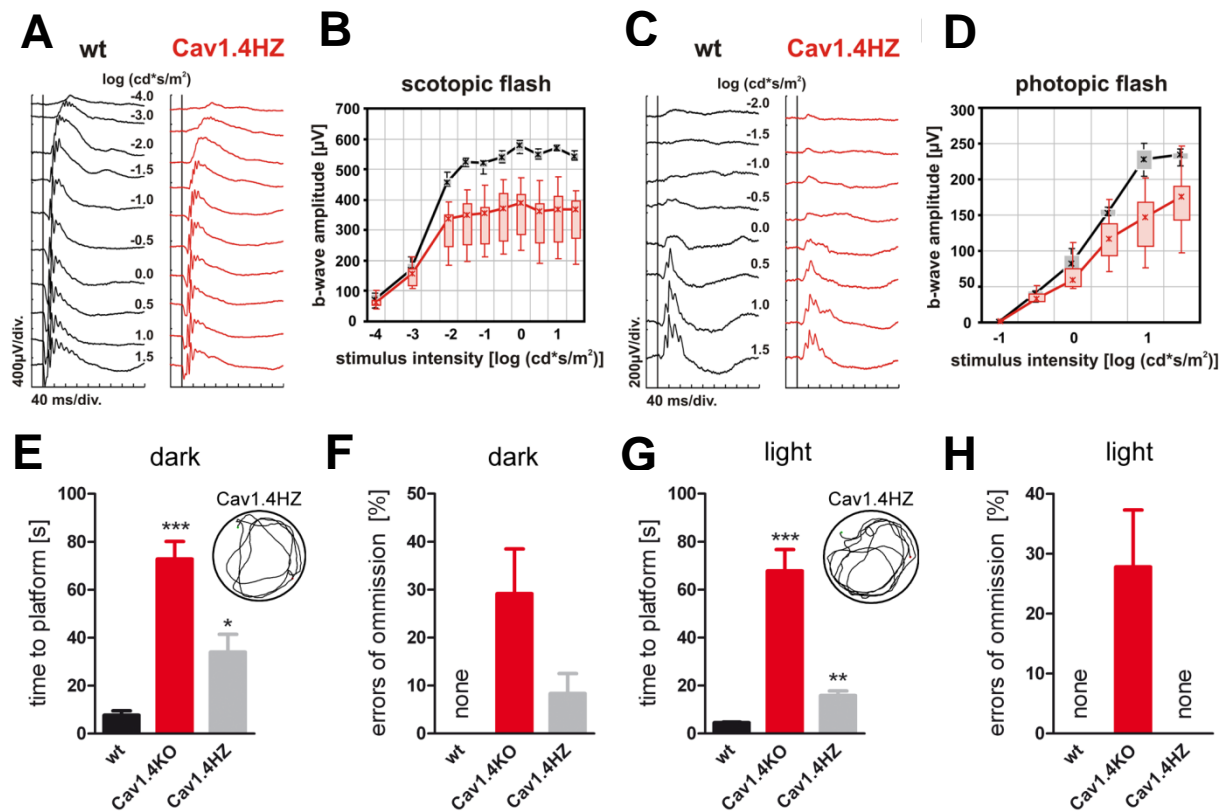


Figure 4.26 – Visual function in $Ca_v1.4$ heterozygous mice. **(A-D)** Electroretinographic analysis of retinal function in $Ca_v1.4HZ$ mice. Representative Ganzfeld-ERG intensity series from dark-adapted **(A)** and light-adapted **(C)** wild type (wt, black traces) and $Ca_v1.4HZ$ mice (red traces). **(B, D)** Quantitative data of the entire group shown as Box-and-Whisker plots, i.e. boxes indicate the 25% and 75% quantile range, whiskers indicate the 5% and 95% quantiles, and the asterisks indicate the median of the data. The amplitude data are plotted as a function of the logarithm of the flash intensity. Performance of $Ca_v1.4HZ$ mice (grey) in a visual water-maze behavioral task under dark **(E-F)** or normal light conditions **(G-H)**. Wild type (wt, black) and $Ca_v1.4$ KO mice (red) are shown for comparison. **(E and G)** Latency to locate a visible platform under dark **(E)** and normal light conditions **(G)**. Example swimming paths of $Ca_v1.4HZ$ mice are shown as insets. Errors of omission under dark **(F)** and normal light conditions **(H)**.

The performance of heterozygous $Ca_v1.4^{+/-}$ mice as judged by the latency to locate the platform (Fig 4.26 E), errors of omission under dark conditions (Fig 4.26 F), swimming paths length and the maximal swimming speed (Fig 4.21), as well as the latency to locate the platform under normal light conditions was in between wild type and $Ca_v1.4$ KO mice (Fig 4.26 G, H).

5. Discussion

5.1 Functional effects of the CaBP4 regulation on the Ca_v1.4 α 1

In the first part of this work, the functional effects of CaBP4 on wild type Ca_v1.4 channels were analyzed. The electrophysiological profile of Ca_v1.4 α 1 channel differs profoundly from that of other LTCCs (Baumann et al., 2004; McRory et al., 2004). Ca_v1.4 has very slow VDI, which leads to an increase in the channel conductance window compared to other LTCCs. The conductance window exists at potentials whereby ion channels are already activated but not yet fully inactivated. This condition is present within the overlapping region under the intersection of activation and inactivation curves of Ca_v1.4 channels. This property enables the channel to provide steady state inward calcium current. The CaBP4, as described in this study, increases the conductance window and the channel availability of Ca_v1.4 even more (Fig. 4.13 G).

The ICDI domain and CaBP4 have opposing functional effects on voltage dependent gating of Ca_v1.4 channels. In wild type Ca_v1.4 channels the ICDI domain shifts the activation curve to more depolarized potentials and increases inactivation. CaBP4 antagonizes these effects by shifting the activation curve of Ca_v1.4 to more hyperpolarized potentials and decreases inactivation. In line with this hypothesis, in the presence of CaBP4 the ICDI domain is functionally silent. Furthermore, in Ca_v1.4 channels lacking the ICDI domain CaBP4 has no effects on the voltage dependence. On the functional level CaBP4 selectively abolishes the effects of the ICDI domain on Ca_v1.4 channel availability. As a consequence, the voltage dependence of channel availability is pushed towards physiological operating voltage range in photoreceptors (Corey et al., 1984; Moriondo et al., 2001; Schneeweis and Schnapf, 2000; Thoreson et al., 2004; Witkovsky et al., 1997). Beside the effects on voltage dependent channel availability, CaBP4 also blocks CDI. This effect is only evident in Ca_v1.4 channels lacking the ICDI domain. With respect to its inhibitory effect on CDI, CaBP4 and the ICDI domain are functionally equivalent (Fig. 5.1).

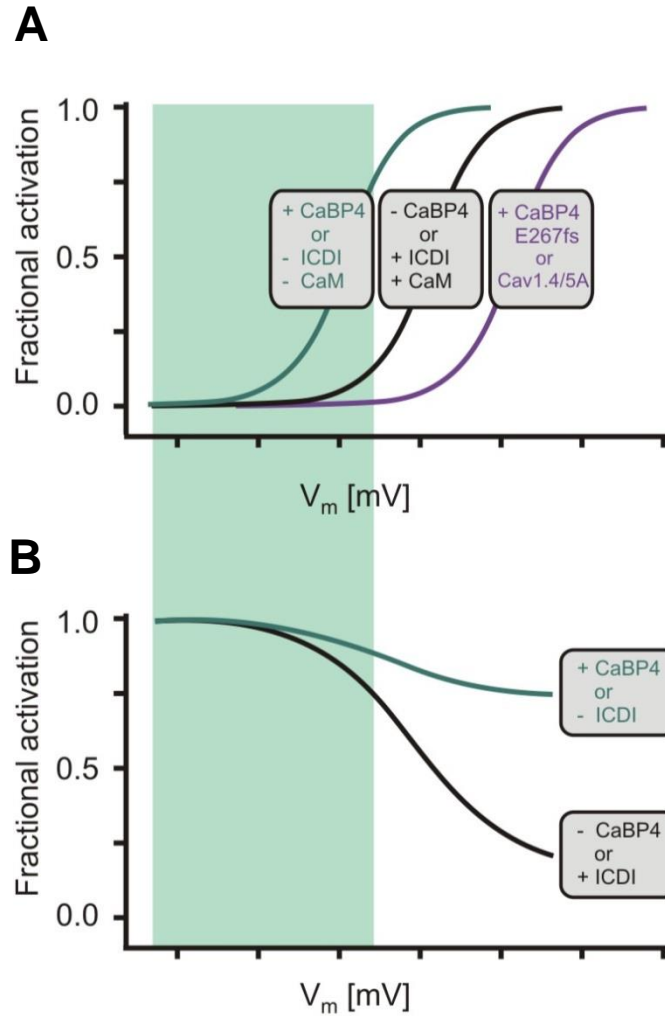


Figure 5.1 – Schematic of CaBP4 and ICDI effects on $Ca_v1.4$ channel activation and inactivation. **(A)** In the absence of CaBP4 the activation curve of $Ca_v1.4$ channels (black curve -CaBP4 +CaM) is at depolarized potentials. CaBP4 shifts activation curve of wild type $Ca_v1.4$ channels to the left (green curve: +CaBP4, -CaM). The same left shift is observed in $Ca_v1.4\Delta$ ICDI channels (green curve: -ICDI). In case of CaBP4-E267fs mutant or the $Ca_v1.4/5A$ variant (purple curve) a shift to even more depolarized potentials can be observed. **(B)** In the absence of CaBP4, there is pronounced inactivation of $Ca_v1.4$ channels (black curve: -CaBP4). CaBP4 decreases $Ca_v1.4$ channel inactivation (green curve: +CaBP4). Similar decrease in $Ca_v1.4$ inactivation is observed in $Ca_v1.4\Delta$ ICDI channels (green curve: -ICDI). Voltage axis in arbitrary units; the physiological voltage range of operation in photoreceptor cells is shown in green. The Boxes summarize the conditions under which the respective activation curve is observed. +ICDI refers to the wild type $Ca_v1.4$ channel -ICDI refers to truncated channels lacking the ICDI domain. Furthermore, in the boxes the presence or absence of endogenous CaM or CaBP4 is given.

DISCUSSION

The FRET experiments (data not shown, made by C.P.) indicate that the CaBP4 interferes structurally with the binding of the ICDI domain to the C-terminus of Ca_v1.4. One possible explanation could be that CaBP4 partially displaces the ICDI domain. Partial departure of the ICDI domain could selectively abolish the effects of the ICDI domain on voltage dependent Ca_v1.4 channel gating.

The FRET experiments provide an evidence that CaBP4 tightly associates with the IQ motif of Ca_v1.4 channels and that CaBP4 is able to displace CaM from binding to the IQ motif at physiological conditions. In line with this interpretation, it was shown that CaBP4 can very efficiently regulate the functional properties of Ca_v1.4 channels in HEK293 cells in which CaM is endogenously expressed at high levels. It is very likely that binding of CaBP4 induces a conformation different from the conformation in the presence of CaM. This difference could be the reason for differential effects of CaBP4 and CaM on CDI in Ca_v1.4ΔICDI channels. Moreover, CaBP4 with its long N-terminus (NT) is a much larger as compared to CaM. The N-terminus (NT) of CaBP4 contains different functional motif domains including a phosphorylation site (S-37). Therefore, it is possible that CaBP4 may bind or interact with the channel also on other interaction site(s) in addition to the IQ motif. The structural domain which may play a critical role in calcium channel inactivation could be the cytoplasmic I-II linker as suggested by (Cens et al., 1999; Kim et al., 2004; Stotz et al., 2000; Tadross et al., 2010). This linker forms a cytoplasmic gating/blocking particle or a lid which is involved in closing the channel pore and initiates the inactivation process of the channel. This domain may serve as one potential additional interaction domain of CaBP4 on Ca_v1.4. The dark green ball which is presented in figures 5.2-5.4 represents any intracellular domain, whereby the I-II linker could be one candidate.

The following mechanisms may explain the presented findings:

First, in the Ca_v1.4 WT channel (Fig. 5.2), the ICDI domain is present in the distal end of the C-terminus (CT). The CaM or CaBP4 bind to the IQ motif and lead to conformational change of the C-terminus, while the ICDI may interact independently with other elements on the channel and inhibit the inactivation process of the channel. In this situation, the inactivation occurs in a strictly voltage dependent manner (VDI). In this case, the ICDI masks the conformational change caused by CaM or CaBP4, and by that eliminates the CDI of the channel. However, the differences between CaBP4 and CaM can be seen by the shift of the activation curve

DISCUSSION

to more hyperpolarized potential and the inhibition of the inactivation process, when CaBP4 is coexpressed.

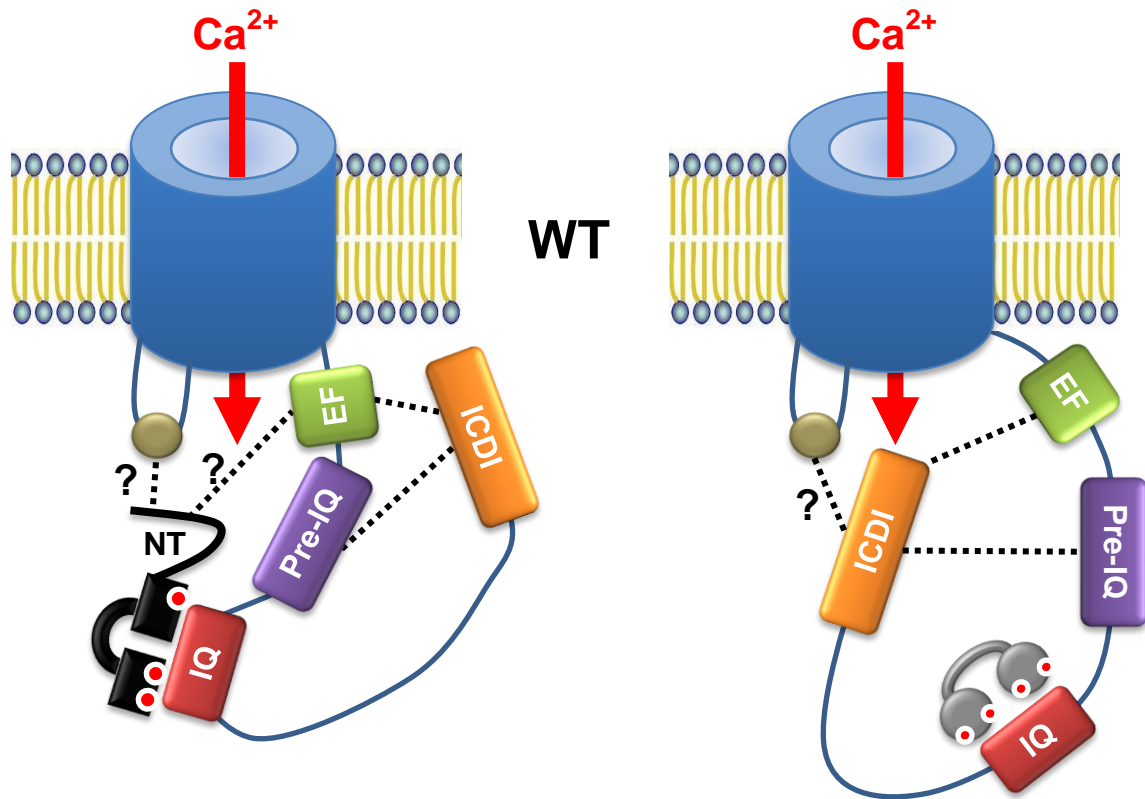


Figure 5.2 – Model showing the inactivation mechanism in $Ca_v1.4$ WT channel. *Left panel*, coexpressed CaBP4 binds to the IQ motif and cause a conformational change in the CT, while its N-terminus (NT) may interact with additional domains on the $Ca_v1.4$ channel. *Right panel*, endogenous CaM binds also to the IQ motif causing a conformational change in a way that the ICDI domain interacts with an intracellular domain to abolish the CDI of the channel.

Second, in the truncated variant of the channel, $Ca_v1.4\Delta ICDI$, the ICDI is absent. $Ca_v1.4$ lacking ICDI shows CDI. However this CDI is abolished when CaBP4 is coexpressed. In the absence of the ICDI domain, the effect of CaBP4 on voltage-dependent gating is abolished. No difference between CaM and CaBP4 can be seen regarding activation and inactivation curves, meaning that deletion of the ICDI affects dramatically all the activation and inactivation properties of the channel (Fig. 5.3).

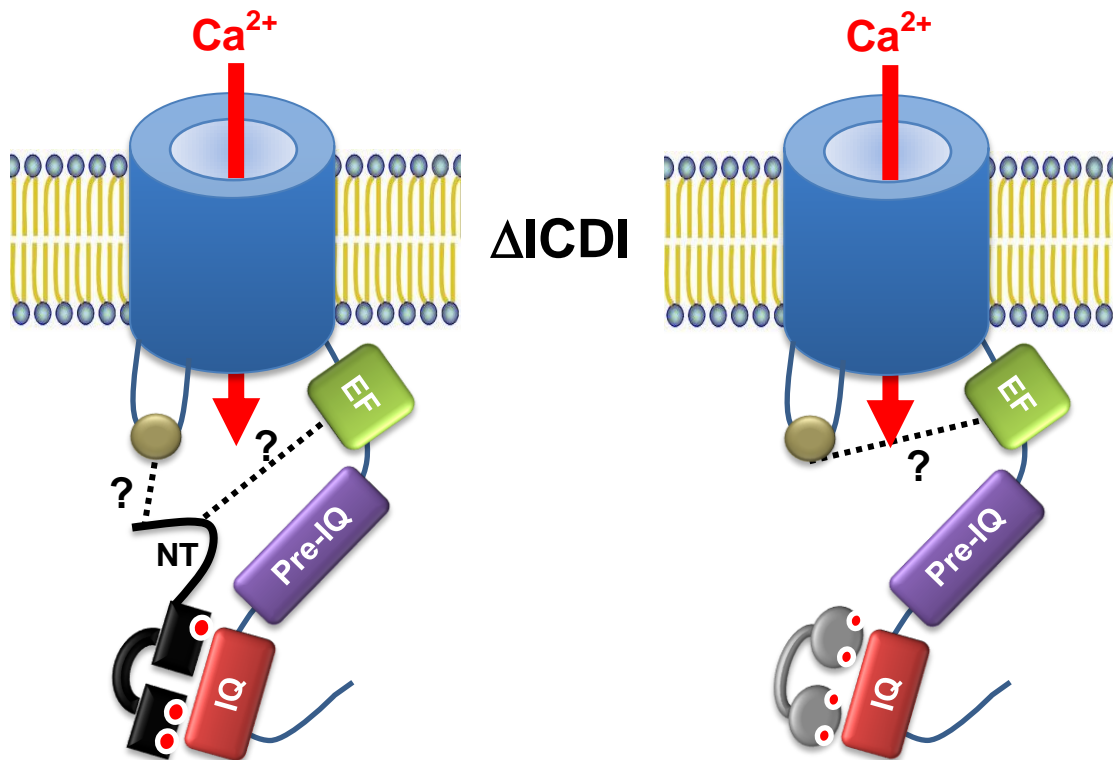


Figure 5.3 – Model showing the inactivation mechanism in $\text{Ca}_v1.4\Delta\text{ICDI}$ channel. *Left panel*, coexpressed CaBP4 binds to the IQ motif and its N-terminus (NT) may still interact with additional domains on the $\text{Ca}_v1.4$ channel, therefore no CDI can be seen. *Right panel*, endogenous CaM binds also to the IQ motif. However, now a direct interaction between intracellular domains like with the EF-hand on the CT of the $\text{Ca}_v1.4$ may speed up channel closure and promotes fast CDI.

The third case deals with $\text{Ca}_v1.4/5A$, in which 5 residues in the IQ motif were replaced by alanines (Fig. 5.4). Here, neither the CaBP4 nor the endogenous CaM binds to the IQ motif and therefore no conformational change of the CT. Both may stay pre-bound to additional motif in a close proximity up or downstream of the IQ sequence.

Patch clamp recordings in $\text{Ca}_v1.4/5A$ HEK cells coexpressing CaBP4 show a surprising result in which the CaBP4 is still able to shift the activation curve by approximately 5mV shift to more hyperpolarized potential, compared to $\text{Ca}_v1.4/5A$ in the absence of CaBP4.

These observations indicate that the CaBP4 is able to bind independently to another binding site on the channel, besides the IQ motif. The CaBP4 may bind with its long NT to any cytoplasmic domain on the channel, like the I-II linker and/or the EF

DISCUSSION

domain, therefore no CDI can be seen. By this interaction, CaBP4 is still partly able to regulate the channel.

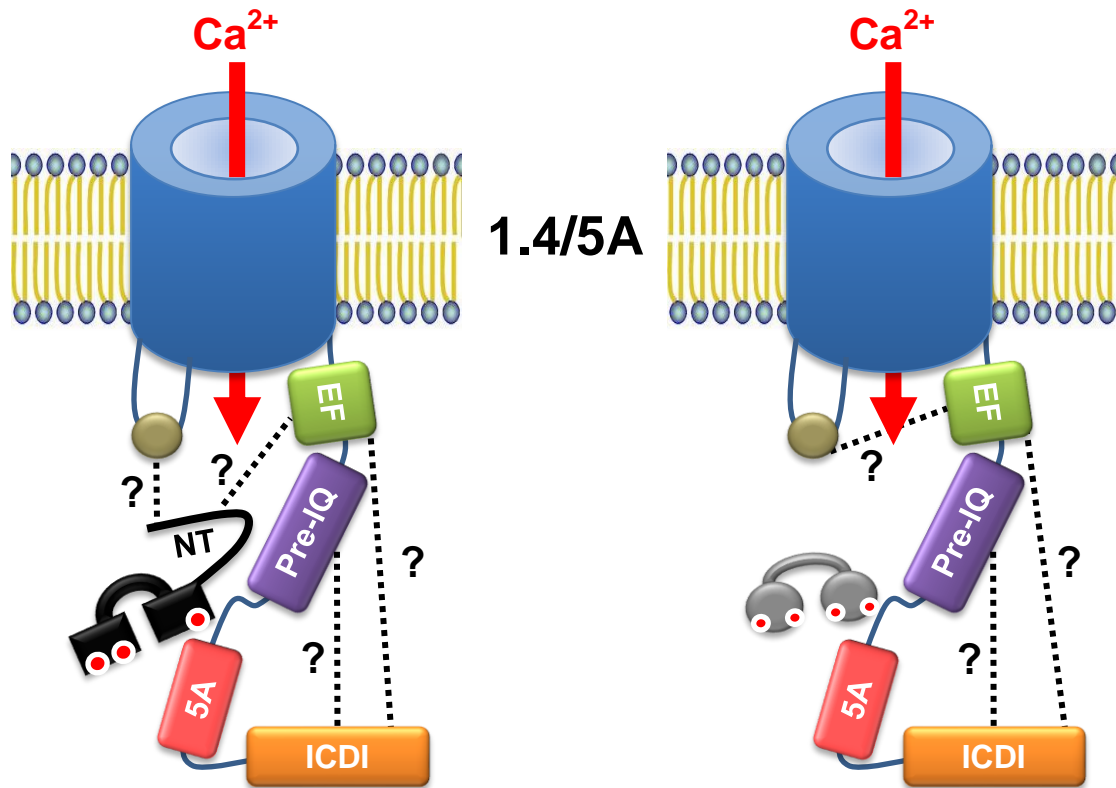


Figure 5.4 – Model showing the inactivation mechanism in Ca_v1.4/5A channel. *Left panel*, coexpressed CaBP4 is prebound to the CT of the channel and its N-terminus (NT) may still interact with additional domains on the Ca_v1.4 channel, therefore no CDI can be seen. *Right panel*, endogenous CaM is also prebound to the IQ motif. However, still a direct interaction between intracellular domains like with the EF-hand on the CT of the Ca_v1.4 may speed up channel closure and promotes fast CDI.

5.2 The patho-mechanism of CaBP4 mutants

Both CaBP4 mutants interact with the C-terminus of Ca_v1.4 but lack most of the effects of wild type CaBP4, suggesting that both lobes of CaBP4 need to be present and act to produce a conformational change that regulates voltage dependent activation and inactivation.

This research provides mechanistical insight how CaBP4 mutants lead to disease. Both of the mutants share a common feature; they significantly reduce the overall channel availability as compared to wild type CaBP4. The two CaBP4 mutants show no negative shift of the voltage dependent activation curve and no change in the slope of the activation curve. This suggests that CaBP4 mutants, even though bound to the channel, cannot antagonize the effect of the ICDI domain on voltage dependent activation.

The CaBP4-R216X mutant is missing the functional C-lobe. The CaBP4-R216X could indeed interact with the channel; however the absence of the C-lobe CaBP4-R216X would not be able to produce the conformational change of the Ca_v1.4-CaBP4 complex which is required for the interference with the ICDI domain.

On the other hand, in the CaBP4-E267fs mutant both lobes are present but the function of the C-lobe could be affected by the exchange of the last amino acid residue in the fourth EF hand and the additional nonsense downstream sequence. Interestingly, for CaBP4-E267fs even a significant shift of the activation curve toward more positive potentials was observed.

A possible explanation is that the CaBP4 mutant stabilizes the channel in a conformational state whereby the endogenous CaM is completely displaced from binding to the channel through IQ motif. This interpretation can be supported by the results obtained with the Ca_v1.4/5A channel, where a right shift toward more positive potentials was observed (Fig. 4.16 A and B). Alternatively, the CaBP4 intensifies the interaction of the ICDI domain with the channel, causing a shift in the activation curve toward more positive potentials.

In both CaBP4 mutants, voltage dependent inactivation was more pronounced than in wild type CaBP4. This indicates that CaBP4 mutants can only partially induce the conformational change induced by wild type CaBP4. The physiological window currents in both CaBP4 mutants were significantly reduced. These effects are more pronounced in CaBP4-R216X.

The appearance of slow CDI in $Ca_v1.4\Delta$ ICDI channels coexpressed with mutant CaBP4 suggests that CaM can access the effector site for CDI at least in some of the channels.

5.3 Functional characterization of $Ca_v1.4$ deficient mice

Here, the retinal phenotype of $Ca_v1.4$ deficient mice (Specht et al., 2009) was analyzed in vivo. Using ERG, the homozygous $Ca_v1.4$ deficient mice show diminished ERG b-waves under scotopic and photopic light conditions compared to wild type mice, demonstrating that this mouse line is a true functional knockout. Additionally, the $Ca_v1.4$ KO mice performed very poorly in a water maze-based vision test, suggesting that they are essentially blind.

In line with this finding, retinal morphology of $Ca_v1.4$ KO mice was markedly changed. Further morphological analysis of the $Ca_v1.4$ KO retinas demonstrated thinning of the *opl*, pronounced outgrowth of postsynaptic structures like rod bipolar cells dendrites and horizontal cell neurites into the *onl* and retraction of presynaptic elements to the *onl*, leading to ectopic synapse formation in the *onl*. These changes concurred with pronounced degeneration and loss of cone, but not of rod photoreceptors. Those results demonstrate that $Ca_v1.4$ channels are essential for both rod and cone neurotransmission and the functional and structural integrity of photoreceptor synapses in mice. These observations are consistent with similar findings from an independent genetically engineered $Ca_v1.4$ deficient mouse model, which was previously reported (Mansergh et al., 2005; Raven et al., 2008).

$Ca_v1.4$ channels are encoded by the X-chromosomal *CACNA1F* gene. In some cases, mutations in *CACNA1F* lead to distinct forms of congenital stationary blindness type 2 associated with clinical symptoms in carrier females (Hemara-Wahanui et al., 2005; Hope et al., 2005; Jalkanen et al., 2007; Rigaudiere et al., 2003). Therefore, it was important to extend this study to heterozygous mice. The analysis of $Ca_v1.4$ heterozygosity on retinal function and morphology revealed several new aspects of $Ca_v1.4$ channel in vivo function. In $Ca_v1.4$ aged heterozygous mice, retinal patches with typical changes observed in the $Ca_v1.4$ deficient mouse retina have been seen side by side with patches of wild type-like morphology. It is very likely that the patchy pattern is caused by random X-chromosomal inactivation of the healthy or the affected *Cacna1f* gene copy early in retinal precursor cells. During development, inactivation of the X-chromosome carrying wild type $Ca_v1.4$

DISCUSSION

gene leads to cells deficient of $Ca_v1.4$ in heterozygous $Ca_v1.4$ mice, organized precisely in radial columns (Reese and Galli-Resta, 2002). Importantly, this means that all pathological and morphological changes observed in the heterozygous affected patches including the synaptopathy as well as the degenerative changes (e.g. loss of cone pedicle structure and patchy activation of Müller glial cells) spread radially and cannot be compensated by neighboring unaffected and functional retinal cells.

However, closer observation of the border regions between affected and non-affected retinal patches suggests a functional interaction. Pre- and postsynaptic elements in affected retinal patches appear different when they are in close proximity to cells within non-affected parts of the heterozygous retina. For instance, labeling of the postsynaptic VDCC $Ca_v1.1$ or the ribbon protein *Ctbp2* are lost in the knockout retina and in affected parts of the heterozygous retina, but are present, though with ectopic localization within the *onl*, in the border area between affected and non-affected retinal regions in the heterozygous mouse. These observations may suggest that non-affected rod cell bodies are able to form an ectopic synapse with bipolar cell neurites originating from postsynaptic partners within the neighboring affected retinal column.

These findings suggest that retinal function in the heterozygous $Ca_v1.4$ retina should be impaired for two reasons:

1. The affected retinal columns cannot contribute to light detection and signal transmission through the visual pathway.
2. Aberrant crosstalk between affected and non-affected retinal patches in the border regions might interfere with normal retinal processing.

In line with this, aged heterozygous mice presented reduction in ERG b-wave amplitudes side by side with intermediate performance in the vision-guided behaviour test which was in between that of wild type and $Ca_v1.4$ deficient mice. Notably, this phenotype was observed under scotopic and photopic light conditions, arguing for defects in rod and cone function.

For most X chromosome-linked diseases carrier females are not affected (Migeon, 2006). However, the results presented in this study suggest, that patients carrying an allele with a null mutation should present with a phenotype. Nevertheless, one needs to take into account that the human retina differs extensively from the mouse

DISCUSSION

retina. Moreover, it is still not clear if human cones (or rods) express other L-type VDCCs (e.g. $Ca_v1.3$) in addition to $Ca_v1.4$ that might compensate for the loss of $Ca_v1.4$ function.

Taken together, this work shows for the first time that *CACNA1F* heterozygosity in female carrier mice has deleterious effects on rod and cone-mediated vision.

6. Summary

Synapses of retinal photoreceptors and bipolar neurons are characterized by their ability to release the neurotransmitter glutamate in a sustained and tonic fashion.

Several ion channels contribute to this hallmark property, among which a member of the L-Type calcium channel family, $Ca_v1.4$, which has a particular significance. $Ca_v1.4$ differs from most other calcium channels by its ultra-slow kinetics of voltage-dependent inactivation (VDI). Moreover, $Ca_v1.4$ does not display feedback inhibition by permeating Ca^{2+} (CDI, calcium-dependent inactivation), that is found in other calcium channels.

Recent studies suggested that the activity of $Ca_v1.4$ is regulated by a specific Ca^{2+} -binding protein (CaBP4). In this thesis, this issue was explored in detail. Using heterologous expression in HEK293 cells, CaBP4 was found to dramatically increase $Ca_v1.4$ channel availability ("window conductance") at the physiological range of membrane potentials. This effect crucially depends on the presence of the C-terminal inhibitory domain of $Ca_v1.4$ (ICDI, inhibitor of Ca^{2+} -dependent inactivation).

Consequently, the effect of CaBP4 was lost in a $Ca_v1.4$ mutant lacking the ICDI. CaBP4 was found to interact with a specific C-terminal motif of $Ca_v1.4$ ("IQ motif") and to interfere with the binding of the ICDI domain. These findings suggest that CaBP4 increases $Ca_v1.4$ channel availability by relieving the inhibitory effects of the ICDI domain on voltage-dependent $Ca_v1.4$ channel gating. In addition, two CaBP4 mutants which are associated with a congenital variant of human night blindness (CSNB2) were analyzed. Although both mutants interact with $Ca_v1.4$ channels, the functional effects of CaBP4 mutants are only partially preserved, leading to a reduction of $Ca_v1.4$ channel availability and loss of function. The heterologous expression studies were corroborated by the analysis of a $Ca_v1.4$ -deficient mouse model that displays several clinical aspects of human CSNB2. The effects of $Ca_v1.4$ deletion on the retinal structure and visual function were examined in detail as part of this thesis. A particular focus was set on the phenotype of heterozygous female mice, since $Ca_v1.4$ is encoded by the X-chromosome and can be transcriptionally silenced. In conclusion, this study sheds new light on the functional regulation of $Ca_v1.4$ by CaBP4. Moreover, it provides insights into the mechanism by which CaBP4 mutants lead to loss of $Ca_v1.4$ function and to retinal disease. Finally, the analysis of $Ca_v1.4$ -deficient mice has provided important information with regard to the pathophysiological processes taking place in the CSNB2 retina.

7. Literature

Aldahmesh, M.A., Al-Owain, M., Alqahtani, F., Hazzaa, S., and Alkuraya, F.S. (2010). A null mutation in CABP4 causes Leber's congenital amaurosis-like phenotype. *Molecular vision* 16, 207-212.

Ball, S.L., Powers, P.A., Shin, H.S., Morgans, C.W., Peachey, N.S., and Gregg, R.G. (2002). Role of the beta(2) subunit of voltage-dependent calcium channels in the retinal outer plexiform layer. *Investigative ophthalmology & visual science* 43, 1595-1603.

Barnes, S., and Kelly, M.E. (2002). Calcium channels at the photoreceptor synapse. *Advances in experimental medicine and biology* 514, 465-476.

Barry, P.H. (1994). JPCalc, a software package for calculating liquid junction potential corrections in patch-clamp, intracellular, epithelial and bilayer measurements and for correcting junction potential measurements. *Journal of neuroscience methods* 51, 107-116.

Bauer, C.S., Tran-Van-Minh, A., Kadurin, I., and Dolphin, A.C. (2010). A new look at calcium channel alpha2delta subunits. *Current opinion in neurobiology* 20, 563-571.

Baumann, L., Gerstner, A., Zong, X., Biel, M., and Wahl-Schott, C. (2004). Functional characterization of the L-type Ca²⁺ channel Cav1.4alpha1 from mouse retina. *Investigative ophthalmology & visual science* 45, 708-713.

Bech-Hansen, N.T., Naylor, M.J., Maybaum, T.A., Pearce, W.G., Koop, B., Fishman, G.A., Mets, M., Musarella, M.A., and Boycott, K.M. (1998). Loss-of-function mutations in a calcium-channel alpha1-subunit gene in Xp11.23 cause incomplete X-linked congenital stationary night blindness. *Nature genetics* 19, 264-267.

Berridge, M.J. (2004). Calcium signal transduction and cellular control mechanisms. *Biochimica et biophysica acta* 1742, 3-7.

Bers, D.M. (2002). Cardiac excitation-contraction coupling. *Nature* 415, 198-205.

Bidaud, I., Mezghrani, A., Swayne, L.A., Monteil, A., and Lory, P. (2006). Voltage-gated calcium channels in genetic diseases. *Biochimica et biophysica acta* 1763, 1169-1174.

Biel, M., Ruth, P., Bosse, E., Hullin, R., Stuhmer, W., Flockerzi, V., and Hofmann, F. (1990). Primary structure and functional expression of a high voltage activated calcium channel from rabbit lung. *FEBS letters* 269, 409-412.

Birnbaumer, L., Campbell, K.P., Catterall, W.A., Harpold, M.M., Hofmann, F., Horne, W.A., Mori, Y., Schwartz, A., Snutch, T.P., Tanabe, T., and et al. (1994). The naming of voltage-gated calcium channels. *Neuron* 13, 505-506.

Birnboim, H.C., and Doly, J. (1979). A rapid alkaline extraction procedure for screening recombinant plasmid DNA. *Nucleic acids research* 7, 1513-1523.

LITERATURE

Blaich, A., Welling, A., Fischer, S., Wegener, J.W., Kostner, K., Hofmann, F., and Moosmang, S. (2010). Facilitation of murine cardiac L-type Ca(v)1.2 channel is modulated by calmodulin kinase II-dependent phosphorylation of S1512 and S1570. *Proceedings of the National Academy of Sciences of the United States of America* 107, 10285-10289.

Bodi, I., Mikala, G., Koch, S.E., Akhter, S.A., and Schwartz, A. (2005). The L-type calcium channel in the heart: the beat goes on. *The Journal of clinical investigation* 115, 3306-3317.

Bohn, G., Moosmang, S., Conrad, H., Ludwig, A., Hofmann, F., and Klugbauer, N. (2000). Expression of T- and L-type calcium channel mRNA in murine sinoatrial node. *FEBS letters* 481, 73-76.

Boycott, K., Maybaum, T., Naylor, M., Weleber, R., Robitaille, J., Miyake, Y., Bergen, A., Pierpont, M., Pearce, W., and Bech-Hansen, N. (2001). A summary of 20 CACNA1F mutations identified in 36 families with incomplete X-linked congenital stationary night blindness, and characterization of splice variants. *Human Genetics* 108, 91-97.

Bradford, M.M. (1976). A rapid and sensitive method for the quantitation of microgram quantities of protein utilizing the principle of protein-dye binding. *Analytical biochemistry* 72, 248-254.

Budde, T., Meuth, S., and Pape, H.C. (2002). Calcium-dependent inactivation of neuronal calcium channels. *Nature reviews. Neuroscience* 3, 873-883.

Burgoyne, R.D., and Weiss, J.L. (2001). The neuronal calcium sensor family of Ca²⁺-binding proteins. *The Biochemical journal* 353, 1-12.

Catterall, W.A. (2000). Structure and regulation of voltage-gated Ca²⁺ channels. *Annual review of cell and developmental biology* 16, 521-555.

Catterall, W.A. (2010). Signaling complexes of voltage-gated sodium and calcium channels. *Neuroscience letters* 486, 107-116.

Catterall, W.A., Perez-Reyes, E., Snutch, T.P., and Striessnig, J. (2005). International Union of Pharmacology. XLVIII. Nomenclature and structure-function relationships of voltage-gated calcium channels. *Pharmacological reviews* 57, 411-425.

Cens, T., Restituito, S., Galas, S., and Charnet, P. (1999). Voltage and calcium use the same molecular determinants to inactivate calcium channels. *The Journal of biological chemistry* 274, 5483-5490.

Chemin, J., Monteil, A., Briquaire, C., Richard, S., Perez-Reyes, E., Nargeot, J., and Lory, P. (2000). Overexpression of T-type calcium channels in HEK-293 cells increases intracellular calcium without affecting cellular proliferation. *FEBS letters* 478, 166-172.

Chen, X., Wang, Q., Ni, F., and Ma, J. (2010). Structure of the full-length Shaker potassium channel Kv1.2 by normal-mode-based X-ray crystallographic refinement. *Proceedings of the National Academy of Sciences of the United States of America* 107, 11352-11357.

LITERATURE

Chin, D., and Means, A.R. (2000). Calmodulin: a prototypical calcium sensor. *Trends in cell biology* 10, 322-328.

Christel, C., and Lee, A. (2012). Ca²⁺-dependent modulation of voltage-gated Ca²⁺ channels. *Biochimica et biophysica acta* 1820, 1243-1252.

Corey, D.P., Dubinsky, J.M., and Schwartz, E.A. (1984). The calcium current in inner segments of rods from the salamander (*Ambystoma tigrinum*) retina. *The Journal of physiology* 354, 557-575.

Cribbs, L.L., Lee, J.H., Yang, J., Satin, J., Zhang, Y., Daud, A., Barclay, J., Williamson, M.P., Fox, M., Rees, M., and Perez-Reyes, E. (1998). Cloning and characterization of alpha1H from human heart, a member of the T-type Ca²⁺ channel gene family. *Circulation research* 83, 103-109.

Cui, G., Meyer, A.C., Calin-Jageman, I., Neef, J., Haeseleer, F., Moser, T., and Lee, A. (2007). Ca²⁺-binding proteins tune Ca²⁺-feedback to Cav1.3 channels in mouse auditory hair cells. *The Journal of physiology* 585, 791-803.

de Leon, M., Wang, Y., Jones, L., Perez-Reyes, E., Wei, X., Soong, T.W., Snutch, T.P., and Yue, D.T. (1995). Essential Ca²⁺-binding motif for Ca²⁺-sensitive inactivation of L-type Ca²⁺ channels. *Science* 270, 1502-1506.

DeMaria, C.D., Soong, T.W., Alseikhan, B.A., Alvania, R.S., and Yue, D.T. (2001). Calmodulin bifurcates the local Ca²⁺ signal that modulates P/Q-type Ca²⁺ channels. *Nature* 411, 484-489.

Dick, I.E., Tadross, M.R., Liang, H., Tay, L.H., Yang, W., and Yue, D.T. (2008). A modular switch for spatial Ca²⁺ selectivity in the calmodulin regulation of Ca_v channels. *Nature* 451, 830-834.

Doering, C.J., Hamid, J., Simms, B., McRory, J.E., and Zamponi, G.W. (2005). Cav1.4 encodes a calcium channel with low open probability and unitary conductance. *Biophysical journal* 89, 3042-3048.

Doering, C.J., Peloquin, J.B., and McRory, J.E. (2007). The Ca_v1.4 calcium channel: more than meets the eye. *Channels (Austin)* 1, 3-10.

Dolmetsch, R.E., Pajvani, U., Fife, K., Spotts, J.M., and Greenberg, M.E. (2001). Signaling to the nucleus by an L-type calcium channel-calmodulin complex through the MAP kinase pathway. *Science* 294, 333-339.

Dolphin, A.C. (2012). Calcium channel auxiliary alpha2delta and beta subunits: trafficking and one step beyond. *Nature reviews. Neuroscience* 13, 542-555.

Dubel, S.J., Starr, T.V., Hell, J., Ahljianian, M.K., Enyeart, J.J., Catterall, W.A., and Snutch, T.P. (1992). Molecular cloning of the alpha-1 subunit of an omega-conotoxin-sensitive calcium channel. *Proceedings of the National Academy of Sciences of the United States of America* 89, 5058-5062.

LITERATURE

Ertel, E.A., Campbell, K.P., Harpold, M.M., Hofmann, F., Mori, Y., Perez-Reyes, E., Schwartz, A., Snutch, T.P., Tanabe, T., Birnbaumer, L., *et al.* (2000). Nomenclature of voltage-gated calcium channels. *Neuron* 25, 533-535.

Few, A.P., Nanou, E., Scheuer, T., and Catterall, W.A. (2011). Molecular determinants of CaV2.1 channel regulation by calcium-binding protein-1. *The Journal of biological chemistry* 286, 41917-41923.

Firth, S.I., Morgan, I.G., Boelen, M.K., and Morgans, C.W. (2001). Localization of voltage-sensitive L-type calcium channels in the chicken retina. *Clinical & experimental ophthalmology* 29, 183-187.

Franke, F.E., Schachenmayr, W., Osborn, M., and Altmannsberger, M. (1991). Unexpected immunoreactivities of intermediate filament antibodies in human brain and brain tumors. *The American journal of pathology* 139, 67-79.

Gao, T., Chien, A.J., and Hosey, M.M. (1999). Complexes of the alpha1C and beta subunits generate the necessary signal for membrane targeting of class C L-type calcium channels. *The Journal of biological chemistry* 274, 2137-2144.

Garipey, J., and Hodges, R.S. (1983). Primary sequence analysis and folding behavior of EF hands in relation to the mechanism of action of troponin C and calmodulin. *FEBS letters* 160, 1-6.

Griessmeier, K., Cuny, H., Rotzer, K., Griesbeck, O., Harz, H., Biel, M., and Wahl-Schott, C. (2009). Calmodulin is a functional regulator of Cav1.4 L-type Ca²⁺ channels. *The Journal of biological chemistry* 284, 29809-29816.

Gurney, A.M., Charnet, P., Pye, J.M., and Nargeot, J. (1989). Augmentation of cardiac calcium current by flash photolysis of intracellular caged-Ca²⁺ molecules. *Nature* 341, 65-68.

Haeseleer, F., Imanishi, Y., Maeda, T., Possin, D.E., Maeda, A., Lee, A., Rieke, F., and Palczewski, K. (2004). Essential role of Ca²⁺-binding protein 4, a Cav1.4 channel regulator, in photoreceptor synaptic function. *Nature neuroscience* 7, 1079-1087.

Haeseleer, F., Imanishi, Y., Sokal, I., Filipek, S., and Palczewski, K. (2002). Calcium-binding proteins: intracellular sensors from the calmodulin superfamily. *Biochemical and biophysical research communications* 290, 615-623.

Haeseleer, F., and Palczewski, K. (2002). Calmodulin and Ca²⁺-binding proteins (CaBPs): variations on a theme. *Advances in experimental medicine and biology* 514, 303-317.

Haeseleer, F., Sokal, I., Verlinde, C.L., Erdjument-Bromage, H., Tempst, P., Pronin, A.N., Benovic, J.L., Fariss, R.N., and Palczewski, K. (2000). Five members of a novel Ca(2+)-binding protein (CABP) subfamily with similarity to calmodulin. *The Journal of biological chemistry* 275, 1247-1260.

Halling, D.B., Aracena-Parks, P., and Hamilton, S.L. (2006). Regulation of voltage-gated Ca²⁺ channels by calmodulin. *Science's STKE : signal transduction knowledge environment* 2006, er1.

LITERATURE

Halling, D.B., Georgiou, D.K., Black, D.J., Yang, G., Fallon, J.L., Quijcho, F.A., Pedersen, S.E., and Hamilton, S.L. (2009). Determinants in CaV1 channels that regulate the Ca²⁺ sensitivity of bound calmodulin. *The Journal of biological chemistry* 284, 20041-20051.

Haynes, L.P., McCue, H.V., and Burgoyne, R.D. (2012). Evolution and functional diversity of the Calcium Binding Proteins (CaBPs). *Frontiers in molecular neuroscience* 5, 9.

Hell, J.W., Westenbroek, R.E., Warner, C., Ahljianian, M.K., Prystay, W., Gilbert, M.M., Snutch, T.P., and Catterall, W.A. (1993). Identification and differential subcellular localization of the neuronal class C and class D L-type calcium channel alpha 1 subunits. *The Journal of cell biology* 123, 949-962.

Hell, J.W., Yokoyama, C.T., Breeze, L.J., Chavkin, C., and Catterall, W.A. (1995). Phosphorylation of presynaptic and postsynaptic calcium channels by cAMP-dependent protein kinase in hippocampal neurons. *The EMBO journal* 14, 3036-3044.

Hemara-Wahanui, A., Berjukow, S., Hope, C.I., Dearden, P.K., Wu, S.B., Wilson-Wheeler, J., Sharp, D.M., Landon-Treweek, P., Clover, G.M., Hoda, J.C., *et al.* (2005). A CACNA1F mutation identified in an X-linked retinal disorder shifts the voltage dependence of Cav1.4 channel activation. *Proceedings of the National Academy of Sciences of the United States of America* 102, 7553-7558.

Hofmann, F., Lacinova, L., and Klugbauer, N. (1999). Voltage-dependent calcium channels: from structure to function. *Reviews of physiology, biochemistry and pharmacology* 139, 33-87.

Hope, C.I., Sharp, D.M., Hemara-Wahanui, A., Sissingh, J.I., Landon, P., Mitchell, E.A., Maw, M.A., and Clover, G.M. (2005). Clinical manifestations of a unique X-linked retinal disorder in a large New Zealand family with a novel mutation in CACNA1F, the gene responsible for CSNB2. *Clinical & experimental ophthalmology* 33, 129-136.

Jalkanen, R., Bech-Hansen, N.T., Tobias, R., Sankila, E.M., Mantyjarvi, M., Forsius, H., de la Chapelle, A., and Alitalo, T. (2007). A novel CACNA1F gene mutation causes Aland Island eye disease. *Investigative ophthalmology & visual science* 48, 2498-2502.

Jalkanen, R., Mantyjarvi, M., Tobias, R., Isosomppi, J., Sankila, E.M., Alitalo, T., and Bech-Hansen, N.T. (2006). X linked cone-rod dystrophy, CORDX3, is caused by a mutation in the CACNA1F gene. *Journal of medical genetics* 43, 699-704.

Kabanarou, S.A., Holder, G.E., Fitzke, F.W., Bird, A.C., and Webster, A.R. (2004). Congenital stationary night blindness and a "Schubert-Bornschein" type electrophysiology in a family with dominant inheritance. *The British journal of ophthalmology* 88, 1018-1022.

Kim, J., Ghosh, S., Nunziato, D.A., and Pitt, G.S. (2004). Identification of the components controlling inactivation of voltage-gated Ca²⁺ channels. *Neuron* 41, 745-754.

Koch, S., Sothilingam, V., Garcia Garrido, M., Tanimoto, N., Becirovic, E., Koch, F., Seide, C., Beck, S.C., Seeliger, M.W., Biel, M., *et al.* (2012). Gene therapy restores vision and delays degeneration in the CNGB1(-/-) mouse model of retinitis pigmentosa. *Human molecular genetics* 21, 4486-4496.

LITERATURE

Kollmar, R., Fak, J., Montgomery, L.G., and Hudspeth, A.J. (1997). Hair cell-specific splicing of mRNA for the alpha1D subunit of voltage-gated Ca²⁺ channels in the chicken's cochlea. *Proceedings of the National Academy of Sciences of the United States of America* 94, 14889-14893.

Koschak, A., Reimer, D., Walter, D., Hoda, J.C., Heinzle, T., Grabner, M., and Striessnig, J. (2003). Cav1.4alpha1 subunits can form slowly inactivating dihydropyridine-sensitive L-type Ca²⁺ channels lacking Ca²⁺-dependent inactivation. *The Journal of neuroscience : the official journal of the Society for Neuroscience* 23, 6041-6049.

Laemmli, U.K. (1970). Cleavage of structural proteins during the assembly of the head of bacteriophage T4. *Nature* 227, 680-685.

Lee, A., Jimenez, A., Cui, G., and Haeseleer, F. (2007). Phosphorylation of the Ca²⁺-binding protein CaBP4 by protein kinase C zeta in photoreceptors. *The Journal of neuroscience : the official journal of the Society for Neuroscience* 27, 12743-12754.

Lee, A., Westenbroek, R.E., Haeseleer, F., Palczewski, K., Scheuer, T., and Catterall, W.A. (2002). Differential modulation of Ca(v)2.1 channels by calmodulin and Ca²⁺-binding protein 1. *Nature neuroscience* 5, 210-217.

Lee, J.H., Daud, A.N., Cribbs, L.L., Lacerda, A.E., Pereverzev, A., Klockner, U., Schneider, T., and Perez-Reyes, E. (1999). Cloning and expression of a novel member of the low voltage-activated T-type calcium channel family. *The Journal of neuroscience : the official journal of the Society for Neuroscience* 19, 1912-1921.

Liang, H., DeMaria, C.D., Erickson, M.G., Mori, M.X., Alseikhan, B.A., and Yue, D.T. (2003). Unified mechanisms of Ca²⁺ regulation across the Ca²⁺ channel family. *Neuron* 39, 951-960.

Liao, P., Yong, T.F., Liang, M.C., Yue, D.T., and Soong, T.W. (2005). Splicing for alternative structures of Cav1.2 Ca²⁺ channels in cardiac and smooth muscles. *Cardiovascular research* 68, 197-203.

Liao, P., Yu, D., Li, G., Yong, T.F., Soon, J.L., Chua, Y.L., and Soong, T.W. (2007). A smooth muscle Cav1.2 calcium channel splice variant underlies hyperpolarized window current and enhanced state-dependent inhibition by nifedipine. *The Journal of biological chemistry* 282, 35133-35142.

Littink, K.W., van Genderen, M.M., Collin, R.W., Roosing, S., de Brouwer, A.P., Riemsdag, F.C., Venselaar, H., Thiadens, A.A., Hoyng, C.B., Rohrschneider, K., *et al.* (2009). A novel homozygous nonsense mutation in CABP4 causes congenital cone-rod synaptic disorder. *Investigative ophthalmology & visual science* 50, 2344-2350.

Long, S.B., Campbell, E.B., and Mackinnon, R. (2005). Crystal structure of a mammalian voltage-dependent Shaker family K⁺ channel. *Science* 309, 897-903.

Mansergh, F., Orton, N.C., Vessey, J.P., Lalonde, M.R., Stell, W.K., Tremblay, F., Barnes, S., Rancourt, D.E., and Bech-Hansen, N.T. (2005). Mutation of the calcium channel gene *Cacna1f* disrupts calcium signaling, synaptic transmission and cellular organization in mouse retina. *Human molecular genetics* 14, 3035-3046.

LITERATURE

Marcantoni, A., Baldelli, P., Hernandez-Guijo, J.M., Comunanza, V., Carabelli, V., and Carbone, E. (2007). L-type calcium channels in adrenal chromaffin cells: role in pace-making and secretion. *Cell calcium* 42, 397-408.

McCue, H.V., Haynes, L.P., and Burgoyne, R.D. (2010). Bioinformatic analysis of CaBP/calneuron proteins reveals a family of highly conserved vertebrate Ca²⁺-binding proteins. *BMC research notes* 3, 118.

McRory, J.E., Hamid, J., Doering, C.J., Garcia, E., Parker, R., Hamming, K., Chen, L., Hildebrand, M., Beedle, A.M., Feldcamp, L., *et al.* (2004). The CACNA1F gene encodes an L-type calcium channel with unique biophysical properties and tissue distribution. *The Journal of neuroscience : the official journal of the Society for Neuroscience* 24, 1707-1718.

Michalakis, S., Geiger, H., Haverkamp, S., Hofmann, F., Gerstner, A., and Biel, M. (2005). Impaired opsin targeting and cone photoreceptor migration in the retina of mice lacking the cyclic nucleotide-gated channel CNGA3. *Investigative ophthalmology & visual science* 46, 1516-1524.

Michalakis, S., Muhlfriedel, R., Tanimoto, N., Krishnamoorthy, V., Koch, S., Fischer, M.D., Becirovic, E., Bai, L., Huber, G., Beck, S.C., *et al.* (2010). Restoration of cone vision in the CNGA3^{-/-} mouse model of congenital complete lack of cone photoreceptor function. *Molecular therapy : the journal of the American Society of Gene Therapy* 18, 2057-2063.

Michalakis, S., Schaferhoff, K., Spiwoks-Becker, I., Zabouri, N., Koch, S., Koch, F., Bonin, M., Biel, M., and Haverkamp, S. (2012). Characterization of neurite outgrowth and ectopic synaptogenesis in response to photoreceptor dysfunction. *Cellular and molecular life sciences : CMLS*.

Migeon, B.R. (2006). The role of X inactivation and cellular mosaicism in women's health and sex-specific diseases. *JAMA : the journal of the American Medical Association* 295, 1428-1433.

Mikami, A., Imoto, K., Tanabe, T., Niidome, T., Mori, Y., Takeshima, H., Narumiya, S., and Numa, S. (1989). Primary structure and functional expression of the cardiac dihydropyridine-sensitive calcium channel. *Nature* 340, 230-233.

Mikhaylova, M., Hradsky, J., and Kreutz, M.R. (2011). Between promiscuity and specificity: novel roles of EF-hand calcium sensors in neuronal Ca²⁺ signalling. *Journal of neurochemistry* 118, 695-713.

Mikhaylova, M., Reddy, P.P., Munsch, T., Landgraf, P., Suman, S.K., Smalla, K.H., Gundelfinger, E.D., Sharma, Y., and Kreutz, M.R. (2009). Calneurons provide a calcium threshold for trans-Golgi network to plasma membrane trafficking. *Proceedings of the National Academy of Sciences of the United States of America* 106, 9093-9098.

Minor, D.L., Jr., and Findeisen, F. (2010). Progress in the structural understanding of voltage-gated calcium channel (Ca_v) function and modulation. *Channels (Austin)* 4, 459-474.

Moosmang, S., Haider, N., Bruderl, B., Welling, A., and Hofmann, F. (2006). Antihypertensive effects of the putative T-type calcium channel antagonist mibefradil are mediated by the L-type calcium channel Cav1.2. *Circulation research* 98, 105-110.

LITERATURE

Moosmang, S., Schulla, V., Welling, A., Feil, R., Feil, S., Wegener, J.W., Hofmann, F., and Klugbauer, N. (2003). Dominant role of smooth muscle L-type calcium channel Cav1.2 for blood pressure regulation. *The EMBO journal* 22, 6027-6034.

Morgans, C.W. (2001). Localization of the alpha(1F) calcium channel subunit in the rat retina. *Investigative ophthalmology & visual science* 42, 2414-2418.

Mori, Y., Friedrich, T., Kim, M.S., Mikami, A., Nakai, J., Ruth, P., Bosse, E., Hofmann, F., Flockerzi, V., Furuichi, T., and et al. (1991). Primary structure and functional expression from complementary DNA of a brain calcium channel. *Nature* 350, 398-402.

Moriondo, A., Pelucchi, B., and Rispoli, G. (2001). Calcium-activated potassium current clamps the dark potential of vertebrate rods. *The European journal of neuroscience* 14, 19-26.

Mullis, K.B., and Faloona, F.A. (1987). Specific synthesis of DNA in vitro via a polymerase-catalyzed chain reaction. *Methods in enzymology* 155, 335-350.

Niidome, T., Kim, M.S., Friedrich, T., and Mori, Y. (1992). Molecular cloning and characterization of a novel calcium channel from rabbit brain. *FEBS letters* 308, 7-13.

Noble, S., and Shimoni, Y. (1981a). The calcium and frequency dependence of the slow inward current 'staircase' in frog atrium. *The Journal of physiology* 310, 57-75.

Noble, S., and Shimoni, Y. (1981b). Voltage-dependent potentiation of the slow inward current in frog atrium. *The Journal of physiology* 310, 77-95.

Nowycky, M.C., Fox, A.P., and Tsien, R.W. (1985). Three types of neuronal calcium channel with different calcium agonist sensitivity. *Nature* 316, 440-443.

Oliveria, S.F., Dell'Acqua, M.L., and Sather, W.A. (2007). AKAP79/150 anchoring of calcineurin controls neuronal L-type Ca²⁺ channel activity and nuclear signaling. *Neuron* 55, 261-275.

Oz, S., Tsemakhovich, V., Christel, C.J., Lee, A., and Dascal, N. (2011). CaBP1 regulates voltage-dependent inactivation and activation of Ca(V)1.2 (L-type) calcium channels. *The Journal of biological chemistry* 286, 13945-13953.

Pang, J.J., Chang, B., Kumar, A., Nusinowitz, S., Noorwez, S.M., Li, J., Rani, A., Foster, T.C., Chiodo, V.A., Doyle, T., et al. (2006). Gene therapy restores vision-dependent behavior as well as retinal structure and function in a mouse model of RPE65 Leber congenital amaurosis. *Molecular therapy : the journal of the American Society of Gene Therapy* 13, 565-572.

Pate, P., Mochca-Morales, J., Wu, Y., Zhang, J.Z., Rodney, G.G., Serysheva, II, Williams, B.Y., Anderson, M.E., and Hamilton, S.L. (2000). Determinants for calmodulin binding on voltage-dependent Ca²⁺ channels. *The Journal of biological chemistry* 275, 39786-39792.

Peloquin, J.B., Doering, C.J., Rehak, R., and McRory, J.E. (2008). Temperature dependence of Cav1.4 calcium channel gating. *Neuroscience* 151, 1066-1083.

LITERATURE

Perez-Reyes, E. (1998). Molecular characterization of a novel family of low voltage-activated, T-type, calcium channels. *Journal of bioenergetics and biomembranes* 30, 313-318.

Peterson, B.Z., DeMaria, C.D., Adelman, J.P., and Yue, D.T. (1999). Calmodulin is the Ca²⁺ sensor for Ca²⁺-dependent inactivation of L-type calcium channels. *Neuron* 22, 549-558.

Peterson, B.Z., Lee, J.S., Mulle, J.G., Wang, Y., de Leon, M., and Yue, D.T. (2000). Critical determinants of Ca(2+)-dependent inactivation within an EF-hand motif of L-type Ca(2+) channels. *Biophysical journal* 78, 1906-1920.

Pfeiffer-Guglielmi, B., Fleckenstein, B., Jung, G., and Hamprecht, B. (2003). Immunocytochemical localization of glycogen phosphorylase isozymes in rat nervous tissues by using isozyme-specific antibodies. *J Neurochem* 85, 73-81.

Pitt, G.S., Zuhlke, R.D., Hudmon, A., Schulman, H., Reuter, H., and Tsien, R.W. (2001). Molecular basis of calmodulin tethering and Ca²⁺-dependent inactivation of L-type Ca²⁺ channels. *The Journal of biological chemistry* 276, 30794-30802.

Platzer, J., Engel, J., Schrott-Fischer, A., Stephan, K., Bova, S., Chen, H., Zheng, H., and Striessnig, J. (2000). Congenital deafness and sinoatrial node dysfunction in mice lacking class D L-type Ca²⁺ channels. *Cell* 102, 89-97.

Poche, R.A., and Reese, B.E. (2009). Retinal horizontal cells: challenging paradigms of neural development and cancer biology. *Development* 136, 2141-2151.

Pragnell, M., De Waard, M., Mori, Y., Tanabe, T., Snutch, T.P., and Campbell, K.P. (1994). Calcium channel beta-subunit binds to a conserved motif in the I-II cytoplasmic linker of the alpha 1-subunit. *Nature* 368, 67-70.

Raven, M.A., Orton, N.C., Nassar, H., Williams, G.A., Stell, W.K., Jacobs, G.H., Bech-Hansen, N.T., and Reese, B.E. (2008). Early afferent signaling in the outer plexiform layer regulates development of horizontal cell morphology. *The Journal of comparative neurology* 506, 745-758.

Reese, B.E., and Galli-Resta, L. (2002). The role of tangential dispersion in retinal mosaic formation. *Progress in retinal and eye research* 21, 153-168.

Reim, K., Wegmeyer, H., Brandstatter, J.H., Xue, M., Rosenmund, C., Dresbach, T., Hofmann, K., and Brose, N. (2005). Structurally and functionally unique complexins at retinal ribbon synapses. *The Journal of cell biology* 169, 669-680.

Rieke, F., Lee, A., and Haeseleer, F. (2008). Characterization of Ca²⁺-binding protein 5 knockout mouse retina. *Investigative ophthalmology & visual science* 49, 5126-5135.

Rigaudiere, F., Roux, C., Lachapelle, P., Rosolen, S.G., Bitoun, P., Gay-Duval, A., and Le Gargasson, J.F. (2003). ERGs in female carriers of incomplete congenital stationary night blindness (I-CSNB). A family report. *Documenta ophthalmologica. Advances in ophthalmology* 107, 203-212.

LITERATURE

Rios, E., Pizarro, G., and Stefani, E. (1992). Charge movement and the nature of signal transduction in skeletal muscle excitation-contraction coupling. *Annual review of physiology* 54, 109-133.

Romanin, C., Gamsjaeger, R., Kahr, H., Schaufler, D., Carlson, O., Abernethy, D.R., and Soldatov, N.M. (2000). Ca(2+) sensors of L-type Ca(2+) channel. *FEBS letters* 487, 301-306.

Sambrook, J., and Russell, D.W. (2001). *Molecular Cloning: A Laboratory Manual* (Cold Spring Harbor Laboratory Press).

Schieder, M., Rotzer, K., Bruggemann, A., Biel, M., and Wahl-Schott, C.A. (2010). Characterization of two-pore channel 2 (TPCN2)-mediated Ca²⁺ currents in isolated lysosomes. *The Journal of biological chemistry* 285, 21219-21222.

Schneeweis, D.M., and Schnapf, J.L. (2000). Noise and light adaptation in rods of the macaque monkey. *Visual neuroscience* 17, 659-666.

Schrauwen, I., Helfmann, S., Inagaki, A., Predoehl, F., Tabatabaiefar, M.A., Picher, M.M., Sommen, M., Seco, C.Z., Oostrik, J., Kremer, H., *et al.* (2012). A mutation in CABP2, expressed in cochlear hair cells, causes autosomal-recessive hearing impairment. *American journal of human genetics* 91, 636-645.

Schulla, V., Renstrom, E., Feil, R., Feil, S., Franklin, I., Gjinovci, A., Jing, X.J., Laux, D., Lundquist, I., Magnuson, M.A., *et al.* (2003). Impaired insulin secretion and glucose tolerance in beta cell-selective Ca(v)1.2 Ca²⁺ channel null mice. *The EMBO journal* 22, 3844-3854.

Seeliger, M.W., Grimm, C., Stahlberg, F., Friedburg, C., Jaissle, G., Zrenner, E., Guo, H., Reme, C.E., Humphries, P., Hofmann, F., *et al.* (2001). New views on RPE65 deficiency: the rod system is the source of vision in a mouse model of Leber congenital amaurosis. *Nature genetics* 29, 70-74.

Seino, S., Chen, L., Seino, M., Blondel, O., Takeda, J., Johnson, J.H., and Bell, G.I. (1992). Cloning of the alpha 1 subunit of a voltage-dependent calcium channel expressed in pancreatic beta cells. *Proceedings of the National Academy of Sciences of the United States of America* 89, 584-588.

Seisenberger, C., Specht, V., Welling, A., Platzer, J., Pfeifer, A., Kuhbandner, S., Striessnig, J., Klugbauer, N., Feil, R., and Hofmann, F. (2000). Functional embryonic cardiomyocytes after disruption of the L-type alpha1C (Cav1.2) calcium channel gene in the mouse. *The Journal of biological chemistry* 275, 39193-39199.

Shaltiel, L., Pappas, C., Fenske, S., Hassan, S., Gruner, C., Roetzer, K., Biel, M., and Wahl-Schott, C.A. (2012). Complex regulation of voltage dependent activation and inactivation properties of retinal voltage gated L-type Ca²⁺ channels Cav1.4 by Ca²⁺ binding protein 4 (CaBP4). *The Journal of biological chemistry*.

Shih, P.Y., Lin, C.L., Cheng, P.W., Liao, J.H., and Pan, C.Y. (2009). Calneuron I inhibits Ca(2+) channel activity in bovine chromaffin cells. *Biochemical and biophysical research communications* 388, 549-553.

LITERATURE

Shistik, E., Ivanina, T., Puri, T., Hosey, M., and Dascal, N. (1995). Ca²⁺ current enhancement by alpha 2/delta and beta subunits in *Xenopus* oocytes: contribution of changes in channel gating and alpha 1 protein level. *The Journal of physiology* 489 (Pt 1), 55-62.

Singh, A., Hamedinger, D., Hoda, J.C., Gebhart, M., Koschak, A., Romanin, C., and Striessnig, J. (2006). C-terminal modulator controls Ca²⁺-dependent gating of Ca(v)1.4 L-type Ca²⁺ channels. *Nature neuroscience* 9, 1108-1116.

Southern, E.M. (1975). Detection of specific sequences among DNA fragments separated by gel electrophoresis. *Journal of molecular biology* 98, 503-517.

Specht, D., Wu, S.B., Turner, P., Dearden, P., Koentgen, F., Wolfrum, U., Maw, M., Brandstatter, J.H., and tom Dieck, S. (2009). Effects of presynaptic mutations on a postsynaptic Cacna1s calcium channel colocalized with mGluR6 at mouse photoreceptor ribbon synapses. *Invest Ophthalmol Vis Sci* 50, 505-515.

Splawski, I., Timothy, K.W., Decher, N., Kumar, P., Sachse, F.B., Beggs, A.H., Sanguinetti, M.C., and Keating, M.T. (2005). Severe arrhythmia disorder caused by cardiac L-type calcium channel mutations. *Proceedings of the National Academy of Sciences of the United States of America* 102, 8089-8096; discussion 8086-8088.

Splawski, I., Timothy, K.W., Sharpe, L.M., Decher, N., Kumar, P., Bloise, R., Napolitano, C., Schwartz, P.J., Joseph, R.M., Condouris, K., *et al.* (2004). Ca(V)1.2 calcium channel dysfunction causes a multisystem disorder including arrhythmia and autism. *Cell* 119, 19-31.

Starr, T.V., Prystay, W., and Snutch, T.P. (1991). Primary structure of a calcium channel that is highly expressed in the rat cerebellum. *Proceedings of the National Academy of Sciences of the United States of America* 88, 5621-5625.

Stockner, T., and Koschak, A. (2013). What can naturally occurring mutations tell us about Cav1.x channel function? *Biochimica et biophysica acta* 1828, 1598-1607.

Stotz, S.C., Hamid, J., Spaetgens, R.L., Jarvis, S.E., and Zamponi, G.W. (2000). Fast inactivation of voltage-dependent calcium channels. A hinged-lid mechanism? *The Journal of biological chemistry* 275, 24575-24582.

Striessnig, J. (1999). Pharmacology, structure and function of cardiac L-type Ca(2+) channels. *Cellular physiology and biochemistry : international journal of experimental cellular physiology, biochemistry, and pharmacology* 9, 242-269.

Striessnig, J., Bolz, H.J., and Koschak, A. (2010). Channelopathies in Cav1.1, Cav1.3, and Cav1.4 voltage-gated L-type Ca²⁺ channels. *Pflugers Archiv : European journal of physiology* 460, 361-374.

Striessnig, J., Hoda, J.C., Koschak, A., Zaghetto, F., Mullner, C., Sinnegger-Brauns, M.J., Wild, C., Watschinger, K., Trockenbacher, A., and Pelster, G. (2004). L-type Ca²⁺ channels in Ca²⁺ channelopathies. *Biochemical and biophysical research communications* 322, 1341-1346.

LITERATURE

Strom, T.M., Nyakatura, G., Apfelstedt-Sylla, E., Hellebrand, H., Lorenz, B., Weber, B.H., Wutz, K., Gutwillinger, N., Ruther, K., Drescher, B., *et al.* (1998). An L-type calcium-channel gene mutated in incomplete X-linked congenital stationary night blindness. *Nature genetics* 19, 260-263.

Tadross, M.R., Ben Johny, M., and Yue, D.T. (2010). Molecular endpoints of Ca²⁺/calmodulin- and voltage-dependent inactivation of Ca(v)1.3 channels. *The Journal of general physiology* 135, 197-215.

Tanabe, T., Takeshima, H., Mikami, A., Flockerzi, V., Takahashi, H., Kangawa, K., Kojima, M., Matsuo, H., Hirose, T., and Numa, S. (1987). Primary structure of the receptor for calcium channel blockers from skeletal muscle. *Nature* 328, 313-318.

Tanimoto, N., Muehlfriedel, R.L., Fischer, M.D., Fahl, E., Humphries, P., Biel, M., and Seeliger, M.W. (2009). Vision tests in the mouse: Functional phenotyping with electroretinography. *Frontiers in bioscience : a journal and virtual library* 14, 2730-2737.

Taylor, W.R., and Morgans, C. (1998). Localization and properties of voltage-gated calcium channels in cone photoreceptors of *Tupaia belangeri*. *Visual neuroscience* 15, 541-552.

Thoreson, W.B. (2007). Kinetics of synaptic transmission at ribbon synapses of rods and cones. *Molecular neurobiology* 36, 205-223.

Thoreson, W.B., Rabl, K., Townes-Anderson, E., and Heidelberger, R. (2004). A highly Ca²⁺-sensitive pool of vesicles contributes to linearity at the rod photoreceptor ribbon synapse. *Neuron* 42, 595-605.

Tsien, R.W., Lipscombe, D., Madison, D.V., Bley, K.R., and Fox, A.P. (1988). Multiple types of neuronal calcium channels and their selective modulation. *Trends in neurosciences* 11, 431-438.

Tuluc, P., Molenda, N., Schlick, B., Obermair, G.J., Flucher, B.E., and Jurkat-Rott, K. (2009). A CaV1.1 Ca²⁺ channel splice variant with high conductance and voltage-sensitivity alters EC coupling in developing skeletal muscle. *Biophysical journal* 96, 35-44.

Turner, R.W., Anderson, D., and Zamponi, G.W. (2011). Signaling complexes of voltage-gated calcium channels. *Channels (Austin)* 5, 440-448.

van der Heyden, M.A., Wijnhoven, T.J., and Opthof, T. (2005). Molecular aspects of adrenergic modulation of cardiac L-type Ca²⁺ channels. *Cardiovascular research* 65, 28-39.

Vincent, A., Wright, T., Day, M.A., Westall, C.A., and Heon, E. (2011). A novel p.Gly603Arg mutation in CACNA1F causes Aland island eye disease and incomplete congenital stationary night blindness phenotypes in a family. *Molecular vision* 17, 3262-3270.

Wahl-Schott, C., Baumann, L., Cuny, H., Eckert, C., Griessmeier, K., and Biel, M. (2006). Switching off calcium-dependent inactivation in L-type calcium channels by an autoinhibitory domain. *Proceedings of the National Academy of Sciences of the United States of America* 103, 15657-15662.

LITERATURE

Williams, M.E., Brust, P.F., Feldman, D.H., Patthi, S., Simerson, S., Maroufi, A., McCue, A.F., Velicelebi, G., Ellis, S.B., and Harpold, M.M. (1992). Structure and functional expression of an omega-conotoxin-sensitive human N-type calcium channel. *Science* 257, 389-395.

Witkovsky, P., Schmitz, Y., Akopian, A., Krizaj, D., and Tranchina, D. (1997). Gain of rod to horizontal cell synaptic transfer: relation to glutamate release and a dihydropyridine-sensitive calcium current. *The Journal of neuroscience : the official journal of the Society for Neuroscience* 17, 7297-7306.

Wutz, K., Sauer, C., Zrenner, E., Lorenz, B., Alitalo, T., Broghammer, M., Hergersberg, M., de la Chapelle, A., Weber, B.H., Wissinger, B., *et al.* (2002). Thirty distinct CACNA1F mutations in 33 families with incomplete type of XLCSNB and *Cacna1f* expression profiling in mouse retina. *European journal of human genetics : EJHG* 10, 449-456.

Wyatt, C.N., Campbell, V., Brodbeck, J., Brice, N.L., Page, K.M., Berrow, N.S., Brickley, K., Terracciano, C.M., Naqvi, R.U., MacLeod, K.T., and Dolphin, A.C. (1997). Voltage-dependent binding and calcium channel current inhibition by an anti-alpha 1D subunit antibody in rat dorsal root ganglion neurones and guinea-pig myocytes. *The Journal of physiology* 502 (Pt 2), 307-319.

Yaari, Y., Hamon, B., and Lux, H.D. (1987). Development of two types of calcium channels in cultured mammalian hippocampal neurons. *Science* 235, 680-682.

Yang, P.S., Alseikhan, B.A., Hiel, H., Grant, L., Mori, M.X., Yang, W., Fuchs, P.A., and Yue, D.T. (2006). Switching of Ca²⁺-dependent inactivation of Ca(v)1.3 channels by calcium binding proteins of auditory hair cells. *The Journal of neuroscience : the official journal of the Society for Neuroscience* 26, 10677-10689.

Yang, S.N., and Berggren, P.O. (2006). The role of voltage-gated calcium channels in pancreatic beta-cell physiology and pathophysiology. *Endocrine reviews* 27, 621-676.

Yap, K.L., Ames, J.B., Swindells, M.B., and Ikura, M. (1999). Diversity of conformational states and changes within the EF-hand protein superfamily. *Proteins* 37, 499-507.

Young, S., Rothbard, J., and Parker, P.J. (1988). A monoclonal antibody recognising the site of limited proteolysis of protein kinase C. Inhibition of down-regulation in vivo. *European journal of biochemistry / FEBS* 173, 247-252.

Zeitz, C., Kloeckener-Gruissem, B., Forster, U., Kohl, S., Magyar, I., Wissinger, B., Matyas, G., Borruat, F.X., Schorderet, D.F., Zrenner, E., *et al.* (2006). Mutations in CABP4, the gene encoding the Ca²⁺-binding protein 4, cause autosomal recessive night blindness. *American journal of human genetics* 79, 657-667.

Zhang, Q., Timofeyev, V., Qiu, H., Lu, L., Li, N., Singapuri, A., Torado, C.L., Shin, H.S., and Chiamvimonvat, N. (2011). Expression and roles of Cav1.3 (alpha1D) L-type Ca(2)⁺ channel in atrioventricular node automaticity. *Journal of molecular and cellular cardiology* 50, 194-202.

LITERATURE

Zhang, Z., He, Y., Tuteja, D., Xu, D., Timofeyev, V., Zhang, Q., Glatter, K.A., Xu, Y., Shin, H.S., Low, R., and Chiamvimonvat, N. (2005). Functional roles of Cav1.3(alpha1D) calcium channels in atria: insights gained from gene-targeted null mutant mice. *Circulation* 112, 1936-1944.

Zhou, H., Kim, S.A., Kirk, E.A., Tippens, A.L., Sun, H., Haeseleer, F., and Lee, A. (2004). Ca²⁺-binding protein-1 facilitates and forms a postsynaptic complex with Cav1.2 (L-type) Ca²⁺ channels. *The Journal of neuroscience : the official journal of the Society for Neuroscience* 24, 4698-4708.

Zhou, H., Yu, K., McCoy, K.L., and Lee, A. (2005). Molecular mechanism for divergent regulation of Cav1.2 Ca²⁺ channels by calmodulin and Ca²⁺-binding protein-1. *The Journal of biological chemistry* 280, 29612-29619.

Zhou, J., Olcese, R., Qin, N., Noceti, F., Birnbaumer, L., and Stefani, E. (1997). Feedback inhibition of Ca²⁺ channels by Ca²⁺ depends on a short sequence of the C terminus that does not include the Ca²⁺ -binding function of a motif with similarity to Ca²⁺ -binding domains. *Proceedings of the National Academy of Sciences of the United States of America* 94, 2301-2305.

Zhou, Y., Morais-Cabral, J.H., Kaufman, A., and MacKinnon, R. (2001). Chemistry of ion coordination and hydration revealed by a K⁺ channel-Fab complex at 2.0 Å resolution. *Nature* 414, 43-48.

Zuhlke, R.D., Pitt, G.S., Deisseroth, K., Tsien, R.W., and Reuter, H. (1999). Calmodulin supports both inactivation and facilitation of L-type calcium channels. *Nature* 399, 159-162.

Zuhlke, R.D., Pitt, G.S., Tsien, R.W., and Reuter, H. (2000). Ca²⁺-sensitive inactivation and facilitation of L-type Ca²⁺ channels both depend on specific amino acid residues in a consensus calmodulin-binding motif in the(alpha)1C subunit. *The Journal of biological chemistry* 275, 21121-21129.

Zuhlke, R.D., and Reuter, H. (1998). Ca²⁺-sensitive inactivation of L-type Ca²⁺ channels depends on multiple cytoplasmic amino acid sequences of the alpha1C subunit. *Proceedings of the National Academy of Sciences of the United States of America* 95, 3287-3294.

8. Appendix

8.1 Sequence of the murine Ca_v1.4α1 cDNA

1 **ATC**TCGGAATCTGAAGTCGGGAAAGATACAACCCAGAGCCCAGTCCAGCCAATGGGACT
 1 **M**S E S E V G K D T T P E P S P A N G T
 61 GGCCCTGGCCCTGAATGGGGCTCTGTCTGGCCCTCCAAGTGTGGGGACTGATACCAGC
 21 G P G P E W G L C P G P P T V G T D T S
 121 GGGGCGTCAGGCCTGGGGACCCCAAGAAGAAGGACCCAGCACAAACACAAGACTGTG
 41 G A S G L G T P R R R T Q H N K H K T V
 181 GCGGTGGCCAGTGTCTCAGAGATCACCTCGAGCGCTCTTCTGCCTCACCCTTACTAATCCC
 61 A V A S A Q R S P R A L F C L T L T N P
 241 ATTCGTCGGTCTGCATCAGCATTGTAGAGTGGAAAG**CCTTTTGATATTCTCATCCTCCTG**
 81 I R R S C I S I V E W K **P F D I L I L L**
 301 **ACAATCTTTGCCAACTGCGTGGCATTGGGGGTATATATCCCTTCCCTGAGGACGACTCC**
 101 **T I F A N C V A L G V** Y I P F P E D D S
 361 AACACTGCTAACCACAACCTTGAACAG**GTAGAATACGTGTTCTGGTGATTTTCACCGTG**
 121 N T A N H N L E Q **V E Y V F L V I F T V**
 421 **GAGACAGTGTCAAGATCGTAGCCTATGGGCTGGTGCTCCATCCCAGCGCCTATATTTCGC**
 141 **E T V L K I V A Y** G L V L H P S A Y I R
 481 AAT**GGCTGGAACCTGCTCGACTTCATCATCGTCTGGTGGGCTGTTTCAGCGTGCTGCTG**
 161 N **G W N L L D F I I V V V G L F S V L L**
 541 GAACAAGGACCTGGGCGGCCAGGAGATGCCCCGATACTGGAGGAAAGCCAGGAGGCTTC
 181 E Q G P G R P G D A P H T G G K P G G F
 601 GAT**GTAAGGCACTGCGGGCATTTAGGGTGCTACGACCTCTAAGGCTAGTGTCTGGGGTC**
 201 D **V K A L R A F R V L R P L R L V S G V**
 661 CCGAGTCTGCACATAGTGCTCAATTCCATCATGAAGGCGCTTGTGCCGCTGCTGCACATT
 221 P S L H I V L N S I M K A L V P L L H **I**
 721 **GCCCTGTTGGTGCTCTTCGTCAATTATCATTTACGCCATCATCGGACTCGAGCTATTCTC**
 241 **A L L V L F V I I I Y A I I G L E L F** L
 781 GGACGAATGCACAAGACATGCTACTTCTGGGATCTGATATGGAAGCAGAGGAGGACCCA
 261 G R M H K T C Y F L G S D M E A E E D P
 841 TCACCTTGTGCATCTTCTGGCTCTGGGCGTTCATGCACACTGAACCATACCGAGTGCCGC
 281 S P C A S S G S G R S C T L N H T E C R
 901 GGGCGCTGGCCAGGACCCAACGGTGGCATCACGAACTTCGACAATTTTTTCTTTGCCATG
 301 G R W P G P N G G I T N F D N F F F A M
 961 CTAAGTGTGTTCCAGTGTATTACCATGGAAGGCTGGACAGACGCTCTACTGGATGCAG
 321 L T V F Q C I T M E G W T D V L Y W M Q
 1021 GATGCCATGGGGTATGAGCTG**CCTTGGGTGTA**CTTTGTGAGCCTTGTGCATCTTTGGGTCC
 341 D A M G Y E L **P W V Y F V S L V I F G S**
 1081 **TTCTTTGTCCTCAACCTTGTGCTTGGAGTCCTAAGC****GGGAGTTCTCCAAGGAAAGAGAA**
 361 **F F V L N L V L G V L S** G E F S K E R E

APPENDIX

1141 AAGGCAAAGCACGAGGTGACTTTCAGAAGCTTCGGGAGAAGCAGCAGATGGAAGAAGAC
381 K A K A R G D F Q K L R E K Q Q M E E D

1201 CTTCCGGGGCTACCTGGACTGGATCACACAGGCTGAGGAGTTAGACCTTCATGACCCCTCA
401 L R G Y L D W I T Q A E E L D L H D P S

1261 GTAGACGGCAACTTGGCTTCTCTTGTGAAGAGGGACGGGCGGGCCATCGGCCAACCTG
421 V D G N L A S L A E E G R A G H R P Q L

1321 TCAGAGCTGACCAATAGGAGGCGGGACGGCTGCGATGGTTCAGCCACTCTACTCGCTCC
441 S E L T N R R R G R L R W F S H S T R S

1381 ACACACTCCACCAGCAGCCACGCCAGCCTCCCAGCCAGTGACACTGGCTCCATGACAGAC
461 T H S T S S H A S L P A S D T G S M T D

1441 ACCCCTGGAGATGAGGATGAAGAAGAGGGGACCATGGCTAGCTGTACACGCTGCCTAAAC
481 T P G D E D E E E G T M A S C T R C L N

1501 AAGATTATGAAAACAAGGATCTGCCGCCACTTCCGCCGAGCCAACCGGGTCTCCGTGCA
501 K I M K T R I C R H F R R A N R G L R A

1561 CGCTGCCGCCGGGCGTCAAGTCCAACGCCTGCTACTGGGCTGTACTGTTGCTCGTCTTC
521 R C R R A V K S N A C Y W A V L L L V F

1621 CTCAACACGTTGACCATAGCTTCAGAGCACCATGGGCAGCCTTTGTGGCTCACCCAGACC
541 L N T L T I A S E H H G Q P L W L T Q T

1681 CAAGAGTATGCCAACAAAGTTCTGCTCTGCCTCTTCACTGTGGAGATGCTCCTCAAACCTG
561 Q E Y A N K V L L C L F T V E M L L K L

1741 TACGGCCTGGGCCCTCTGTCTACGTTGCCTCCTTTTTCAACCGCTTTGACTGCTTCGTG
581 Y G L G P S V Y V A S F F N R F D C F V

1801 GTCTGTGGGGGCATCCTAGAAACCACTTTGGTGGAGGTGGGGCCATGCAGCCTCTTGGC
601 V C G G I L E T T L V E V G A M Q P L G

1861 ATCTCAGTGCTCCGATGTGTACGTCTCCTCAGGATCTTCAAGTCCAGGCCTGGGCA
621 I S V L R C V R L L R I F K V T R H W A

1921 TCCCTGAGCAATCTGGTGGCATCTTTGCTCAATTCCATGAAGTCCATCGCCTCCTTGCTG
641 S L S N L V A S L L N S M K S I A S L L

1981 CTTCTCCTCTTTCTCTTCATCATCATCTTCTCCCTGCTTGGCATGCAGCTGTTTGGGGC
661 L L L F L F I I I F S L L G M Q L F G G

2041 AAGTTCAACTTTGACCAGACCCACACCAAGAGGACACCTTTGATACCTTCCCCAAGCC
681 K F N F D Q T H T K R S T F D T F P Q A

2101 CTCCTCACTGTCTTTCAGATCCTGACTGGTGGAGATTGGAACGTTGTCATGTATGATGGT
701 L L T V F Q I L T G E D W N V V M Y D G

2161 ATCATGGCCTACGGTGGGCCCTTCTTCCCAGGGATGCTGGTGTGTGTTTATTTTCATCATC
721 I M A Y G G P F F P G M L V C V Y F I I

2221 CTCTTCATCTGTGGCAACTACATCCTGCTGAACGTGTTTCTTGCCATTGCCGTGGATAAC
741 L F I C G N Y I L L N V F L A I A V D N

2281 CTAGCCAGCGGGGATGCAGGCACTGCCAAAGACAAGGGCAGAGAGAAGAGCAGTGAAGGA
761 L A S G D A G T A K D K G R E K S S E G

2341 AACCTCCAAAGGAGAACAAGTATTGGTGCCTGGTGGAGAGAATGAGGACGCAAAGGGT
781 N P P K E N K V L V P G G E N E D A K G

APPENDIX

3661 TTTAACTATGCCATGGACATCCTCAACATGGTCTTCACTGGCCTCTTACCATTGAGATG
1221 F N Y A M D I L N M V F T G L F T I E M

3721 GTGCTCAAATCATCGCCTTTAAACCCAAGCATTACTTTGCAGATGCCTGGAATACGTTT
1241 V L K I I A F K P K H Y F A D A W N T F

3781 GATGCTCTCATTGTAGTGGGCAGTGTAGTCGACATCGCCGTCACAGAAAGTCAATAACGGA
1261 D A L I V V G S V V D I A V T E V N N G

3841 GGCCATCTTGGCGAGAGTTTCAAGAGACAGCTCCCCGATATCTATCACGTTCTTTTCGCCTC
1281 G H L G E S S E D S S R I S I T F F R L

3901 TTCCGAGTCATGAGGCTGGTCAAGCTTCTGAGTAAGGGTGGAGGGATCCGCACACTGCTC
1301 F R V M R L V K L L S K G E G I R T L L

3961 TGGACATTCATCAAGTCTTTCCAGGCCTTGCCCTATGTGGCACTTCTCATAGCAATGATA
1321 W T F I K S F Q A L P Y V A L L I A M I

4021 TTCTTCATCTATGCAGTCATTGGCATGCAGATGTTTGGCAAGGTGGCTCTTCAGGACGGC
1341 F F I Y A V I G M Q M F G K V A L Q D G

4081 ACGCAGATAAATCGAAACAACAATTTCCAGACCTTTCCGCAGGCTGTGCTGCTTCTGTTC
1361 T Q I N R N N N F Q T F P Q A V L L L F

4141 AGGTGTGCCACTGGTGAGGCCTGGCAAGAGATAATGCTAGCCAGCCTTCCAGGAAATCGA
1381 R C A T G E A W Q E I M L A S L P G N R

4201 TGTGACCCTGAGTCTGACTTTGGCCCAGGCGAGGAATTTACCTGTGGTAGCAGTTTTGCC
1401 C D P E S D F G P G E E F T C G S S F A

4261 ATCGTCTACTTCATCAGCTTCTTTATGCTCTGTGCCTTCTGATTATAAATCTCTTTGTG
1421 I V Y F I S F F M L C A F L I I N L F V

4321 GCTGTAATCATGGATAACTTTGATTACCTAACCAGAGATTGGTCTATCCTGGACCCAC
1441 A V I M D N F D Y L T R D W S I L G P H

4381 CACCTTGATGAATTCAAGAGGATCTGGTCTGAATATGACCCCGGAGCCAAGGGCCGCATC
1461 H L D E F K R I W S E Y D P G A K G R I EF

4441 AAGCACTTGGATGTGGTTGCCCTGCTGAGACGCATCCAGCCCCATTTGGGATTTGGAAAG
1481 K H L D V V A L L R R I Q P P L G F G K

4501 CTATGCCACACCGAGTGGCCTGCAAGAGACTCGTGGAATGAATGTGCCCTCAACTCA
1501 L C P H R V A C K R L V A M N V P L N S

4561 GATGGAACAGTGACATTCAACGCTACACTCTTTGCCCTGGTGCGGACATCCCTGAAGATC
1521 D G T V T F N A T L F A L V R T S L K I Pre-IQ

4621 AAGACAGAAGGGAACCTGGATCAAGCCAACCAGGAGCTTCGGATGGTCATCAAAAAGATC
1541 K T E G N L D Q A N Q E L R M V I K K I

4681 TGGAAGCGGATAAAGCAGAAATTGTTGGATGAGGTCATCCCTCCTCCCGATGAGGAGGAG
1561 W K R I K Q K L L D E V I P P P D E E E

4741 GTCACTGTGGGAAAATTCTATGCCACATTCTGATCCAAGATTATTCGAAAATTCCGG
1581 V T V G K F Y A T F L I Q D Y F R K F R IQ

4801 AGAAGGAAAGAAAAGGGGCTACTAGGAGAGAGGGCCCCAACAAGCACATCCTCTGCCCTC
1601 R R K E K G L L G R E A P T S T S S A L

4861 CAGGCTGGTCTAAGGAGCCTGCAGGACTTGGGTCTGAGATCCGTCAGCCCTCACCTAT
1621 Q A G L R S L Q D L G P E I R Q A L T Y

APPENDIX

4921 GACACTGAGGAAGAAGAGGAAGAGGAAGAGGCAGTGGGTCAGGAGGCTGAGGAAGAGGAA
 1641 D T E E E E E E E E A V G Q E A E E E E

4981 GCTGAGAACAACCCAGAACCATACAAAGACTCCATAGACTCCCAGCCCCAATCTCGATGG
 1661 A E N N P E P Y K D S I D S Q P Q S R W

5041 AACTCTAGGATTTCCGGTGTCTCTACCTGTAAAGGAGAACTTCCAGATTCTCTCTCAACT
 1681 N S R I S V S L P V K E K L P D S L S T

5101 GGGCCGAGTGATGATGATGGGCTGGCTCCCAACTCCAGGCAGCCCAGTGTGATACAGGCT
 1701 G P S D D D G L A P N S R Q P S V I Q A

5161 GGCTCCCAACCACACAGGAGAAGCTCTGGGGTTTTTCATGTTCACTATCCCGGAAGAAGGA
 1721 G S Q P H R R S S G V F M F T I P E E G

5221 AGTATTCAGCTCAAGGGAAGCTCAAGGGCAGGACAATCAGAATGAGGAACAGGAAGTCCCT
 1741 S I Q L K G T Q G Q D N Q N E E Q E V P

5281 GACTGGACTCCTGACCTGGATGAGCAGGCCGGGACTCCTTCGAACCCAGTCTTTTACCA
 1761 D W T P D L D E Q A G T P S N P V L L P

5341 CCTCACTGGTCCCAGCAACACGTAAACGGGCACCATGTGCCACGCCGACGTTTGCTGCCC
 1781 P H W S Q Q H V N G H H V P R R R L L P

5401 CCCACGCCTGCAGGTCGGAAGCCCTCCTTCACCATCCAGTGTCTGCAACGCCAGGGCAGT
 1801 P T P A G R K P S F T I Q C L Q R Q G S

5461 TGTGAAGATTTACCTATCCCAGGCACCTACCATCGTGGACGGACCTCAGGACCAAGCAGG
 1821 C E D L P I P G T Y H R G R T S G P S R

5521 GCTCAGGGTTCCTGGGCAGCCCCTCCTCAGAAGGGTTCGACTGCTATATGCCCCCTGTTG
 1841 A Q G S W A A P P Q K G R L L Y A P L L

5581 TTGGTGGAGGAATCTACAGTGGGTGAAGGATACCTTGGCAAACCTGGCGGCCACTGCGT
 1861 L V E E S T V G E G Y L G K L G G P L R

5641 ACCTTACCTGTCTGCAAGTGCCTGGAGCTCATCCGAATCCCAGCCACCGCAAGAGGGGC
 1881 T F T C L Q V P G A H P N P S H R K R G

5701 AGTGCTGACAGTTTGGTGGAGGCTGTGCTCATCTCCGAAGGCCTAGGTCTCTTTGCCCAA
 1901 S A D S L V E A V L I S E G L G L F A Q

5761 GACCCACGATTTGTGGCCCTGGCCAAGCAGGAGATTGCAGATGCATGTCACCTGACCCTG
 1921 D P R F V A L A K Q E I A D A C H L T L

5821 GATGAGATGGACAGTGCTGCCAGTGACTGCTGGCACAGAGAACCACCTCCCTTTACAGT
 1941 D E M D S A A S D L L A Q R T T S L Y S

5881 GATGAGGAGTCTATTCTTTCCCGCTTTGATGAAGAGGACCTGGGAGATGAGATGGCCTGT
 1961 D E E S I L S R F D E E D L G D E M A C

5941 GTCCATGCCCTCTAA
 1981 V H A L *

ICDI

Transmembrane segments

NNN – loops 1/2/3 sequences

8.2 Multiple sequence alignment of the CaBPs

hCaBP1		0
hCaBP2		0
hCaBP3		0
hCaBP4	MTTEQARGQQGPNLAI GRQKPPAGVVTPKSDAEEPPLTRK	40
hCaBP5		0
hCaBP7		0
hCaBP8		0
hCaM		0

hCaBP1	MGNVCV KYPLRNLSRKMCQEEQTSY MVVQTSEEG	33
hCaBP2	MGNCAKRPWRRGPKDPLQWLGSPPRGSCPS PSS	33
hCaBP3		0
hCaBP4	RSKKERGLRGSRKRTGSSGEQTGPEAPGSSNNPPSTGEGP	80
hCaBP5		0
hCaBP7		0
hCaBP8		0
hCaM		0

hCaBP1	LAADAELPGPLLMLAQNCAVMHNL LGPACIFLRKGF AENR	73
hCaBP2	SPKEQGD PAPG.VQG..YSVLNSLVGPACIFLRPSIAATQ	70
hCaBP3	MLP...AALQSHLVVVFPAVSQQCLSS	25
hCaBP4	AGAPPASPGPASSRQSHRHRPDSLHDAAQRTYGPLLNRVF	120
hCaBP5	MQFPMGPACIFLRKGI A EKQ	20
hCaBP7	MPFHPVTAALMYRGIYTVPNLLS...E	24
hCaBP8	MPFHHVTAGLLYKGNLNRSL SAGSDS	27
hCaM		0

EF-1

hCaBP1	QPDRSLRPEEIEELREAFREFDKDKDGYINCRDLGN....	109
hCaBP2	L.DREL RPEEIEELQVAFQEFDRDRDGYIGCRELGA....	105
hCaBP3	R.RCRRGPGWGTAWRGGVELAGHQSQDGPSSLLPVGAQPPY	64
hCaBP4	GKDRELGP EELDELQAAFEFDTDRDGYISHRELGD....	156
hCaBP5	R.ERPLGQDEIEELREAFLEFDKDRDGFISCKDLGN....	55
hCaBP7	QRPVDIPEDELEEIREAFKVFDRDGNGFISKQELGT....	60
hCaBP8	EQLANISVEELDEIREAFRVLDRDGNGFISKQELGM....	63
hCaM	MADQLTEEQIAEFKEAFSLFDKGDGTITTKELGT....	35

EF-2

hCaBP1	.CMRTMG.....YMPTEMELIELSQQINMNLG GHVD	139
hCaBP2	.CMRTL G.....YMPTEMELIEISQQIS...GKVD	132
hCaBP3	LLQHSFATSSCLSWLLLRSRCLRAVTAGLEIRMNLG GRVD	104
hCaBP4	.CMRTL G.....YMPTEMELLEVSQH IKMRMG GRVD	186
hCaBP5	.LMRTMG.....YMPTEMELIELGQQIRMN LG GRVD	85
hCaBP7	.AMRSLG.....YMPNEVELEVI IQRLDMDGDGQVD	90
hCaBP8	.AMRSLG.....YMPSEVELAIIMQRLDMDGDGQVD	93
hCaM	.VMRSLG.....QNPTEAELQDMINEVDADGN GTID	65

APPENDIX

	...EF-2	EF-3	
hCaBP1	FDDFVELMGPKLLAETAD.	MIGVKELRDAFREEDTNGDGE	178
hCaBP2	FEDFVELMGPKLLAETAD.	MIGVREL RDAFREEDTNGDGR	171
hCaBP3	FDDFVELMTPKLLAETAG.	MIGVQEMRDAFKEEDTNGDGE	143
hCaBP4	FEFVELIGPKLREETAH.	MLGVRELRIAFREEDRDRDGR	225
hCaBP5	FDDFVELMTPKLLAETAG.	MIGVQEMRDAFKEEDTNGDGE	124
hCaBP7	FEFVTL LGPKLSTSGIPEKFGHT	DFDTVFWKQDMQK...	127
hCaBP8	FDEFMTILGPKLVSSEGRDGLGNTIDSIFWQ	EDMQR...	130
hCaM	FPEFLTMMARKMKDTS.....	EEIIEAFRVEDKDGNGY	100

	...EF-3	EF-4		
hCaBP1	ISTSELREAMRKL LGHQV	GHRDI EEIIRDVD.....	LNGD	213
hCaBP2	ISVGE LRAALKALLGERLS	QREVD EILQDVD.....	LNGD	206
hCaBP3	ITLAE LQQAMQRL LGERLTPREI	SEVVREAD.....	VNGD	178
hCaBP4	ITVAELREAVPALLGEPL	AGPELDEMLREVD.....	LNGD	260
hCaBP5	ITLVELLQQAMQRL LGERLTPREI	SEVVREAD.....	VNGD	159
hCaBP7	LTVDELKRLLYDTFCEHL	SMKDIENIIMTEEESH	LGTAEE	167
hCaBP8	ITLEELKHILYHAFRDHL	TMKDIENIINEEES	LNETS GN	170
hCaM	ISAAELRHVMTN.LGEKLT	DEEVDEMIREAD.....	IDGD	134

	...EF-4		
hCaBP1	GRVDFEEFVRMMSR	227	
hCaBP2	GLVDFEEFVRMMSR	220	
hCaBP3	GTVDFEEFVKMMSR	192	
hCaBP4	GTVDFDEFVMMLSRH	275	
hCaBP5	GTVDFEEFVKMMSR	173	
hCaBP7	CPVDVETCSNQ.QIRQTCVRKSLICAF	AFIISVMLIAA	206
hCaBP8	CQTEFEGVHSQKQNRQTCVRKSLICAF	FAMAFIISVMLIAA	210
hCaM	GQVNYEEFVQMMTAK	149	

hCaBP1		
hCaBP2		
hCaBP3		
hCaBP4		
hCaBP5		
hCaBP7	NQVLRSGM	214
hCaBP8	NQILRSGM	218
hCaM		

APPENDIX

8.3 Sequence alignment of the CaBP4 protein variants

CaBP4_WT	MATEHNVQLVPGSQKIPKGVVSPRSAAEGPALTRRRSKKE	40
CaBP4_E267fs	MATEHNVQLVPGSQKIPKGVVSPRSAAEGPALTRRRSKKE	40
CaBP4_R216X	MATEHNVQLVPGSQKIPKGVVSPRSAAEGPALTRRRSKKE	40
Consensus	matehmvqlvpgsqkipkgvvsprsaaegpaltrrrskke	
CaBP4_WT	SWHPGSQKASSGDQSSSQGSEASGSSKHPPRTKVGQEEPS	80
CaBP4_E267fs	SWHPGSQKASSGDQSSSQGSEASGSSKHPPRTKVGQEEPS	80
CaBP4_R216X	SWHPGSQKASSGDQSSSQGSEASGSSKHPPRTKVGQEEPS	80
Consensus	swhpgsqkassgdqsssqgseasgsskhpprtkvgqeeps	
CaBP4_WT	SAPARPASHRHRSHRHRSDPQQDAAQRTYGPLLNRMFGKDR	120
CaBP4_E267fs	SAPARPASHRHRSHRHRSDPQQDAAQRTYGPLLNRMFGKDR	120
CaBP4_R216X	SAPARPASHRHRSHRHRSDPQQDAAQRTYGPLLNRMFGKDR	120
Consensus	saparpashrhrshrhrsdpqddaaqrtygpllrmfkgdr	
CaBP4_WT	ELGPEELEELQAAFEEDFTDQDGYIGYRELGDCMRTLGYM	160
CaBP4_E267fs	ELGPEELEELQAAFEEDFTDQDGYIGYRELGDCMRTLGYM	160
CaBP4_R216X	ELGPEELEELQAAFEEDFTDQDGYIGYRELGDCMRTLGYM	160
Consensus	elgpeeleelqaafeefdtddqgyigyrelgdcmrtygm	
CaBP4_WT	PTEMELLEVSQHVKMRMGGFVDFEETFVELISPKLREETAH	200
CaBP4_E267fs	PTEMELLEVSQHVKMRMGGFVDFEETFVELISPKLREETAH	200
CaBP4_R216X	PTEMELLEVSQHVKMRMGGFVDFEETFVELISPKLREETAH	200
Consensus	ptemellevsqhvkmrmggfvdfefvelispklreetah	
CaBP4_WT	MLGVRELRIAFREFDKDRDGRITVAELRQAAPALLGEPLE	240
CaBP4_E267fs	MLGVRELRIAFREFDKDRDGRITVAELRQAAPALLGEPLE	240
CaBP4_R216X	MLGVRELRIAF	211
Consensus	mlgvrelriafrefdkdrdgritvaelrqaapallgeple	
CaBP4_WT	GTELDEMLREMDLNGDGTIDFDEFVMMMLSTG	271
CaBP4_E267fs	GTELDEMLREMDLNGDGTIDFdvcdaiyrlrhlggqptg	280
Consensus	gteldemlremdlngdgtidfd	
CaBP4_E267fs	pggqdtshrqtttpfsmekspfpqagspphhtqlqslpv	320
CaBP4_E267fs	lsspipklwrekkn	334

8.4 Primers and Restriction enzymes

Name	5'-Sequence-3'	Length (bp)	Restriction enzyme	Construct
LS_CaBP4_F	CATCTT AGATCT GCCGCCAC CATGGCAACAGAGCACAATG	40	BglII	CaBP4 in pIRES
LS_CaBP4ΔNT_F	CAAG AGATCT GCCGCCACCA TGTTTGGAAAGGATCG	36	BglII	CaBP4ΔNT in pIRES
LS_CaBP4_R	CATAAA GTCGAC TCAGCCTG TAGATAGCATC	31	SalI	CaBP4 in pIRES
CaBP4_R216X_R	GTGTT GTCGAC TCAGAAGGC GATGCGTAGCTCC	33	SalI	CaBP4 R216X in pIRES
CaBP4_R216X_R2	CCGCCG GTCGAG TCAGAAGG CGATGCGTAGCTCC	34	XhoI	CaBP4 R216X for FRET
CaBP4-3' UTR_R	CAATGTCGACAAATCATGTT CTCCAGTG	28	SalI	CaBP4-E267fs in pIRES
CaBP4-delAG_F	CACCATAGACTTTGACGTTT GTAATGATGCTATC	34	Overlap PCR	CaBP4-E267fs
CaBP4-delAG_R	GATAGCATCATTACAAACGT CAAAGTCTATGGTG	34	Overlap PCR	CaBP4-E267fs
LS_NTCaBP4_R	CATT GTCGAC TCAGCGGTTG AGCAAGGGC	29	SalI	NTCaBP4 in pIRES
LS_NTCaBP4_R2	CATT GTCGAG TCAGCGGTTG AGCAAGGGC	29	XhoI	NTCaBP4 for FRET
Neoext_F	CACTCCAGACATCCTGCTGA	20	Genotyping	Old WT allele PCR (ca. 290bp)
Kout1f_R1	GTCAACCCATGCTGTCTCCT	20		
Kout1f_F	ACCAAACCCCTAGCCCATACC	20	Genotyping	Old KO allele PCR (ca. 150bp)
Neoext_R	CCACATCAGAGGGAAAGGAA	20		
Ca _v 1.4_for	CCAACCAAACCCTAGCCCAT ACC	23	Genotyping	New PCR for genotyping the Ca _v 1.4 mice WT band = 398bp KO band = 169bp
Ca _v 1.4_WT_Rev	CATGCATACATACCTGGTGA CC	22		
Ca _v 1.4_KO_Rev	GATGTGTGCTTGCGAGATCC AC	22		

8.5 Materials and Equipment

8.5.1 Devices

Name	Company
Certomat [®] S (Bacterial culture shaker)	B.Braun Biotech international
CemiDoc [™] MP imaging system (for Western blots)	Biorad
E143, E835, EV202 (Voltage source for gel electrophoresis)	Consort
Gel Doc 2000 (for agarose gels)	Biorad
Incubator Cell culture – Hera safe	Heraeus
Incubator Bactria – Hera function line	Heraeus
Microwave R-212	Sharp
MilliQ-UF gradient	Millipore
Balance BP1215 (fine) and BP 4105	Sartorius
Plastic materials (petri dishes, plates, falcon, cups)	Sarstedt \ Greiner Bio-one
Photometer (BioPhotometer [™])	Eppendorf
Glass cuvette	Hellma
Agarose gel chamber	PeqLab
pH meter PH110	VWR international
Thermomixer compact	Eppendorf
Ultraviolet crosslinler CL-1000	UVP
Thermocycler T1(PCR)	Biometra
Mastercycler nexus gradient (PCR)	Eppendorf
Vacuum Concentrator	Bachofer
VortexMixer	VWR international
Refrigerator premium	Liebherr
Freezer confort no-frost	Liebherr
-80 ⁰ C freezer	Heraeus
P21 / K10 / B3 + DC10 (Water bath)	Haake
Western blot system	Biorad
Cryotome CM 30505	Leica
Hera guard – linear fume-chamber	Heraeus
Hera safe Cell culture fume-chamber	Heraeus
MR-3001K (magnet rotor) Rotamax120	Heidolph
Microscopes	Zeiss
Centrifuge: Eppendorf Centrifuge 5415 R\D J2-MC Centrifuge (Rotor: JA-10; JS-13.1) L-80K Ultracentrifuge Labofuge200\fresco\primo\pico Galaxy mini or mini-spin(tabletop centrifuge)	Eppendorf Beckmann Beckmann Heraeus VWR international\Eppendorf
Patch Clamp setup: Light source SNT12V 100W + Axiovert200 microscope Axopatch 200B (Amplifier) Polychrome V Digitizer digidata 1440A Control system SM1 Puller DMZ universal Borosilicate glass cappillaries SC150FT-8	Zeiss Axon instruments Till photonics Axon instruments Luigs & Neumann WZ Harvard Apparatus

APPENDIX

8.5.2 Chemicals

Name	Company
Ampicillin	Roth
Agarose	Peqlab
Seakem [®] LE-Agar	Biozym
Bacto-yeast extract	Aplichem
Bacto- tryptone	Aplichem
Boric acid	Sigma
Bromophenol blue	Sigma
DMSO (dimethyl sulfoxide)	Sigma
DNA extension ladder (standard markers)	Fermentas
dNTPs	Roth
EDTA (ethylenediamine-N, N, N', N'-tetraacetic acid)	Roth
Acetic acid	Roth
Ethanol	Roth
Ethidium bromide	Roth
Glucose	Roth
Glycerol	Sigma
Glycin	Roth
Glycerin	Roth
HCl (hydrochloric acid)	Roth
Isopropanol	Roth
potassium acetate	Sigma
KCl (potassium chloride)	Sigma
MgSO ₄ (magnesium sulfate)	Sigma
NaCl (sodium chloride)	VWR
NaOH (sodium hydroxide)	VWR
Phenol/Chlorophorm/Isoamylalkohol-Mix	Roth
Rnase A	Roche
SDS (Sodium dodecyl sulfate)	Roth
Tris (α, α, α-tris (hydroxymethyl) methylamine)	VWR
Tris-Cl	VWR
tRNA	Roche
Xylencyanol	Sigma
FBS	Biochrom
DMEM 4,5 g Glc + Pyruvat, DMEM 1 g Glc + Pyruvat	Invitrogen
Proteinase K	Roche
ECL	Santa Cruz
Fugene	Roche
Restriction enzymes	NEB \ Fermentas
Ligation kit and Maxi kit	Roche
Protease-Inhibitor	Roche
Herculase	Agilent
Pen/Strep	Biochrom
PureYield™ Midiprep system	Promega
REDTaq [®] ReadyMix	Sigma-Aldrich
Phusion polymerase	Finnzymes

8.6 Summary of the electrophysiological measurements

8.6.1 Voltages for half-maximum activation ($V_{0.5,act}$) and slope values (k_{act}) from the patch clamp measurements

	Concentration of charge carrier [mM]	$V_{0.5,act} Ca^{2+}$					$V_{0.5,act} Ba^{2+}$				
		$V_{0.5}$	SEM	Slope (k_{act})	SEM	n	$V_{0.5}$	SEM	Slope (k_{act})	SEM	n
Cav1.4	10mM	-9.41 ^{##}	± 1.88	7.88 ^{###}	± 0.23	7	-13.39 ^{###}	± 0.60	7.00 ^{###}	± 0.17	18
Cav1.4	2mM	-15.09 [*]	± 1.36	6.88 ^{**}	± 0.14	9					
Cav1.4 + CaBP4	10mM	-18.38 ^{**}	± 2.15	5.26 ^{***}	± 0.50	4	-18.89 ^{***}	± 1.53	5.39 ^{***}	± 0.36	6
Cav1.4 + R216X	10mM	-9.47 ^{##}	± 0.84	7.77 ^{##}	± 0.21	5	-15.16	± 1.36	6.18	± 0.47	9
Cav1.4 + E267fs	10mM	-3.62 ^{*,###}	± 1.07	7.88 ^{##}	± 0.43	5	-10.45 ^{**,###}	± 0.51	6.51 ^{*,###}	± 0.10	14
Cav1.4ΔICDI	10mM	-16.75 ^{**}	± 0.95	6.83 ^{**}	± 0.29	10	-21.30 ^{***}	± 0.64	5.42 ^{***}	± 0.14	23
Cav1.4ΔICDI + CaBP4	10mM	-17.09 ^{**}	± 1.47	5.51 ^{***}	± 0.22	13	-21.75 ^{***}	± 0.92	4.75 ^{***}	± 0.23	17

8.6.2 Voltages for half-maximum inactivation ($V_{0.5,inact}$) and slope values (k_{inact}) from the patch clamp measurements

	Concentration of charge carrier [mM]	$V_{0.5,inact} Ca^{2+}$					$V_{0.5,inact} Ba^{2+}$				
		$V_{0.5}$	SEM	Slope (k_{inact})	SEM	n	$V_{0.5}$	SEM	Slope (k_{inact})	SEM	n
Cav1.4	10mM	-2.77	± 5.00	17.41	± 1.62	4	-23.63 ^{##}	± 2.00	15.16	± 0.83	5
Cav1.4	2mM	-5.12	± 2.23	16.93	± 1.22	12					
Cav1.4 + CaBP4	10mM	-13.27	± 4.67	20.24	± 3.37	3	-13.55 ^{**}	± 2.72	17.42	± 2.26	8
Cav1.4 + R216X	10mM	-13.47	± 3.29	15.45	± 1.42	4	9.48 ^{***,###}	± 2.71	19.57 [*]	± 1.23	6
Cav1.4 + E267fs	10mM	13.55 [#]	± 6.35	19.37	± 2.66	6	14.25 ^{***,###}	± 2.26	20.21 [*]	± 1.07	12
Cav1.4ΔICDI	10mM	-20.50 ^{**}	± 2.12	14.97	± 2.48	4	-11.55 ^{**}	± 2.75	21.72 [*]	± 1.77	12
Cav1.4ΔICDI + CaBP4	10mM	-22.95 ^{**}	± 2.07	11.64	± 2.34	5	-16.45	± 3.02	10.54 ^{*,#}	± 0.85	11

8.7 List of Abbreviations

A	Adenine
aa	Amino acid
Å	Angstrom (10^{-10} meter)
AC	Amacrine cells
AIED	Iceland Åland eye disease
Amp ^R	Ampicillin
ANOVA	Analysis of variance
ApoCaM	Apo-calmodulin
APS	Ammonium peroxosulphate
ATP	Adenosine triphosphate
Ba ²⁺	Barium
BaCl ₂	Barium chloride
BBS	BES-buffered saline
BES	N,N-Bis(2-hydroxyethyl)-2-aminoethanesulfonic acid
bp	Basepairs
BP	Bipolar cells
BTZ	Benzothiazepines
BSA	Bovine serum albumin
C	Cytosine
c	Concentration
Ca ²⁺	Calcium
CaCl ₂	Calcium chloride
CaM	Calmodulin
Ca _v	Voltage gated calcium channel
CACNA1F	Gene of Cav1.4 channel
CDI	Calcium-dependent inactivation
cDNA	Complementary DNA
CIP	Calf intestinal phosphatase
cm	Centimeter
CMV	Cytomegalovirus
CO ₂	Carbon Dioxide
CORDX3	X-linked rod-cone dystrophy type 3
CT	Carboxyl terminus of proteins and peptides
CSNB	Congenital stationary night blindness
DHP	Dihydropyridines
DMEM	Dulbecco's modified Eagle medium
DMSO	Dimethylsulfoxide
DNA	Deoxyribonucleic acid
dNTP	2'-deoxynucleoside 5'-triphosphate

APPENDIX

DTT	Dithiothreitol
eCFP	Enhanced cyan fluorescent protein
E. coli	Escherichia coli
EDTA	Ethylenediaminetetraacetic
e.g.	For example
EGFP	Enhanced green fluorescent protein
EGTA	Ethyleneglycol-bis (2-aminoethyl ether)-N, N'-N'-tetraacetic acid
EtOH	Ethanol
ER	Endoplasmic reticulum
ERG	Electroretinography
FBS	Fetal bovine serum (fetal bovine serum)
FRET	Fluorescence resonance energy transfer
g	Grams
G	Guanosine
GC	Ganglion cells
h	hour
HC	Horizontal cells
HCl	Hydrochloric acid
HEK293	Human embryonic kidney cell line, clone 293
HEPES	2 - [4 - (2-hydroxyethyl)-1-piperazinyl] ethanesulfonic acid
H ₂ O	Water
H ₃ PO ₄	Phosphorous acid
HVA	High voltage-activated
HZ	Heterozygote
ICDI	Inhibitor of calcium-dependent inactivation
IQ motif	Isoleucine-glutamine motif
IRES	Internal ribosome entry site
Kan ^R	Kanamycin
kb	Kilobases
KCl	Potassium chloride
kDa	Kilodaltons
KH ₂ PO ₄	Potassium dihydrogen phosphate
KO	Knock out
L	Liter
LB	Luria-Bertani
LTCC	L-type calcium channel
LVA	Low voltage-activated
μ	Micro (10 ⁻⁶)
M	Moles per liter
m	Milli (10 ⁻³)
mA	Milliamperes

APPENDIX

MCS	Multiple cloning site
MgATP	Magnesium-ATP
MgCl ₂	Magnesium chloride
MgSO ₄	Magnesium sulfate
min	Minutes
n	Nano (10 ⁻⁹)
NaCl	Sodium chloride
NaOH	Sodium hydroxide
NCSs	Neuronal Ca ²⁺ sensors
Neo ^R	Neomycin
n.s.	Not significant
O.D	Optical density
pA	Picoamperes
PAA	Phenylalkylamine
PAGE	Polyacrylamide gel electrophoresis
PB	Phosphate buffer
PBS	Phosphate buffered electrolyte solution
PCR	Polymerase chain reaction
PEG	Polyethylene glycol
PFA	Paraformaldehyde
Ph	Photoreceptors
rpm	Rounds per minute
RT	Room temperature
SDS	Sodium dodecyl sulfate
SEM	Standard error of the mean
T	Tyrosine
TE	Tris-EDTA buffer
TBE	Tris-borate-EDTA buffer
TBS	Tris-borate-NaCl buffer
TEA	Tetraethylammonium
TEMED	N, N, N', N'-tetramethylethylenediamine
Tris	Tris (hydroxymethyl) aminomethane
U	Unit
UV	Ultraviolet
V	Volts
VDI	Voltage-dependent inactivation
vs.	Versus
WT	Wildtype

9. Curriculum Vitae

Personal Data

Name: Lior Shaltiel

Date of birth: 20th September 1979

Place of birth: Ramat-Gan, Israel

Nationality: Israeli, Dutch

School Education

1994-1997 Macabim-Re'ut high school, Israel. Full matriculation certificate enhanced: Biology, Chemistry, Mathematics and Arabic.

Military Service

1997-2001 Full military service. Military rank: Staff Sergeant. Excellency unit award.

Education

2001-2005 B.Sc (*summa cum laude*), department of Chemical Engineering, Specialization in biotechnology, Ben-Gurion University of the Negev (BGU), Israel.

2005-2007 M.Med.Sc degree, department of Physiology, BGU, Israel.

2006-2009 Visiting student at the institute of Pharmacology and Toxicology in the Technical University of Munich (TUM).

Professional Experience

2003-2005 Research assistant investigating intracellular signal transduction. Department of Life Sciences, BGU, Israel.

2004-2005 Research assistant in a project between BGU and Mediowound Ltd, Israel.

07-10/2002 Laboratory assistant in the analytic lab, Israel.

Promotion

2009-2013 Ph.D. student in the international graduate school Life Science Munich (LSM) under **Prof. Chirstian Wahl-Schott**, department of Pharmacy, LMU Munich. Granted by the Bavarian research foundation for the research: "Regulation of retinal calcium channels by calcium-binding proteins".

10. Publications

- Michalakis S*, **Shaltiel L***, Sothilingam V, Koch S, Zabouri N, Haverkamp S, Garcia Garrido M, Tanimoto N, Seeliger MW, Biel M and Wahl-Schott CA. Mosaic synaptopathy and functional defects in Cav1.4 heterozygous mice. (2013) Manuscript in preparation.
- **Shaltiel L***, Paparizos C*, Fenske S*, Hassan S, Gruner C, Rötzer K, Biel M, Wahl-Schott CA. Complex regulation of voltage dependent activation and inactivation properties of retinal voltage gated L-type Ca²⁺ channels Cav1.4 by Ca²⁺ binding protein 4 (CaBP4). (2012) J Biol Chem. 2012 Oct 19;287(43):36312-21, Epub 2012 Aug 30.
- Fenske S, Mader R, Scharr A, Paparizos C, Cao-Ehlker X, Michalakis S, **Shaltiel L**, Weidinger M, Stieber J, Feil S, Feil R, Hofmann F, Wahl-Schott C, Biel M. HCN3 Contributes to the Ventricular Action Potential Waveform in the Murine Heart. (2011) Circ Res. Oct 14;109(9):1015-23.
- Levy S, Beharier O, Etzion Y, Mor M, Buzaglo L, **Shaltiel L**, Gheber LA, Kahn J, Muslin AJ, Katz A, Gitler D, Moran A. The molecular basis for ZnT-1 action as an endogenous inhibitor of L-type calcium channels. (2009) J Biol Chem. Nov 20;284(47):32434-43.
- Gurfinkel R, Lavon I, Cagnano E, Volgin K, **Shaltiel L**, Grossman N, Kost J, Singer AJ, Rosenberg L. Combined ultrasonic and enzymatic debridement of necrotic eschars in an animal model (2009) J Burn Care Res. 30(3):505-13.

11. Acknowledgements

First, I would like sincerely thank Prof. Dr. Martin Biel, who accepted me as a PhD student in his group. His office door was always open for questions and support.

My special thanks go to my direct supervisor, Prof. Dr. Christian Wahl-Schott, for the excellent care and support. Dear Christian, I have learned from you an incredible amount of knowledge! Especially, I would like to thank you for the extensive personal instruction into the electrophysiology field.

I would like to thank PD Dr. Stylianos Michalakis for the excellent guidance and the mutual work on the characterization of visual phenotype on the $Ca_v1.4$ Heterozygote mice. In this context, I would like additionally to thank the research group of Prof. Seeliger (University of Tübingen), especially Dr. Regine Mühlfriedel, for the very good cooperation and collaboration.

I would like to thank also Christos Papparizos who was more than a colleague. It was great working together and I am sure we will stay in contact outside of the lab.

I am so happy that I could work in a lab with such good working climate, and this is due to the fact that I had such great colleagues! I thank all our lab members, in the past and the present, especially to Elvir, Sami, Kristina, Verena, Prakti, Susanne and the two Steffis, for so many beautiful memories: parties, barbecues, Oktoberfest visits, retreats and many more. Without you, this thesis would have been done with much less fun!

Special thanks also to my two favorite TAs Katrin Rötzer and Berit Noack. I am so happy we could work together, without you this work would have lasted longer.

Last but not least, I would like to thank the Bavarian Research Foundation (BFS) for supporting this work.



Additionally, I am thankful for the opportunity I had during my PhD study to be part of the graduate school Life Science Munich (LSM) and the excellence Ernst Ludwig Ehrlich Scholarship (ELES) program.



